Nonequilibrium Thermodynamics and Fitness Costs Associated with Information Preservation May Explain Longevity Differences between Species

by

Brett Neal Augsburger

A dissertation submitted to the Graduate Faculty of
Auburn University
in partial fulfillment of the
requirements for the Degree of
Doctor of Philosophy

Auburn, Alabama
May 7, 2016

Keywords: aging, entropy, second law, allometry

Approved by

Richard C. Bird, Co-chair, Professor of Pathobiology
Michael H. Irwin, Co-chair, Research Professor of Pathobiology
Robert R. Arnold, Associate Professor of Drug Discovery and Development
Bruce F. Smith, Professor of Pathobiology

Abstract

The aging process in most organisms is enormously complex, involving a multitude of integrated molecular pathways that define and modulate the gradual cellular, tissue and system-level changes that evoke the aging phenotype. Despite this sophistication, the root causes underlying the susceptibility of an organism to aging may be comparatively straightforward. Here, I posit that biological aging can be explained using established principles from physics (nonequilibrium thermodynamics and Newtonian), evolutionary theory, and information theory. A logical conclusion of the theory presented here is that aging is inevitable in all individual organisms given sufficient time. It is also argued here how stipulations derived from the second law of thermodynamics and Newtonian physics may be critical in defining evolutionary fitness landscapes that vary according to the ability of an organism to resist the loss of data in information-encoding biomolecules (DNA), and possibly other biocomponents subject to irreversible fidelity loss in some organisms, and that this may largely explain the differences in longevity amongst many organisms.

Acknowledgments

First and foremost, I would like to thank my major professor, Dr. Michael H. Irwin, for allowing me to pursue a topic that most major professors would consider too controversial and risky for a doctoral research project. His encouragement and support were vital. Dr. Irwin spent many hours discussing concepts with me and providing constructive feedback. This work would truly not have been possible without him.

I would like to thank my committee co-chair, Dr. Richard C. Bird, as well as the other members of my dissertation committee, Drs. Bruce F. Smith and Rusty Arnold, for their guidance and scientific input. I am also extremely appreciative to Dr. Jacek Wower for serving as university reader and for providing valuable feedback and constructive criticism.

I am very thankful to Dr. Leonard Hayflick for his encouragement and feedback. His work in the field of aging has greatly influenced my own efforts. I would also like to thank Dr. Carl A. Pinkert for accepting me into his lab before his transition to the dark side (i.e. the University of Alabama) and Dr. Vishnu Suppiramaniam for mentoring me early on in my graduate studies. I would like to thank Drs. Narendra K. Singh and John C. Quindry for their guidance and assistance with entering graduate school. I would like to thank the other members of the Irwin Laboratory, Jonathan Marable and Michelle Hoffman, for all of their help and efforts. Last, but certainly not least, I would like to thank my wife, Kelly, and children, Aidan and Avery, for their patience and for believing in me.

Table of Contents

List of Tables

List of Figures

List of Abbreviations and Symbols

BMR	basal metabolic rate
COT	mass-specific cost of transport
CFPS	cell-free protein synthesis
DDM	n-Dodecyl β-D-maltopyranoside
FMR	field metabolic rate
IMM	inner mitochondrial membrane
Mfn1/2	mitofusin 1/2
MLSP	maximum lifespan
mtDNA	mitochondrial DNA
OMM	outer mitochondrial membrane
ROI	return on investment
ROS	reactive oxygen species

Symbols

d_eS/dt	external entropy production rate
d_iS/dt	internal entropy production rate
D	degradation state
$\bar{I}_{DNA}$	average mutual information retained in a DNA ensemble
$l(x)$	survival up to age x

$m(x)$	fecundity at age x
M_b	body mass
$\dot{N}_{rc}$	biomolecule/biocomponent replacement rate
P	biomolecule/biocomponent performance
r	fitness
$\dot{S}_i$	average rate of internal entropy production

Forward

This work consists of two parts: a primary theoretical portion and a secondary experimental supplement. The major portion (Chapters 1-10) puts forth a novel theory of aging which attempts to explain the paramount importance of fundamental physical law in determining organismal longevity in concert with principles derived from evolutionary theory and information theory. The second part of this work is an experimental supplement that describes a design for a proteoliposome mitochondrial DNA delivery vehicle and outlines the experimental progress towards realizing the initial proof-of-concept stage for this delivery vehicle.

Chapter 1 - Introduction

Biological aging is the gradual loss of physiological function that occurs with the passing of time in individual organisms after reproductive maturity. This functional deficit leads to progressively decreased fecundity, increased mortality risk, and an increased risk of failure of most tissues, organs, and systems. Many theories have been proposed that attempt to explain why organisms age. Concepts from evolutionary theory, genetics, biochemistry, and cellular and molecular biology are most often used as the basis of these theories. Despite the fact that these efforts have resulted in a multitude of theories, each with serious anomalies, the focus over the last half century has remained in these areas—more fundamental physical law has been under or incorrectly applied, or simply ignored altogether. Notwithstanding the fact that deterioration is implicated nearly universally in the aging process, the connection to nonequilibrium thermodynamics and entropy production has not been firmly established and is infrequently mentioned. There have been a few notable exceptions; for example, Hayflick contends that entropy alone is sufficient to explain biological aging (Hayflick, 2007a; 2000; 2004; 2007b).

The second law of thermodynamics (hereafter abbreviated to "second law") stipulates that all energy, regardless of form, has a propensity to transition from a localized state to one that is more spread out, dispersed in space, at a rate that is determined by the ability of contributing external factors to counteract this tendency. In any system that is not at thermodynamic equilibrium, this tendency will result in entropy production by means of irreversible processes. A nonequilibrium system will continue to produce entropy indefinitely until equilibrium is reached, resulting in a transition from a higher

concentration of molecular bond energy to a lower bond energy concentration (Demirel, 2014a).

It has been argued that the second law only relates to closed systems and that since organisms are open systems the second law does not apply (Mitteldorf, 2010). This is false—the second law is universally applicable and always satisfied (Kondepudi and Prigogine, 2014). According to modern nonequilibrium thermodynamics, the second law describes the tendency for internal entropy to be produced by any system that is not in equilibrium. Clearly organisms are not in thermodynamic equilibrium and therefore internal entropy is produced continuously in all organisms.

Organisms combat entropy increases by exchanging heat and other forms of energy with their surroundings and importing/exporting entropy in the form of metabolites and catabolites. It has been suggested that any entropy increase in an organism can always be counteracted without repercussions by simply expending energy; from this, some have concluded that there is no thermodynamic stipulation for aging to occur and no role for thermodynamics in explaining aging. This is a rather obvious *non sequitur*—yet this notion has been perpetuated in the aging literature, both explicitly and implicitly (Kirkwood, 1999; Mitteldorf, 2010; Trindade et al., 2013). It will be demonstrated here why this inference is a logical fallacy and how it neglects to consider the effects of internal entropy production within an organism—particularly the influence of internal entropy production on the flow of biomolecular-encoded information over time.

Despite existing in a nonequilibrium state, individual organisms resist the decay towards equilibrium, which eventually results in death, long enough to allow them to mature and reproduce. The term “longevity”, as used in this discussion, refers to the

average period of time that individuals of a species live under ideal conditions. This can vary from hours to centuries depending on the species.

It will be demonstrated how internal entropy production is combatted within an organism and why various classes of biomolecules are impacted differently by thermodynamically-explained phenomena. For example, DNA molecules face inevitable reductions in mutual genetic information as a result of internal entropy production. While death due to other circumstances may occur first, individuals must eventually succumb to this effect with adequate time. Although germ cells will also inevitably lose mutual DNA information, species are able to survive and adapt due to selective pressures favoring the resulting genotypes that maximize fitness—losses in genetic information (i.e. mutations) that reduce species fitness are gradually eliminated from the gene pool.

It will also be established how strategies that increase or decrease the rate of loss of mutual DNA information in the individuals of a species may produce concomitant changes in other factors that impact fitness. Long-established allometric trends related to longevity can predict the state of many of these factors across a diverse range of species. The described logic suggests the existence of correlations between longevity, the rate of loss of mutual DNA information in individuals of a species and these fitness-modulating factors.

Chapter 2 - Nonequilibrium Thermodynamics Stipulates Biomolecular Damage in Living Organisms

Thermodynamic equilibrium can be characterized as the total absence of thermodynamic potentials within a system. Free energy is minimized in systems that have reached thermodynamic equilibrium. In living organisms, energy remains highly concentrated due to the chemical bonds that hold biomolecules together. For this reason, considerable thermodynamic potentials exist and therefore organisms are not in thermodynamic equilibrium. Organisms establish an ordered structure with low entropy by utilizing energy and matter that is exchanged with the environment. In terms of the preservation of overall biomolecular[1] integrity, an organism could be characterized as a near steady-state nonequilibrium system—at least if considered over a snapshot-in-time that is short compared to total lifespan. As the atomic arrangement of biomolecules fails to maximize free energy[2], the second law stipulates that irreversible processes driving the system in the direction of equilibrium will occur and impose insults on biomolecular

---

[1] Unless otherwise noted, the biomolecules being referred to are the proteins, carbohydrates, lipids, nucleic acids, and other macromolecules that define the structure of an organism and facilitate function.

[2] Not to be confused with free-energy minimization during protein folding and the conformational changes of other biomolecules. In these examples, the free-energy being minimized only considers conformation options for a given atomic structure (transitions that can occur within a very short time period). Even in its lowest free-energy conformation, any given biomolecule will still possess considerable excess energy, largely stored in the bonds between its atoms, compared to an equilibrium state where this energy has been maximally dispersed.

structure. This degradative phenomenon must be counteracted by the organism to prevent loss of biomolecular integrity.

Within any organism, thermodynamic fluxes (thermal, chemical, mechanical, electrical and others) exist and contain significant spatial and temporal heterogeneity at both the mesoscopic and macroscopic levels. As a result, a multitude of opportunities exist for biomolecular interactions that result in transitions to undesirable structural states. Mechanical force-based unfolding of proteins and unzipping or shearing of nucleic acids can occur, as can protein folding alterations and improper protein associations due to crowding (Zhou, 2010). DNA is subject to hydrolysis, oxidation, and methylation reactions among others (Lindahl, 1993). Denaturation of DNA and protein from excessive temperature is also possible. The disruption of hydrophobic interactions can occur in many situations and can alter protein structure such that it is nonfunctional. These are some of the more obvious ways by which a biomolecule could be damaged in a living organism. It should be apparent that while it is beneficial to the organism for the probabilities of these occurrences to be minimized, it is impossible to reduce them to zero.

Section 1 - A Model System for Analyzing Thermodynamically-Derived Biomolecular Degradation

As stipulated by thermodynamic principles, biomolecules face degradation even in conditions of relative homogeneity. For example, biomolecular structure can be compromised by a variety of undesirable chemical reactions that directly alter the molecular arrangement. To demonstrate the degradative effects of thermodynamic chemical forces on biomolecules, we will consider a system consisting of a fixed volume of cytosol. The analysis will focus on a single type of biomolecule; this could be an expressed protein, synthesized lipid or any other biomolecule that is produced by the

organism's cellular machinery. We will assume for this example that the biomolecule of interest is a protein. The temperature and pressure of the system are in equilibrium with the surroundings and equivalent to physiological values. The concentrations of all molecules aside from the protein of interest are held constant by chemiostats. The system is assumed to remain in thermomechanical equilibrium at all times but not chemical equilibrium. Chemical reactions not involving the protein of interest are inhibited (reaction rates and affinities are zeroed), as are all biomolecular repair and replacement mechanisms. At time t_0, every molecule of the protein of interest is in a state consistent with that immediately following successful protein synthesis, proper folding and post-translational modification (if applicable).

In accordance with the second law, the described system will produce internal entropy and transition irreversibly from an initial state at time t_0 through a very large number of nonequilibrium states until all chemical reaction affinities have been reduced to zero. Since the system as defined has no means of counteracting internal entropy production, the second law requires that the only stable or steady state is the chemical equilibrium state. Although some reaction affinities may be low, even the most improbably reactions must have nonzero reaction rates. The presence of reactive oxygen species (ROS) may generate reactions with particularly high affinities but such reactions are not the only source of internal entropy production. During the progression towards chemical equilibrium, the protein can exist in a very large number of alternative internal states representing various

degradative arrangements. The transitions between internal states can be characterized by reactions of the form

$$\sum_{\alpha=1}^{N_a} a_\alpha^{nm} A_\alpha + n \rightleftharpoons m + \sum_{\beta=1}^{N_b} b_\beta^{nm} B_\beta \quad (1)$$

where n and m are the initial and new protein internal states, a_α^{nm} and b_β^{nm} are the number of molecules of reactant (A_α) or product (B_β) involved in the reaction, and N_a and N_b are the number of different reactants and products involved. As these reactions proceed, internal entropy will be produced until the system reaches equilibrium. The rate of internal entropy production $d_i S/dt$ at any time t up until equilibrium can be expressed as

$$\frac{d_i S}{dt} = \sum_{j=1}^{r} \sum_{i=1}^{k} \left(\frac{-v_i^{(j)} \mu_i}{T} \right) \frac{d\varepsilon_j}{dt} > 0 \quad (2)$$

where k is the number of chemical species involved in a particular reaction, r is the total number of reactions taking place in the system, $v_i^{(j)}$ are the stoichiometric coefficients, μ_i are the chemical potentials, and $d\varepsilon_j/dt$ represents the reaction velocity at time t. At thermodynamic equilibrium, both the reaction velocity and the reaction affinity $A_r = \sum_{i=1}^{k} \left(-v_i^{(j)} \mu_i / T \right)$ will be zero.

Nonspontaneous processes can also occur during the degradation towards system equilibrium by way of being driven through thermodynamic coupling (Wang, 2009). Although these processes will usually also result in a biomolecule transitioning into a biologically undesirable internal state, negative entropy may be produced locally. Per the second law, internal entropy production must be non-negative in nonequilibrium systems

at all times. Therefore, any negative internal entropy produced by a nonspontaneous process will be offset by positive internal entropy production elsewhere in the system.

The described system illustrates why biomolecular degradation will occur continuously within all organisms, tissues, and cells—due to both spontaneous and nonspontaneous reactions. For homeostasis (steady-state) to be preserved, this degradation must be combatted by biological mechanisms capable of producing sufficient negative entropy to offset the internal entropy being produced. Obviously, degradative internal entropy production in a living organism is not limited to chemical reactions, as in the system above, but will also include contributions due to heat, mass, and momentum transfer as well as electrical, magnetic, and other effects. Each of these factors can be modelled similarly using modern nonequilibrium thermodynamic theory and the second law in particular, establishing an arrow of time which stipulates that the future can be distinguished from the past by an ever increasing quantity of internal entropy produced.

Section 2 - Preservation of Steady-state Nonequilibrium within a Biomolecular System

Returning to our model system, the ultimate endpoint of this system represents a state where all of the examined biomolecule have fully degraded and internal entropy production has ceased. Once this state is reached, all reaction affinities A_r and reaction velocities $d\varepsilon_j/dt$ will be zero, and the system will be in equilibrium.

The total entropy increase in the system at any time t is

$$dS_{sys,t} = \int_{t_0}^{t} \left(\frac{d_e S}{dt} + \frac{d_i S}{dt} \right) = \frac{Q_{tot}}{T} + \int_{t_0}^{t} \sum_{j=1}^{r} \sum_{i=1}^{k} \left(\frac{-v_i^{(j)} \mu_i}{T} \right) \frac{d\varepsilon_j}{dt} \qquad (3)$$

Here, $d_e S/dt$ represents the rate of entropy gain/loss in the system due to the exchange of energy with the surroundings (heat flowing into or out of the system). Q_{tot} represents

the total heat that has been transferred to/from the system between time t_0 and time t. Utilizing the change in system entropy $dS_{sys,t}$ for any time t and the increase in system entropy corresponding to the equilibrium condition $dS_{sys,max}$, we can define a new parameter to represent the degree to which the biomolecular ensemble under examination has degraded. This will be called "degradation state" D and is calculated

$$D(t) = \frac{dS_{sys,t}}{dS_{sys,max}} \quad (4)$$

A D of 1 corresponds to full degradation, while a value of 0 is representative of a pool of fully intact biomolecules. To prevent the described system from transitioning to an equilibrium state with maximum disorder and to preserve a steady state, the entropy being produced must be counteracted such that the following equation is satisfied

$$\dot{S}_{sys} = \frac{d_e S}{dt} + \frac{d_i S}{dt} = 0 \quad (5)$$

Since the second law stipulates that $d_i S/dt > 0$, in order to maintain a steady state

$$\frac{d_e S}{dt} = -\frac{d_i S}{dt} < 0 \quad (6)$$

As expected, negative entropy must be introduced into the system in order for biomolecular integrity to be preserved (i.e. prevent an increase in system entropy). Suppose that the system incorporates a replacement mechanism that replaces $\dot{N}_{rc}$ moles s^{-1} of

degraded biomolecules with newly expressed or fully-repaired biomolecules. A steady state can be maintained if

$$D_{rep}\frac{-dS_{sys,max}}{N_{tot}}\dot{N}_{rc} = -\frac{d_iS}{dt} \quad (7)$$

where D_{rep} represents the average degradation state of a replaced biomolecule and N_{tot} is the total number of the biomolecule of interest in moles. Eq. (7) can be rearranged to solve for replacement rate. (The rate of internal entropy production will be denoted by $\dot{S}_i$ instead of $\frac{d_iS}{dt}$ for purposes of clarity.)

$$\dot{N}_{rc} = \dot{S}_i N_{tot}\left(D_{rep} * dS_{sys,max}\right)^{-1} \quad (8)$$

The degradation state D of a biomolecular pool specifies the level of degradation of the average biomolecule but it does not indicate how well biomolecules perform at that degradation state. A new term, "biomolecular performance" P, will be used to quantify the relative ability of a biomolecule to perform its intrinsic biological function(s). A value for P of 1 indicates that the average biomolecule in an ensemble is able to perform 100% of its intrinsic biological function(s), or in other words, the ensemble will perform as if all biomolecules were in ideal condition. A P of 0 denotes that the average biomolecule is unable to perform any of its intrinsic biological function. Ultimately, we would like to express biomolecular replacement rate $\dot{N}_{rc}$ as a function of biomolecular performance. Several more relationships must be defined before this is possible.

Let us examine how biomolecular performance relates to degradation state. Biomolecular insults are inevitable and common occurrences; for this reason, biomolecules must retain the ability to perform their intrinsic biological function even when some level

of damage is present. If a biomolecule did not have this capability, only a very small percentage of biomolecules within a pool would be functional at any given time.

Many small singular insults to a biomolecule will have little to no effect on biomolecular performance (although certainly some singular insults can render a biomolecule nonfunctional or significantly compromised). As the number of insults incurred by a biomolecular pool begins to accumulate, biomolecular performance must decrease at a rate which will increase with further degradation. As the degradation state continues to increase, an inflection point will eventually be reached where the rate of decrease in P has achieved a maximum and further increases in degradation state will result in increasingly lower rates of decrease in P. The described relationship between biomolecular performance and degradation state can be approximated by a logistic curve. This can be represented as

$$P(D) = \left[1 + e^{k(D - D_{P50})}\right]^{-1} \quad (9)$$

Parameter D_{P50} specifies the biomolecular degradation state value that corresponds to a biomolecular performance of 0.5. In other words D_{P50} is a way to signify how much degradation a biomolecular ensemble can incur before losing half its performance. D_{P50} can be thought of as a measure of biomolecular durability. The parameter k specifies the steepness of the curve, or the relative ability of a biomolecule to resist decreases in performance with increasing degradation; for this reason, k can be viewed as a measure of biomolecular resiliency (lower values indicate increased resiliency). Fig. 1 illustrates some hypothetical graphs of P as a function of D for various values of k and D_{P50}.

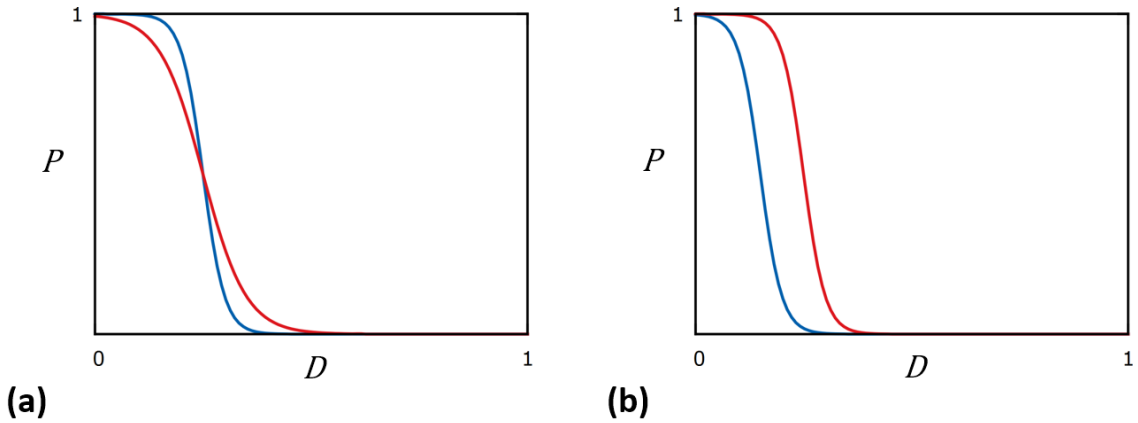

Fig. 1. Hypothetical biomolecular performance—degradation state curves that demonstrate the result of modulating different parameters from Eq. (9).

(a) D_{P50} = 0.25, k = 40 (blue), k = 20 (red). (b) D_{P50} = 0.15 (blue), D_{P50} = 0.25 (red), k = 40.

Next, we will derive a means to express the average degradation state of a biomolecule undergoing turnover in terms of the biomolecular performance of the ensemble. For this purpose, it will be assumed that the biomolecular repair/replacement mechanisms are able to differentiate between the performance state of individual molecules and that the average biomolecular performance of a repaired/replaced biomolecule is $m\%$ of the average biomolecular performance of the ensemble. By rearranging Eq. (9) and incorporating the m term we arrive at the desired expression

$$D_{rep}(P) = D_{P50} + k^{-1}\ln(\frac{100}{mP} - 1) \qquad (10)$$

Obviously, this relation does not perfectly describe the exact behavior of a cellular biomolecular repair and replacement strategy. However, for the purposes of the current discussion this approximation will be sufficient.

Lastly, to express biomolecular replacement rate in terms of biomolecular performance for a steady-state scenario, we require an expression for the rate of internal entropy production as a function of degradation state. Eq. (2) described the rate of internal entropy

production in terms of chemical reaction affinities and velocities. We can approximate a transformation of this equation into one that is a function of degradation state by considering some aspects of the reactions occurring within the system. For the time being, we will disregard radical and other chain-type reactions. We will assume that there are a very large number of potential reactions and that the reaction velocities of these reactions are widely and relatively evenly dispersed. Reactions with high reaction velocities will tend to occur before those with lower reaction velocities. In other words, reactions with high reaction velocities will be more prevalent at low degradation states. As degradation state increases, reactions with lower reaction velocities will begin to represent a larger proportion of the internal entropy being produced. However, there will be fewer total reactions because reactions with higher reaction velocities will have already completed. Therefore, as degradation state increases, the reaction velocity of the average reaction will decrease (reducing $\dot{S}_i$) and there will be fewer total possible reactions (further reducing $\dot{S}_i$). For this reason, $\dot{S}_i$ as a function of degradation state can be approximated by an exponential decay relationship.

$$\dot{S}_i(D) = \dot{S}_{max} e^{-rD} \qquad (11)$$

where $\dot{S}_{max}$ is the maximum rate of internal entropy production (corresponding to a D of zero) and r is the exponential decay constant. Actual values of r should always be greater than 0.

Finally, we have all the requisite relationships to express biomolecular replacement rate $\dot{N}_{rc}$ as a function of biomolecular performance. Combining Eqs. (8) thru (11), and solving for $\dot{N}_{rc}$ yields

$$\dot{N}_{rc}(P) = \dot{S}_{max} e^{-rD_{P50}} (P^{-1} - 1)^{-\frac{r}{k}} \left(D_{P50} + k^{-1} \ln\left(\frac{100}{mP} - 1\right)\right)^{-1} \frac{N_{tot}}{dS_{sys}, max} \quad (12)$$

Biomolecular replacement rate is of particular importance as it closely correlates with the rate of energetic resource consumption required to maintain a specific level of biomolecular performance. The performance of a given biomolecular ensemble must satisfy cellular/organismal requirements. Therefore, it is of interest to consider how biomolecular performance and replacement rate relate to each other and how other parameters may effect this relationship.

In the first hypothetical scenario, we examine the effects of modulating the exponential decay constant r (Fig. 2, Case A). Higher values of r equate to an increase in the rate of decay of internal entropy production with increasing degradation state (demonstrated in Fig. 2A.2 by plotting Eq. (11) for three different values of r). As long as r is not less than or equal to zero (or in other words, provided that internal entropy production decreases with increasing degradation state), there will be a particular performance value above and below which any change in replacement rate will have a diminishing effect on biomolecular performance. This is illustrated by plotting the derivative of Eq. (12), $\frac{d\dot{N}_{rc}}{dP}$ as a function of P, as shown in Fig. 2A.4. The minima in this graph represent the biomolecular performance values where the return on investment (in terms of rate of consumption of cellular energetic resources) towards biomolecular replacement rate is maximized. This

demonstrates the presence of a tradeoff between biomolecular performance and cellular energetic resource return on investment (ROI).

Next we will consider two variations of a biomolecule that share the same degradation state for a particular performance value but differ in resiliency (parameter k) due to differences in biomolecular structure. This is depicted in Fig. 2B.1 for a shared performance value of 0.95. $\dot{S}_i(D)$ is similar for both variations (Fig. 2B.2). Increasing biomolecular resiliency (decreasing k) allows for the same biomolecular performance to be achieved with lower replacement rates (Fig. 2B.3). All else being equal, selective pressure should favor biomolecular configurations that maximize resiliency.

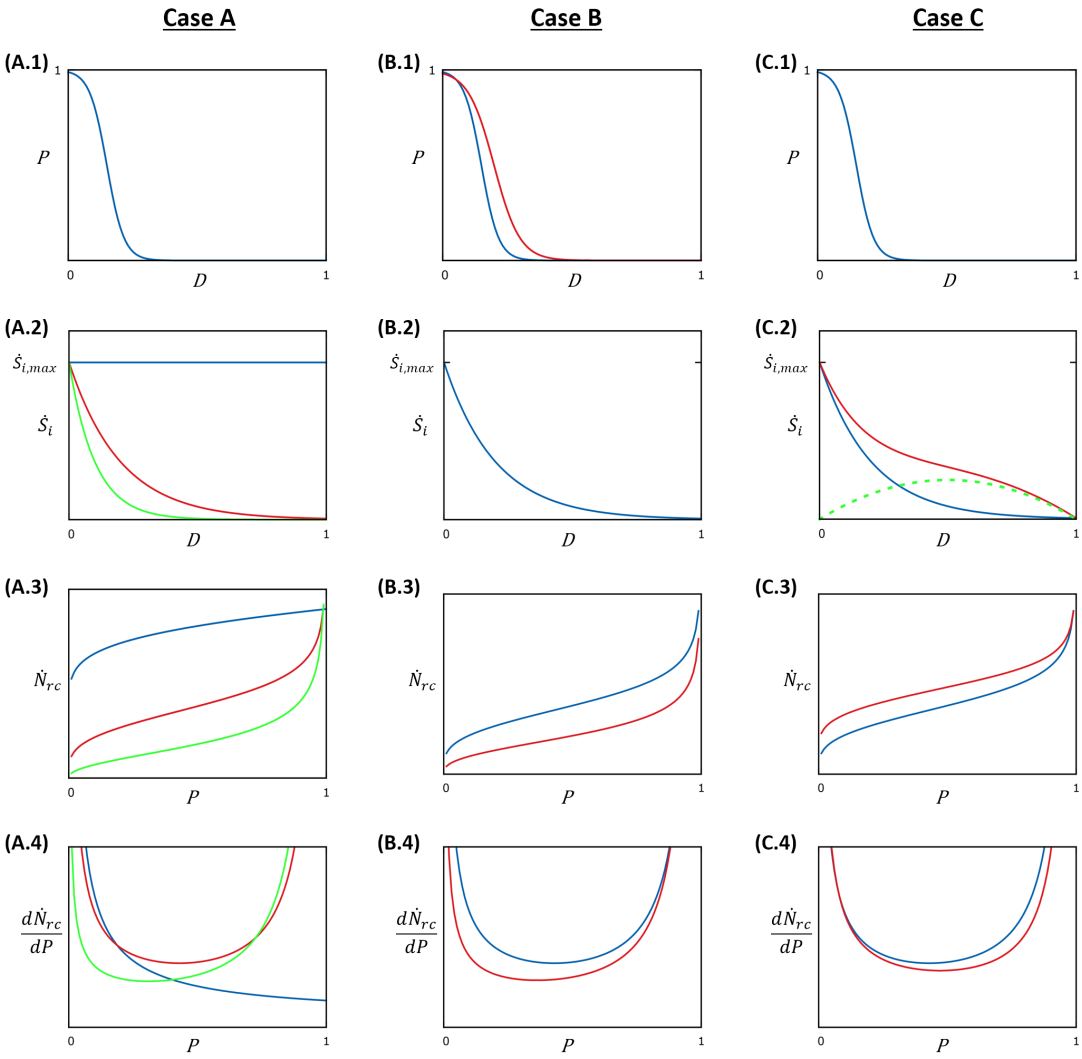

Fig. 2. Three hypothetical biomolecular repair/replacement scenarios demonstrating the relationships between biomolecular performance, degradation state, and repair/replacement rate by plotting Eqs. (9), (11), (12), (14), and (15).

Case A: Effects of altering parameter r. D_{P50} = 0.15, k = 30, m = 10, r = 0 (blue), r = 5 (red), r = 10 (green). Case B: Increasing biomolecular resiliency (lowering k) reduces the biomolecular replacement rate required to achieve a given performance. Both variations have the same degradation state at a performance value of 0.95. D_{P50} = 0.15 (blue), D_{P50} = 0.199 (red, calculated), k = 30 (blue), k = 20 (red), m = 10, r = 5, P_{match} = 0.95. Case C: Introduction of a radical reaction term into the internal entropy production rate equation. D_{P50} = 0.15, k = 30, m = 10, r = 5, h = 1.0.

For the last scenario, we will consider the impact of radical and other chain-type reactions. The presence of these reactions will impact $\dot{S}_i(D)$. At low degradation states, there will be relatively few chain-type reactions as reactive product is required to generate these reactions. As degradation state increases, more reactive product will be available, leading to an increase in the number of chain-type reactions and a corresponding increase in internal entropy production. As the amount of reactive product increases, the amount of available reactant will decrease. At some degradation state value, the amount of reactant remaining will have decreased to the point that the quantity of remaining available reactant becomes the factor limiting the reaction rate. This will result in a maximal contribution to $\dot{S}_i$ at this condition and a continual decrease in the magnitude of the contribution to $\dot{S}_i$ for higher degradation states. If we assume that this switchover occurs at a degradation state of 0.5, we can roughly approximate this behavior with the relation

$$\dot{S}_{i,rad}(D) = \dot{S}_{max} h(D - D^2) \quad (13)$$

where h is a scaling term. The total internal entropy production equation becomes

$$\dot{S}_{i,tot}(D) = \dot{S}_{max}(e^{-rD} + h(D - D^2) \quad (14)$$

Combining this equation with Eqs. (8) thru (10), and solving for $\dot{N}_{rc}$ yields the new expression

$$\begin{aligned}\dot{N}_{rc}(P) = \dot{S}_{max} \Bigg(& e^{-rD_{P50}}(P^{-1} - 1)^{-\frac{r}{k}} \\ & + h(D_{P50} + k^{-1}\ln(P^{-1} - 1) \\ & - (D_{P50} + k^{-1}\ln(P^{-1} - 1))^2) \Bigg) \Bigg(D_{P50} \\ & + k^{-1}\ln\left(\frac{100}{mP} - 1\right)\Bigg)^{-1} \frac{N_{tot}}{dS_{sys},max}\end{aligned} \quad (15)$$

By plotting Eq. (14), we can see the influence of chain-type reactions on total internal entropy production for a hypothetical scenario (Fig. 2C.2). Not surprisingly, per Eq. (15), incorporating chain-type reactions results in increased replacement rates for all performance values (Fig. 2C.3).

Of note is how it is conceivable for a biomolecular pool to have considerable radical-induced damage when functioning at a degradation state corresponding to that which maximizes cellular energetic resource ROI. In addition, it demonstrates that it is reasonable to expect more radical-induced damage (i.e. increased degradation state) in situations where energetic resource availability is limited and energetic resource ROI is more highly prioritized over peak performance. Biomolecular performance levels that maximize energetic resource ROI are likely to correspond with higher levels of biomolecular radical damage compared to the higher performance levels utilized by organisms with lower energetic resource availability restrictions and where maximal biomolecular performance is a higher priority.

The naked mole-rat (*Heterocephalus glaber*) may be an example of this phenomenon in action. The naked mole-rat has a maximum lifespan (MLSP) of ~31 years while their similar-sized cousin, the house mouse (*Mus musculus*), has an MLSP of only ~4 years (Tacutu et al., 2012). Yet, the naked mole-rat has been found to have significantly higher levels of oxidative stress than the house mouse (Andziak et al., 2005). Naked mole-rats also have higher levels of oxidative damage, including increased lipid peroxidation and total protein oxidation (Andziak and Buffenstein, 2006; Andziak et al., 2006). Examination of mitochondrial protein fractions from heart tissue found that mitochondrial proteins are also more damaged on average in naked mole-rats compared to mice (Andziak et al., 2006).

Despite this, naked mole-rats do not have superior biochemical defenses and in fact, they do not possess an antioxidant assemblage that is any more effective or efficient than that of mice (Andziak et al., 2005).

Naked mole-rats live in a hypoxic environment and have extremely low metabolic rates for their size (McNab, 1966). It has been considered a paradox that the naked mole-rat exhibits high levels of oxidative stress and protein damage while having such extreme longevity compared to similarly sized, closely-related species. I believe that not only is this not paradoxical, it is actually predictable and straightforward to explain. The first piece of the puzzle is explaining why oxidative damage levels are substantially elevated in the naked mole-rat. The naked mole-rat's limited access to oxygen restricts the rate of cellular ATP production via oxidative phosphorylation, thereby requiring that a very high priority be placed on the energetic ROI of cellular processes. As demonstrated, biomolecular performance levels that maximize energetic ROI are likely to correspond with higher loads of radical (oxidative) damage. Related species that are not as energetic resource restricted, for example the house mouse, may operate at higher biomolecular performance levels (to help maximize athletic ability, growth rate, etc.) which will correspond to lower levels of oxidative, and other, damage present in their biomolecular pools. Therefore, it should not be surprising that the naked mole-rat has elevated levels of oxidative damage, which is indicative of a higher biomolecular degradation state. The second part of solving the naked mole-rat paradox is explaining why their high biomolecular degradation states do not determine, nor adversely affect, MLSP. This will be addressed in Chapter 7 Section 5.

Chapter 3 - Combatting Degradative Internal Entropy Production within an Organism

From examining Eq. (5) we can see that in order for an individual organism to avoid a permanent increase in total entropy (i.e. to maintain a steady-state in terms of biomolecular degradation), the organism must be capable of producing sufficient negative entropy d_eS/dt to offset any degradative internal entropy that is produced d_iS/dt. Many of the mechanisms utilized for this purpose have been characterized. These mechanisms include biomolecular expression systems, molecular chaperones, degradation systems (proteasomes, lysosomes) and DNA repair enzymes, to name a few. It is clear that organisms would be unable to maintain (or even attain) a developed state without biomolecular repair and replacement mechanisms (Zimniak, 2008). At the cellular level, stem cells and mitotic cell division, together with apoptosis, provide a means to replace entire cells and, in some organisms, even tissues—thereby preserving (or at least attempting to preserve) the degradation state in these populations.

Consideration should also be given to the factors that influence the rate of degradative internal entropy production d_iS/dt within a system, as this will determine the amount of negative entropy required to satisfy a particular steady-state condition. Reducing the rate of internal entropy production will decrease the amount of negative entropy needed, and therefore the energetic investment required, to preserve homeostasis. The rate of internal entropy production is proportional to the sum of the contributions from all thermodynamic potentials acting on a biomolecular ensemble. This includes chemical reactions, heat, mass, momentum transfer, and other effects. The magnitudes of the thermodynamic potentials

depends on the strengths of the respective "damage-inflicting" forces (which may vary significantly with time, particularly when a biomolecule is in an active state) and the ability of an organism's biomolecular structures to resist these forces.

The rate of degradative internal entropy production will tend to decrease with increasing degradation state. The steady-state condition that is achieved will be the state where the rate of negative entropy production from repair and replacement is equivalent in magnitude to the rate of degradative internal entropy production. Regardless of the degradation state, all biomolecular ensembles will consist of biomolecules in various states of degradation. Perfect fidelity cannot be achieved in any biomolecular ensemble. (As degradation state decreases, less and less negative entropy will be produced by each biomolecular repair/replacement event; therefore, infinite resources would be required to attain perfect fidelity, i.e. a degradation state of zero.)

Section 1 - Optimization of Biomolecular Structure

Biomolecular structural optimizations can modulate the effects of degradative thermodynamic potentials by resisting biomolecular state changes. As an illustration, consider how a protein may be affected by hydroxyl radicals, which are capable of generating very strong chemical reaction potentials. The amino acids cysteine and methionine are particularly vulnerable to oxidation reactions (Suto et al., 2006). The inclusion of cysteine in a protein could be avoided, and another amino acid substituted, to protect from aberrant structural modifications due to hydroxyl radical reactions. Alternatively, cysteine could be implemented in non-critical locations within a protein as a sacrificial means to scavenge free radicals and help prevent damage to more critical domains. It should be considered, however, that a cysteine or methionine residue in a

particular location could bestow an advantageous trait to a protein (improved catalytic activity, energy utilization, substrate specificity, etc.)—thus any benefits to inclusion must be weighed against the costs associated with the increased susceptibility to insult.

Some of the other ways that biomolecular structural optimizations could help resist damage-inducing thermodynamic forces include modifications that improve resistance to undesirable hydrophobic interactions capable of generating conformation changes and structural variations that resist temperature-induced denaturation. These biomolecular modifications could result in a deleterious increase in the physical size of the biomolecule or otherwise be disadvantageous, such as limiting the rate at which a biomolecule can perform its intrinsic biological function. Modifications to biomolecular structure could also affect the amount of energetic resources required for the production/replacement/repair of a biomolecule.

On the other hand, high durability/resiliency or low rates of internal entropy production may be sacrificed by structural alterations that maximize the specific rate of work that can be performed by a biomolecule. An example of this is discussed in detail in Chapter 7 Section 4, where it is demonstrated that the polyunsaturated fatty acid content levels of membrane lipids, which varies across species, likely represent evolved tradeoffs between the specific rate of biomolecular work that can be performed by transmembrane proteins and the rate of internal entropy production.

Clearly, biomolecule structural optimization is a multifactorial compromise. It is apparent that through evolution, biomolecular arrangements are "tested" iteratively and through selective pressure converge towards arrangements that provide the appropriate balance between these factors such that evolutionary fitness is maximized in the species.

Section 2 - Microenvironment Optimization

Also relevant to the rate of degradative internal entropy production within an organism are the microenvironmental conditions, as these will define the magnitude of the degradative thermodynamic forces acting upon biomolecules. Temperature, which is a measure of the average kinetic energy of molecules, has a significant effect on reaction velocities and bond forces/energies. Although biomolecular conformation can change when temperature is increased or decreased, lower temperature will generally improve molecular stability and reduce the rate of internal entropy production. However, higher temperatures will produce increased kinetic energy transfer during intermolecular collisions. This will increase the specific rate of biomolecular work that can be performed. Evolution establishes a compromise between these and other temperature-dependent factors such that the defined species body temperature maximizes fitness.

Other attributes of a microenvironment may have less obvious, and even somewhat counterintuitive, ramifications. For example, conditions of higher oxidative stress are expected to increase the magnitude of degradative thermodynamic forces. At first glance, this may seem purely undesirable from a biological standpoint. Yet, it was demonstrated earlier how arrangements that highly prioritize energetic resource ROI may exhibit elevated levels of oxidative stress.

Section 3 - Biomolecular Work Rate can Influence the Magnitude of Degradative Internal Entropy Production Rates

Consider the state of biomolecules actively performing their intrinsic biological function. The process taking place will involve a transfer of energy. This will result in a brief period of time when energy is highly concentrated in close proximity to the biomolecule. The magnitude of the thermodynamic potentials contributing towards

biomolecular degradation will be amplified during this time. For this reason, internal entropy will be produced at an increased rate when biomolecules are in the active state.

All else being equal, a biomolecular pool that is inactive (not performing any intrinsic biological function) will have lower rates of degradative internal entropy production than one where biomolecules spend a significant percentage of time in the active state. The average rate of internal entropy production can be approximated by

$$\dot{S}_i = (100 - p)\dot{S}_{i,static} + p\dot{S}_{i,active} \quad (16)$$

where $\dot{S}_{static}$ is the degradative internal entropy production rate of the system when biomolecules are not performing any intrinsic biological function, $\dot{S}_{active}$ is the rate of internal entropy production when all biomolecules are actively performing their intrinsic biological functions, and p represents the percentage of time the average biomolecule spends in the active state. It should be evident that configurations where biomolecules spend more time in the active state (work rate is higher) will require increased rates of biomolecular repair/replacement to preserve the steady-state condition.

Section 4 - Extrapolation of Degradation State Concepts to Larger Physical Scales

The system described in Chapter 2 applies to biomolecules; many of the same concepts can also be applied to larger physical scales. For example, organelles are repaired and replaced, and face damage due to degradative internal entropy production in much the same manner as the individual biomolecules that they are assembled from. Mitotic cell populations can also be considered as described earlier, with individual cells utilized as the expressed (replicating) unit.

Chapter 4 - Preservation of DNA Molecular Information

Most biomolecules can be replaced directly by expression of a genetic sequence or are the metabolic products of expressed biomolecules. The performance of these biomolecular pools can be preserved through replacement by the successful expression of the appropriate genetic sequence or the relevant metabolic processes, and the removal or repair of any dysfunctional counterparts. With a given rate of turnover and assuming intact expression machinery, the preservation of biomolecular performance within a cell becomes dependent on: (1) the integrity of the genetic material responsible for biomolecular expression, and (2) the cell's ability to remove all dysfunctional biomolecules. It is suggested that, while the last requirement should not be trivialized, this is a very attainable objective: That is to say, the specificity of degradation pathways can afford to err on the side of casting a wider net to help ensure that any dysfunctional biomolecule is eventually recognized since these biomolecules can be resynthesized anew. Indiscriminate purging of cellular content would eventually dispose of any unwanted products—it is much easier to discard in excess to rid of waste than it is to preserve ultimate integrity in a structure. For these reasons, integrity preservation in biomolecules that cannot be expressed, the genetic-encoding biomolecules—DNA, warrants further scrutiny.

Section 1 - Decreases in Mutual Information of DNA Molecules

Combatting degradative internal entropy production via replacement requires intact information-containing biomolecules encoding for both the biomolecules being replaced and the expression machinery. DNA molecules contain the information encoding for all other classes of biomolecules, either directly or as the metabolic products of expressed

products. Furthermore, DNA molecules hold the instructions for all cellular processes. Like all molecules within an organism, DNA is subject to molecular insults resulting from internal entropy production and will incur an insult rate proportional to the damage-inflicting thermodynamic potentials of the microenvironment. DNA molecules are unique among classes of biomolecules as they depend on their own integrity for their replacement.

There are a number of ways that DNA damage can result in base alterations, cross-linking, strand breaks, and other modifications (De Bont and van Larebeke, 2004). Consider some of the possible outcomes when a double-stranded DNA molecule has suffered a single base excision:

1. The damage is properly repaired by endogenous base excision repair (BER) mechanisms
2. The damage is improperly repaired by BER mechanisms
3. An additional insult occurs at this site before repair can take place
4. No repair or further damage occurs for a length of time

DNA replication takes place far from thermodynamic equilibrium. The accuracy of DNA polymerase is largely dependent on the differences in the free energy released or absorbed by the various possible base-pairing combinations of incoming nucleotides to template strand nucleotides (Arias-Gonzalez, 2012). Utilizing thermodynamic theory, polymerase error rates have been estimated and demonstrated to be non-zero, in alignment with empirical findings. Although single-base excision damage is very often repaired by BER (scenario 1), restoring redundancy and preventing changes in stored information, there is always a possibility that a replication error will occur. Additionally, repair machinery must translocate to the site of the insult and perform the repair. This will not

occur instantaneously. If the site is further damaged before repair takes place then information loss could occur.

Only a single level of redundancy is definite at all DNA base pairs—that provided by the pairing base on the opposite strand. Even an insult restricted to a single base will deplete this redundancy and can lead to a permanent change in DNA information. This does not imply that more serious insults are not repairable. For example, double-stranded breaks may be completely repaired by homologous recombination in some cases, but there is no guarantee that a homologous site will exist or that the repair will be successful.

Once a DNA molecule has suffered an insult, there is no means to guarantee restoration of redundancy. As the second law stipulates that molecular insults are inevitable, the genetic data stored in DNA molecules must change with time—indefinite preservation of data is not possible. The concept of "perfect" DNA repair is flawed and unattainable.

The second law can therefore be causally implicated as mandating that losses in mutual DNA information will occur over time. This same conclusion has been drawn previously utilizing information theory; Yockey (1974) suggested that the noisy-channel coding theorem stipulates that, in the right conditions, the stability of the genetic message can be such that the error is "arbitrarily small" but that the probability of error must always be non- zero.

Permanent losses in genetic data are typically discussed in terms of discrete mutations or the rate at which mutations are occurring (Sniegowski et al., 2000). An alternative way to assess these losses is to consider the amount of DNA-encoded information that is

preserved using the concept of mutual information[3], which is a measure of the amount of information shared between two datasets. This provides a means to quantitate the amount of data retained in DNA molecules, be it the same DNA molecule at different points in time or between different DNA molecules. Methods for calculating the mutual information between DNA sequences have been discussed elsewhere (Demirel, 2014b; Grosse et al., 2000; Mahony et al., 2007). As genetic data must change with time, the mutual information of a discrete, non-replicating DNA molecule must also decrease with time; therefore, the rate of change in mutual information of DNA molecules will be negative and can be represented by

$$MIR_{DNA} = \frac{I_{DNA}}{t} < 0 \qquad (17)$$

I_{DNA} represents the amount of mutual information between the data stored in the DNA molecule at any initial time and after a period of time t has passed.

Section 2 - Applicability of the Degradation State Concept to DNA Molecular Ensembles

Synthesized biomolecules depend on the integrity of DNA for their correct expression. If the full integrity of DNA is preserved then, theoretically, negative entropy could be produced at a rate that results in a steady state of performance in any expressed biomolecular pool (as discussed in Chapter 2 Section 2). Since DNA molecules rely on

[3] **Although thermodynamics is useful for examining the causes of DNA molecular insults and assessing the magnitude of the damage-inducing potentials, concepts from information theory are more appropriate for analyzing DNA integrity quantitatively. So as to not confuse the fields, any use of the term entropy in this manuscript can be assumed to refer to thermodynamic entropy. Direct reference to Shannon entropy is avoided.**

their own integrity for identical replacement, this biomolecular replacement scenario is not applicable to DNA molecules.

Section 3 - Considerations for Mutual DNA Information Preservation in Different Cell Types

For a sexually reproducing multicellular organism, the zygote contains the truest representation of the parentally derived genetic data anywhere in the individual and of any stage in life, i.e. the mutual DNA information between parent and offspring is maximal in the zygote. The informational integrity of an organism's DNA at any later point in life can be quantified by comparing to this baseline standard.

Let us consider how the requirements for preservation of mutual DNA information are likely to vary over the course of an individual multicellular organism's life and as a function of cell type. Somatic cellular function must remain at a sufficiently high level for a certain minimum period of time in order for the organism to successfully reproduce. Selective pressure for preservation of function begins to decrease as an individual ages past reproductive maturity (Hamilton, 1966; Medawar, 1952). The progeny of adult stem cells are the replenishment source for somatic cells; therefore, it could be predicted that adult stem cells, on average, must retain a higher degree of mutual DNA information than non-stem somatic cells for any given point in an individual's lifespan.

Singular events that generate losses in mutual DNA information (i.e. mutations) most commonly have little or no effect on offspring fitness. Some mutations will result in decreases in fitness while only the rare insult produces increased fitness (Eyre-Walker and Keightley, 2007; Fisher, 1930). The distribution of these fitness effects can vary considerably between organisms. Evolutionary pressures must be sufficiently strong to select against "negative" mutations in order to prevent a loss of fitness.

The redundancy provided by diploidy/polyploidy, gene duplication, and functional overlap likely provides a degree of robustness that enables non-germ cells to tolerate a certain level of mutual DNA information loss with minimal performance impact on the individual (Medvedev, 1972; Plata and Vitkup, 2013; Riggs, 1994; Yockey, 1974). Similar levels of damage would be more detrimental in germ cells as they would propagate to all cells of the progeny. Therefore, we can confidently state that the average mutual DNA information retained by germ cells must be greater than that of adult stem cells at the time of reproduction, which in turn must be greater than the mutual DNA information retained in non-stem somatic cells at the time of reproduction. This relationship can be written

$$\bar{I}_{DNA}(zyg; som_{rep}) < \bar{I}_{DNA}(zyg; stem_{rep}) < \bar{I}_{DNA}(zyg; germ_{rep}) \quad (18)$$

where $\bar{I}_{DNA}(zyg; som_{rep})$ represents the average mutual information between the non-stem somatic cells of an individual at the time of reproduction and the same individual when it was a zygote, $\bar{I}_{DNA}(zyg; stem_{rep})$ is the average mutual information between adult stem cells and the zygote, and $\bar{I}_{DNA}(zyg; germ_{rep})$ is the average mutual information between germ cells and the zygote.

In addition to the redundancy within DNA base-sequences, which provides some level of tolerance for loss of mutual DNA information, alternative redundancy strategies could help to preserve the mutual DNA information in somatic cells. One such approach is to utilize multiple copies of DNA, as could be provided by cellular populations together with strategies that select for cells containing DNA molecules that retain the most mutual DNA information. This could be accomplished by the collective pooling and segregation of population of cells, together with specialized, rigid insult-detection and data preservation strategies.

In agreement with Eq. (18), organisms appear to come closest to preserving mutual DNA information in germ cells. This is the result of evolved strategies that place extraordinary emphasis on the preservation of both nuclear and mitochondrial genetic data in germ cells. The fidelity of mtDNA is effectively reset during oogenesis through a genetic bottlenecking process that selects for the healthiest mtDNA and eliminates less efficient, mutated mtDNA molecules (Lee et al., 2012; Wai et al., 2008); likewise, nuclear DNA is subject to very strict insult detection mechanisms (Bailly and Gartner, 2013; Hochwagen and Amon, 2006; Jaramillo-Lambert et al., 2010). Germ cells are more likely than somatic cells to undergo apoptosis when DNA damage is detected, rather than attempt to repair the damage (which often results in the loss of mutual DNA information). Germ cells are also sequestered in a protected microenvironment with various support cells whose sole function is the support and maintenance of the germ cells (Schulz et al., 2002).

Assessing the situation from a thermodynamic perspective suggests that the rate of mutual DNA information loss can be minimized by keeping the thermodynamic potentials acting on the DNA molecules as low as possible. Primordial germ cells (gametogonia), as well as oocytes and spermatocytes, have relatively low rates of oxygen consumption (Brinster and Troike, 1979). Most adult stem cells are quiescent and frequently prioritize glycolysis over oxidative phosphorylation for meeting ATP requirements, resulting in relatively low levels of free radicals and ROS (Rossi et al., 2008; Shyh-Chang et al., 2013; Suda et al., 2011; Tothova et al., 2007) and lower mtDNA replication rates. This supports the notion that manipulation of thermodynamic potentials acting on DNA molecules through modulation of cellular processes and manipulation of the microenvironment is a

realizable and effective means of reducing the rate of mutual DNA information loss in cells.

The genetic information in the gametes derived from an individual that is common to the same individual when it was a zygote $I_{DNA}(zyg; gametes)$ will depend not only on the inevitable germ cell mutual information losses caused by internal entropy production over the course of its life but also those losses resulting from genetic recombination during meiosis ΔMI_{recom}:

$$I_{DNA}(zyg; gametes) = I_{DNA}(zyg; germ_{rep}) - \Delta MI_{recom} \quad (19)$$

Since advantageous mutations are rare, loss of mutual information between parent and offspring will result in a loss of fitness of the species absent effective evolutionary selection mechanisms. The proportion of progeny with lower fitness must not be so excessive that evolution cannot successfully select for the neutral and higher fitness offspring. Thus, a minimal limit $I_{DNA}(zyg; gametes_{min})$ is effectively placed on the mutual information of the progeny:

$$I_{DNA}(zyg; gametes) \geq I_{DNA}(zyg; gametes_{min}) \quad (20)$$

Germ cells must be maintained with adequate redundancy levels and a sufficiently stringent support strategy providing fidelity preservation to satisfy Eq. (20). In this way, mutual DNA information is largely preserved generation-to-generation.

There is a direct correlation between the lifetime risk of cancer in a tissue and the number of divisions of the stem cells maintaining that tissue (Tomasetti and Vogelstein, 2015). It is clear that the strategies used to preserve stem cell integrity do not match the fidelity achieved by germ cell preservation strategies. Since the preservation of stem cell mutual DNA information requires dedicated niches with specialized microenvironments,

there must be associated negative fitness costs to scaling these niches excessively—even though doing so may result in further reductions in the rate of mutual DNA information loss in the cell type in question. For this reason, an organism's stem cell niches must be configured to adequately support the respective target tissue over the lifespan of the individual, but not be so unnecessarily burdensome that they lower species fitness.

Chapter 5 - Establishing a Connection between Thermodynamic, Information, and Evolutionary Theory in Biological Aging

Modern nonequilibrium thermodynamic theory stipulates that all biomolecules must suffer degradative insults due to the production of internal entropy. Biological repair and replacement mechanisms cannot guarantee that mutual DNA information is preserved or restored in individual cells. As a result, cellular mutual DNA information must decrease with time. We will next examine what repercussions the irreversible loss of mutual DNA information in discrete cells could have on both the individual and the species as a whole.

Section 1 - In the Individual

Most germline mutations are neutral or detrimental to fitness, with only the rare mutation being beneficial. It follows that mutations occurring in the somatic cells of an individual organism would exhibit this same pattern with regards to their contribution towards the performance of the individual. Therefore, without selection for only those changes that are neutral or beneficial to the individual, mutual DNA information loss in somatic cells would reduce individual performance with time, i.e. individual organisms will age.

Although evolution and selection are traditionally thought of as occurring between generations of a species, similar concepts are in play in the life and death cycles of the cells of a multicellular organism during an individual's life. Single cells are the replicating unit in this scenario. For an individual multicellular organism containing cells undergoing mitosis, natural selection will occur on the cellular level and favor those cells that display

the highest fitness. These configurations may not necessarily be the most beneficial to the individual multicellular organism as a whole. As natural selection will always be present at the level of the replicating unit (Baum et al., 2013; Szathmáry and Smith, 1995)—cells in these cases—the individual must rely on imperfect innate biological mechanisms that attempt to select for only those configurations that do not reduce the viability of the individual.

The only way to guarantee that the mutual DNA information in a cell is perfectly preserved is by comparing the DNA base sequence to a known-good reference sequence base-by-base. This master template does not exist in any organism and there is no means for an organism to perform a comparative DNA sequence analysis. Cells with undesirable base-sequence modifications must be detected by phenotype. In the case of more severe damage, the cell is often able to detect the damage and initiate apoptosis (Zhou and Elledge, 2000). At the other end of the scale, singular mutation events may exhibit very mild or no detectable undesirable phenotype; these cells are likely to avoid detection completely. For example, mutations whose effect is masked by redundancy are likely to have no detectable phenotype. A mutation may also occur in a region of the genome that is not currently active or relevant to the particular cell; as a result there may be no immediate negative phenotype. This genomic region could become active at some later time, at which point the mutation may have already spread to the cell's progeny.

Even in the most ideal embodiment, the effects of multiple mutation events must eventually decrease individual viability; at some point, removing cells determined by biological mechanisms to be undesirable will no longer provide reprieve from losses in viability since cellular mutual DNA information will continue to decrease until all cells

approach the detectable threshold of dysfunction. At this point, there would be no "good" configurations to select for to replace those cells determined to be undesirable, even if such cells could be detected with complete accuracy.

For a period of time, genetic redundancies would likely be able to mostly compensate for the loss of mutual DNA information in an individual—essentially delaying a detectable aging phenotype to at least the age of reproductive maturity (Fig. 3a). A second line of defense is provided by innate mechanisms that identify specific types of cellular dysfunction and eliminate cells displaying those phenotypes (Zhou and Elledge, 2000). Once the utility of these redundancies is expended and ever-increasing numbers of compromised cells circumvent innate detection mechanisms, the individual will no longer be able to avoid a loss of viability. This resulting dysfunction becomes progressively worse with time. As no existing, or theoretical, biological means has been demonstrated or postulated to be capable of selecting only for those changes in cellular DNA information that are neutral or beneficial to the individual, it is inevitable that all individual organisms must eventually age if they live long enough. Due to the impossibility of an organism achieving an indefinitely sustenant phenotype, the claim by Hamilton (1966) that senescence arises inevitably due to declining selection pressure with age at the level of the species, while not challenged here, is redundant.

Additionally, no mechanism selecting for changes benefiting an individual multicellular organism could prevent natural selection from also occurring at the level of the individual cell[4]. Therefore, cancer is also inevitable in any individual organism given

---

[4] Or from selection occurring on a subcellular level amongst DNA-containing organelles (mitochondria and chloroplasts)

sufficient time—despite the fact that cancer has yet to be detected in a small number of studied species. (The naked mole-rat has long been considered one such species. This was challenged in a recent article where cancer was reported in the naked mole-rat for the first time (Delaney et al., 2016)).

Section 2 - In the Species

As previously discussed, gametes must suffer losses in mutual DNA information with time. The total loss suffered between a gamete and the zygote that gave rise to the individual that produced the gamete will generally be less than that which occurs in somatic cells of an individual due to mechanisms that enhance gamete quality (Bailly and Gartner, 2013; Jaramillo-Lambert et al., 2010). By limiting the amount of loss present in the gamete to a level low enough that selection for neutral and higher fitness offspring is possible, the fitness of the species can be preserved and even increase. Natural selection is the only means by which inevitable mutual DNA information losses can be prevented from generating mandatory fitness losses in the species.

Since evolving to maximize species fitness involves genomic changes, configurations that maximize fitness under new selective pressures may generate mutual DNA information losses in the species that are greater than conditions where selection is nearly absent (as calculated by the average mutual DNA information loss between parent and offspring, $\overline{I}_{DNA}(zyg; gametes)$). Fluctuating selective pressures prevent mutual DNA information loss from being minimized in the species.

Consider, however, what would happen if selective pressures were held constant. The rate of mutual DNA information loss will begin at some initial value as fitness of the species increases at some positive rate (Fig. 3b). Through the course of many generations,

fewer configurations will be available that are capable of producing higher fitness than the current configuration. As a result, the rate of mutual DNA information loss must decrease and the rate of fitness increase becomes less rapid across generations. With fewer "positive" mutations available and selection tending to eliminate "negative" mutations, the rate of mutual DNA information loss in a species under static selective pressure could be much lower than $\overline{I}_{DNA}(zyg; gametes)$. In conditions where selective pressure were static, fitness would eventually approach a theoretical limit as the rate of mutual DNA information loss approaches zero.

Since conditions of perfectly static selective pressure are not realizable and variations in selective pressures result in adaptive genetic changes, species mutual DNA information must decrease with time. This logic establishes a correspondence between the directionality of the second law and mutual DNA information loss in both individuals of a species and species themselves.

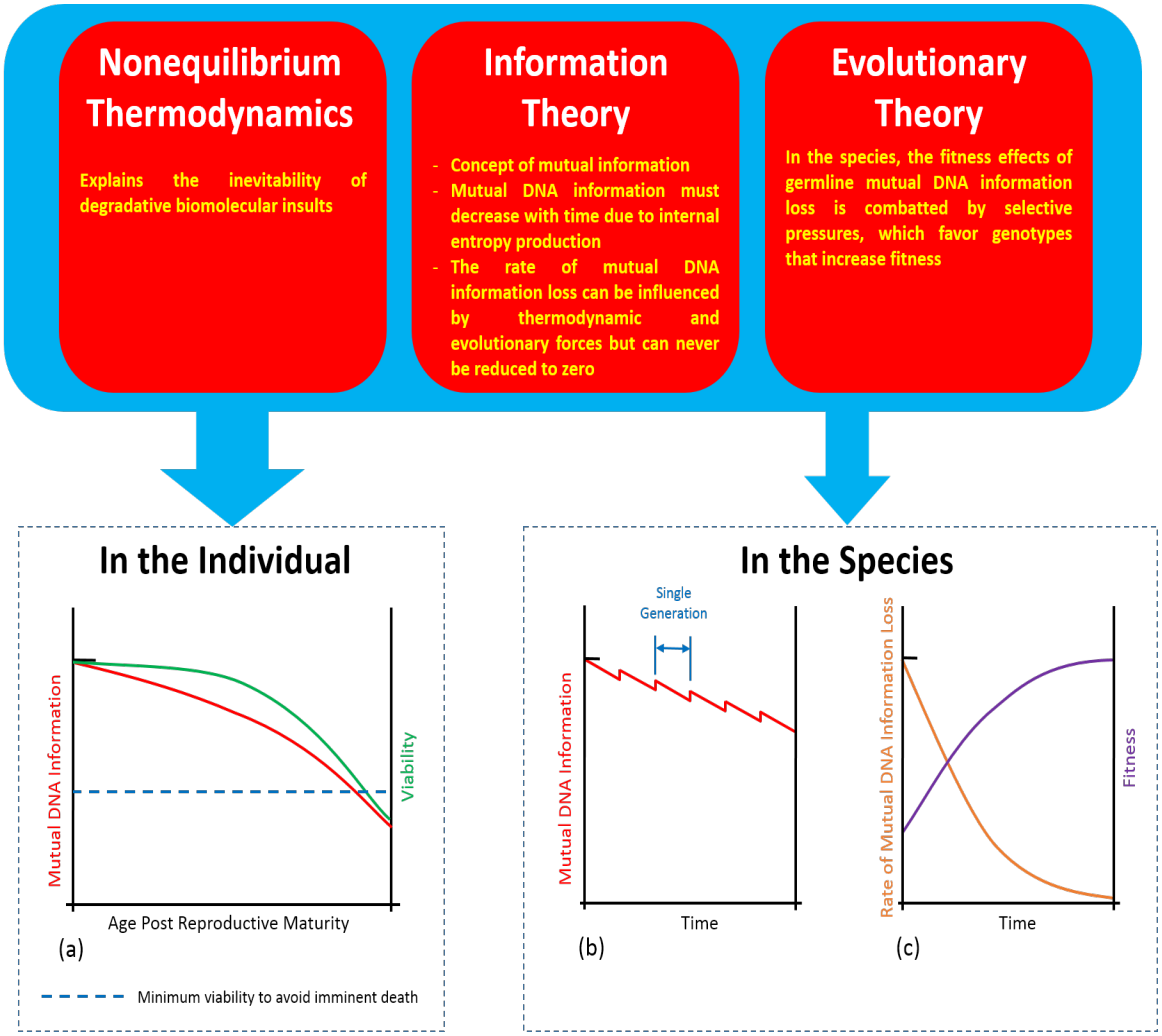

Fig. 3. The proposed connection between thermodynamics, information, and evolutionary theory in generating mandatory mutual DNA information losses in both the individual and the species.

(a) Although a correlation between individual viability and somatic cell mutual DNA information loss is predicted, genetic redundancies and other compensating mechanisms may attenuate reductions in individual viability due to mutual DNA information losses. (b) The average mutual DNA information in cells of all individuals of a species will decline as a generation ages. This loss can be largely reverted in subsequent generations by portioning germ cells in conditions optimized for preservation of genetic data. (Generations have been aligned for illustration purposes.) (c) In conditions of static selective pressures, the rate of mutual DNA information loss is predicted to decrease as fitness approaches a maximum value.

Chapter 6 - Examining Degradation Increases in Aging Organisms

Living organisms are highly ordered entities that exist in a state far from thermodynamic equilibrium. As a result, degradation will occur within organisms as internal entropy is produced. Cellular mechanisms work towards counteracting these damaging effects, establishing what is very close to being a steady state (over a limited time-window) in terms of preservation of biomolecular integrity. Despite these efforts, the overall degradation state (entropy) of an organism increases with age.

Section 1 - Energetic Expenditures towards Biomolecular Repair and Replacement – a Paradox?

Proteins account for the majority of biomolecules within a cell. The rate of total protein synthesis has been empirically determined for a number of species. Smaller organisms synthesize proteins at higher rates than larger species (Fig. 4a). Protein synthesis in mice is estimated to occur at a rate sufficient to replace total body protein mass every 5.27 days, while the same occurs in man approximately every 31.07 days (Table 1). Of course, individual protein turnover rates can vary widely protein-to-protein, from minutes to years (Hetzer, 2013).

Over the course of a lifetime, a long-living human will synthesize enough protein to replace total body protein mass 1439 times over (Table 1). Let us assume for the moment that degraded/dysfunctional proteins are "accumulating" as an organism grows older due to an insufficient amount of energy being spent on repair and replacement, as suggested by the disposable soma theory of aging (Kirkwood, 1977; Kirkwood and Holliday, 1979; Kirkwood and Rose, 1991). Considering a worst-case scenario where all of the protein in

an aged human is in need of replacement, it would only require an estimated 0.07% increase in daily resource investment in protein synthesis to offset the average daily increase in protein degradation state. This translates to 0.23 calories per day[5]. With a daily dietary intake of 2500 calories, this is only 0.0092% of daily energy intake. Although this figure does not include the energetic repair and replacement costs of all classes of biomolecules, the total amount of protein dedicated to translation is 2-15 times greater than that dedicated to transcription and DNA maintenance (Liebermeister et al., 2014); protein synthesis represents a significant fraction of the total energy spent by an organism on biomolecular repair and replacement. In light of the very small additional investment predicted to be needed to offset the increase in protein degradation state in the described scenario, the disposable soma theory's claim that aging is caused by an energetic underinvestment in repair and maintenance resulting in an accumulation of damage (Kirkwood, 1977; Kirkwood and Holliday, 1979; Kirkwood and Rose, 1991) is difficult to accept. Although the numbers above are just estimates, even if they were off by two orders of magnitude this argument would still hold merit. In addition, organisms that turnover their proteins more frequently exhibit decreased longevity—not increased (Fig. 4b). Smaller organisms turnover protein at a higher rate than larger organisms (Fig. 4a) and have reduced longevity (Austad, 2005; Calder, 1984; de Magalhães et al., 2007).

[5] Protein synthesis requires approximately 4.5 kJ of energy per gram of protein (Waterlow, 2006, p.170). Producing 310 g/day of protein (human rate) equates to roughly 1395 kJ or 333 Cal per day; 0.07% of this value is 0.23 Cals per day.

Table 1. Protein synthesis rates, number of days to turnover total body protein mass, and number of turnovers per lifespan for different metazoan species

Species	BW (kg)	Protein synthesis g/day	Protein synthesis g/kg BW per day	Protein synthesis g/kg$^{0.75}$ BW per day	Body Protein Composition (%)	Days to Replace Total Body Protein Mass	Maximum Lifespan (years)[4]	Turnovers Per Life	Synthesis Rate Reference
Honey possum	0.01	0.2798	29.15	9.12	-	6.86	2.00	106.4	Bradshaw and Bradshaw, 2009
Mouse, small	0.02	0.768	38.40	14.44	20.25[1]	5.27	4	276.9	Garlick and Marshall, 1972
Rat	0.35	7.7	22.00	16.92	20.81[1]	9.46	3.80	146.6	Reeds and Harris, 1981
Rabbit	3.6	33	9.17	12.63	19.44[1]	21.20	9.00	154.9	Reeds and Harris, 1981
Cat (HP)	4.8	31.4	6.54	9.68	21.81[1]	33.34	30.00	328.4	Russell et al., 2003
Dog	10.2	123.37	12.10	21.62	22.06[1]	18.24	24	480.2	Everett et al., 1977
Sheep	63	351	5.57	15.70	16.00[2]	28.72	22.80	289.8	Reeds and Harris, 1981
Man	67	310	4.63	13.24	14.38[3]	31.07	122.50	1439.2	Pacy et al., 1994
Cow	575	1740	3.03	14.82	22.50[1]	74.35	20.00	98.2	Reeds and Harris, 1981

Note: Body protein concentration for honey possum not available, used 17% for "days to turnover" calculation. [1]Moulton, 1923. [2]Reid et al., 1968. [3]Mitchell et al., 1945. [4]Tacuta et al., 2012.

Caloric restriction has been demonstrated to extend longevity in some organisms. This also appears to contradict the disposable soma theory. Proponents of the disposable soma theory have attempted to explain this "paradox" by suggesting that caloric restriction generates a shift in resources away from reproduction and towards somatic maintenance (Shanley and Kirkwood, 2000). While extended caloric restriction has been found to attenuate the reduction in protein synthesis in muscle tissue that occurs with advanced age in mice (Zangarelli et al., 2006), recent studies have demonstrated that caloric restriction does not produce a direct increase in the rate of mixed protein synthesis in mice (Miller et al., 2013), nor is mitochondrial protein synthesis significantly affected by caloric restriction in liver, heart, or skeletal muscle (Miller et al., 2011). Although it has been proposed that caloric restriction does indeed increase protein turnover (Tavernarakis and Driscoll, 2002), an examination of supporting data suggests that the decreased attenuation in protein synthesis with age resulting from extended caloric restriction was interpreted as an increase in protein turnover in direct response to caloric restriction—yet these are two distinct phenomena with very different implications.

A corollary of the disposable soma theory suggests that an increase in the amount of energy available to an organism would allow it to devote more resources towards somatic maintenance and thus delay aging; however, studies demonstrating that increased caloric intake increases longevity do not exist—yet it is well-known that obesity leads to increased rates of aging and diabetes (Ahima, 2009). It is clear that energetic expenditures towards repair and replacement alone cannot explain the differences in longevity between species nor does it provide a solid rationale for why aging must occur in the first place.

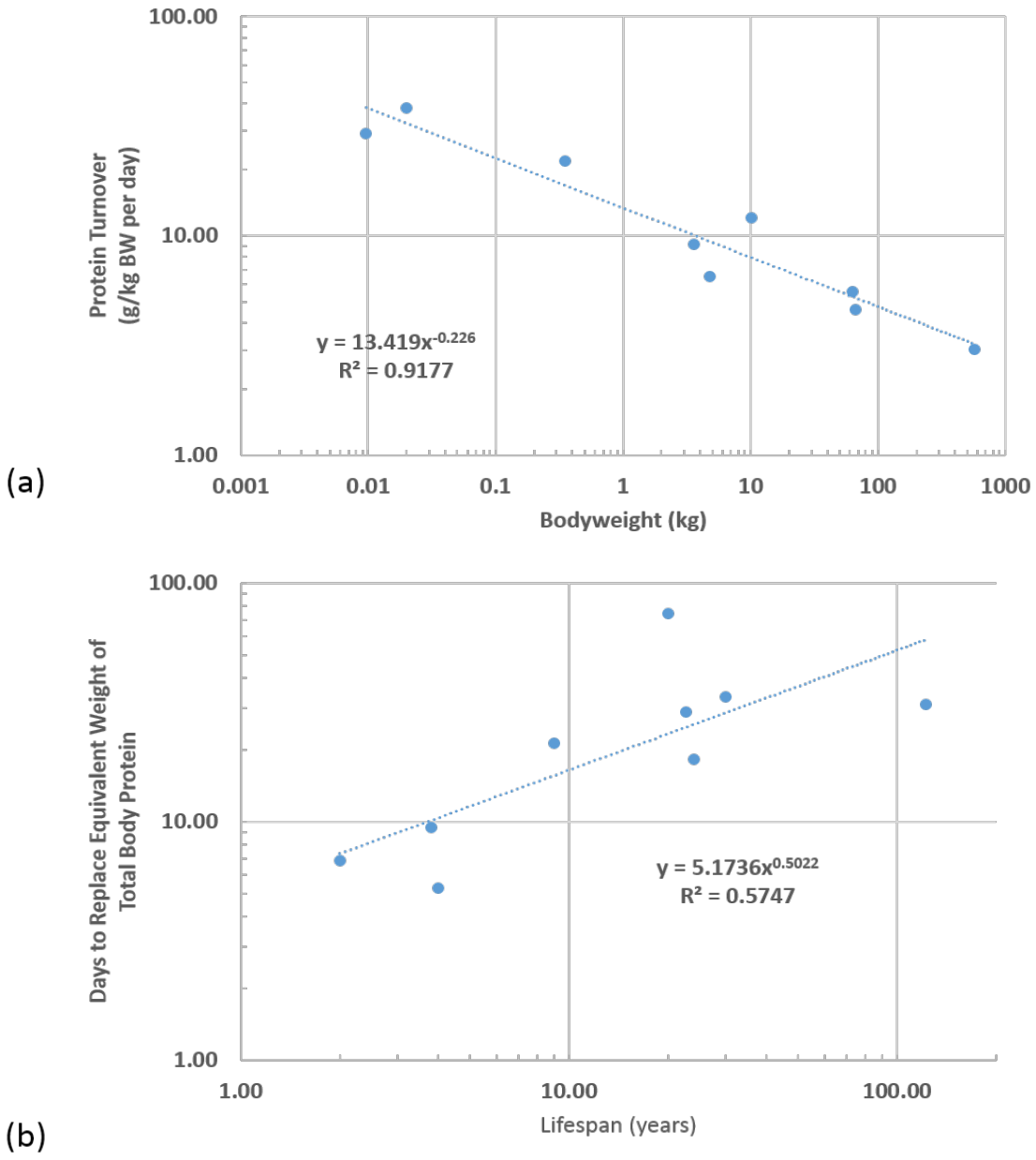

Fig. 4. Protein turnover and replacement across species

(a) Protein turnover as a function of bodyweight for the species listed in Table 1 and (b) frequency at which the equivalent weight of total body protein is synthesized as a function of MLSP. Data from Table 1.

Section 2 – Total Entropy Increases Slowly with Age in Comparison to Internal Entropy Production Rate

The high frequency at which the animals depicted in Table 1 replace their total body protein mass demonstrates that the rate of degradative internal entropy production $d_i S/dt$ within an individual is much greater than the rate at which the total entropy of an individual organism increases with age dS_{age}/dt.

$$\frac{dS_{age}}{dt} \ll \frac{d_i S}{dt} \qquad (21)$$

Eq. (21) is also intuitively evident when the speed at which biological material degrades at biologically relevant temperatures, even when conditions are sterile and optimized, is contrasted against the lifespan of an organism with even moderate longevity. Nevertheless, the overall degradation state of an individual organism eventually worsens with time. The degradation of an aging organism could be viewed as a progression through many discrete steady-state nonequilibrium conditions which ultimately results in an overall degradation state that renders the individual nonviable. But why do organisms transition between these states and why is youthful homeostasis always lost? It was argued earlier that DNA molecules face inevitable losses in mutual DNA information as individual organisms age. This offers an explanation for why this transition occurs in DNA molecules—yet if they are the *only* class of biomolecule in an organism directly subject to inevitable, irreversible loss then the reasons why other classes of biomolecules reach elevated degradation states with age must be more complex.

Section 3 - Biomolecular Degradation - Accumulation versus Homeostatic Shifts

A closer look at the increased degradation exhibited in other classes of biomolecules could help to elucidate what may be occurring. Aging has been described as the

accumulation of unrepaired damage. This implies that all of the biomolecular degradation in an aged individual is the result of lifelong accumulation. Perhaps this assessment is not entirely accurate.

As demonstrated earlier, an organism is unable to sustain a steady-state condition of perfect biomolecular fidelity (a degradations state D of zero) as this would require infinite resources—thus even in a youthful state of "homeostasis" organisms will have some level of biomolecular degradation (a non-zero degradation state). "Misrepair" is not required in order to have degraded biomolecules as degradative internal entropy production is present in all living organisms.

A reduction in biomolecular replacement or repair rates is predicted to increase degradation state (i.e. decrease average biomolecular performance). Should such a transition occur in an organism for a particular biomolecule, it is expected that a new degradation state would eventually be established, at which time no further reductions in biomolecular performance should occur unless outside factors are at play.

This logic suggests that biomolecular replacement and repair rates alone do not explain how an accumulation of damaged biomolecules could occur. Restoration of proteasome function in aged human dermal primary fibroblasts largely restores markers of protein aging to youthful levels (Hwang et al., 2007). This is analogous to a shift in the protein pool from a higher to a lower degradation state, and this demonstrates that the increase in degradation state occurring with age is at least partially reversible. If the degraded protein was truly representative of accumulated, irreparable damage then upregulation of proteasomal function should not eliminate any damage. The fact that the condition is essentially reversible suggests that the increased biomolecular degradation found in aged

individuals is more likely attributable to reduced biomolecular turnover which leads to a corresponding shift in biomolecular degradation state and is not due to damage "accumulation".[6] Consistent with this notion, protein turnover does indeed significantly decline during aging (Rattan, 1996; Richardson and Cheung, 1982; Ryazanov and Nefsky, 2001).

A distinction between "accumulated" dysfunctional biomolecules and a shift in biomolecular degradation state caused by reduced turnover can be made by simply examining whether turnover is occurring. "Damage" that is actively and continuously turned over should not be referred to as accumulated damage, even if the rate of turnover has decreased and the degradation state of the biomolecular pool is high.

This raises further doubt over the disposable soma theory's assertion that aging is caused by an energetic underinvestment in repair and maintenance resulting in an accumulation of damage (Kirkwood, 1977; Kirkwood and Holliday, 1979; Kirkwood and Rose, 1991). The idea of an "energetic underinvestment" is a misnomer as there is no amount of energetic investment that will produce a perfect population of biomolecules (a degradation state of zero). Increasing biomolecular turnover rates will reduce biomolecular

---

[6] A small number of biomolecules evidently *can* accumulate into dysfunctional products when an organism has declined (aged) to a certain degree; for example, advanced glycation end products (AGEs) and certain other aggregates (Verzijl et al., 2000). A decline in global biomolecular repair and replacement processes can lead to biases generating significant differences in repair and replacement rates between biomolecules. With infrequent turnover, the proportion of certain types of damaged product can expand, even when youthful turnover levels prevent accumulation. Superficially, this type of damage could be thought of as "accumulated". An example of this phenomenon was demonstrated by De Baets et al. (2011). I am not aware of any published data suggesting that this accumulation occurs under normal circumstances absent significantly decreased turnover (such as that which occurs with advanced age). Many of the same protein species found to aggregate with age have been shown to be produced, and are concomitantly cleared, in younger individuals.

degradation state but energetic resource ROI will continually worsen as turnover rate is increased. An energetic underinvestment in repair and replacement cannot explain why youthful homeostasis is lost—there must be a higher-level initiating cause.

The fact that biomolecular degradation state is partly determined by resource allocation towards repair and replacement, and therefore must involve factors that affect fitness, suggests that species have evolved to operate at biomolecular degradation states, and with internal entropy production rates, that balance many factors including athletic performance, metabolic rate, physical size, etc. This alone does not provide direct insight into why organisms age. However, the concept of biomolecular degradation states is useful when considered together with the inevitability of mutual DNA information loss in helping to explain why youthful homeostasis cannot be indefinitely preserved.

Section 4 - Entropy-Driven Managed Deterioration – Basic Concepts

The energetic cost of repairing the degraded biomolecules in an aged individual once is small relative to the continuous investment made to sustain viable biomolecular degradation states. So why does biomolecular degradation state increase in an aging individual?

Fig. 5 depicts the basic interrelationships that may explain the progression of the aging phenotype in many metazoans. In this model, the key top-level factor initiating the transition from youthful homeostasis is internal entropy production, which inevitably generates losses in mutual DNA information for both mitochondrial and nuclear DNA. Mutual DNA information losses in mitochondrial DNA (mtDNA) will cause mitochondria from aged individuals to exhibit lower peak energy output (Yaniv et al., 2013). This decline in mutual mtDNA information may be partially modulated by a controlled deceleration in

mitochondrial biogenesis (Figge et al., 2012), which reduces the rate of clonal expansion of degraded mtDNA and limits the exposure of mtDNA to the high thermodynamic stress conditions of replication events. The escalating deficit in cellular energy currency production in the aging individual results in a progressively worsening inability to fund all cellular processes at youthful levels. This generates forced reductions in biomolecular turnover that lead to increased biomolecular degradation states and lower biomolecular performance, representative of a transition away from youthful homeostasis.

Losses in nuclear DNA fidelity will result in a mosaic of stochastic cellular dysfunction that worsens with age (Bahar et al., 2006; Lodato et al., 2015). Together with the described mitochondrial dysfunction, this could be largely responsible for age-linked cellular dysfunction and the overall aging phenotype of the individual. “Longevity optimization” genes may have evolved to attenuate the negative effects of mutual information losses in nuclear and mitochondrial DNA through reallocation of resources and physiological alterations. This model is discussed in more detail in Chapter 8.

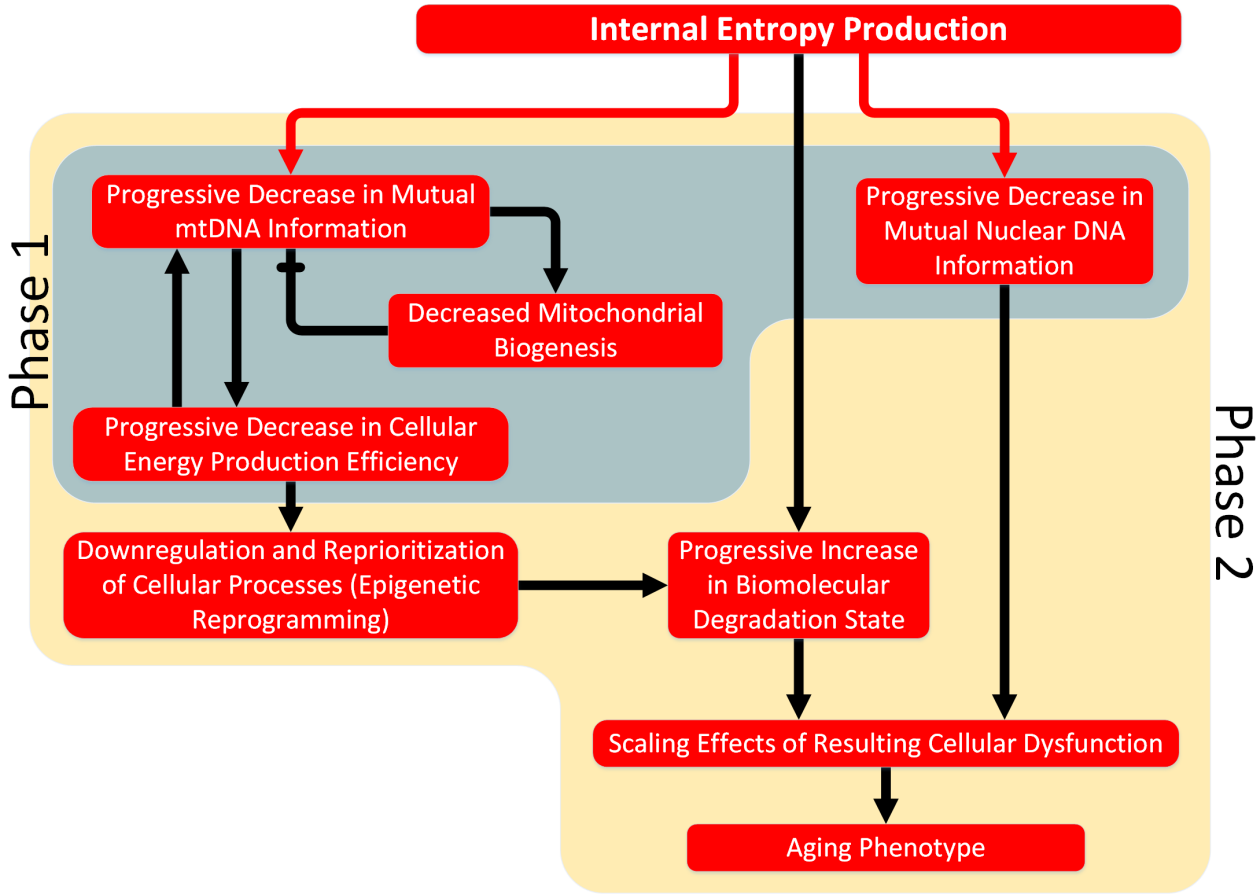

Fig. 5. The basic interrelationships between primary factors that may largely describe the progression of the aging phenotype in many metazoa.

During 'Phase 1' of an individual's life, mutual DNA information loss has not reached levels sufficient to generate an aging phenotype. 'Phase 2' begins when dysfunction has progressed to the point that aspects of the aging phenotype begin to take hold.

Chapter 7 - Longevity Determination

Leonard Hayflick has stated that aging is not driven by genes but by thermodynamics (Hayflick, 2004), while he has argued that the genome does, on the other hand, govern longevity. Additionally, Hayflick maintains that natural selection has led towards biomolecular arrangements that are capable of preserving fidelity until reproductive maturity, but that the survival value for arrangements that exceed this longevity is considerably diminished (Hayflick, 2007b).

If aging is driven by thermodynamics, as suggested by Hayflick and further supported here, then any and all factors that contribute towards resisting (or promoting) permanent thermodynamically-induced changes in any biocomponent subject to irreversible loss are implicated in longevity determination. This includes factors that directly or indirectly affect the magnitude of the thermodynamic stresses on these biostructures as well as factors that specify redundancy levels, which can offer varying degrees of protection from permanent information loss.

The loss of mutual DNA information is inevitable in an individual given sufficient time. If such loss is paramount to aging, then a closer examination of the thermodynamics affecting DNA molecules is warranted and may assist in identifying primary longevity determinants.

Section 1 - Investigating the Rate of Mutual DNA Information Loss in Individuals

To further examine the rate of mutual DNA information loss, it is useful to separate the various contributing conditions and factors. DNA undergoing replication is significantly more likely to undergo mutation due to the impaired stability of single-stranded DNA (Frederico et al., 1990) and the imperfect nature of DNA polymerases (Arias-Gonzalez, 2012). Therefore, replicating and non-replicating conditions should be considered independently. In a living cell, many DNA insults are eliminated by damage-detection and

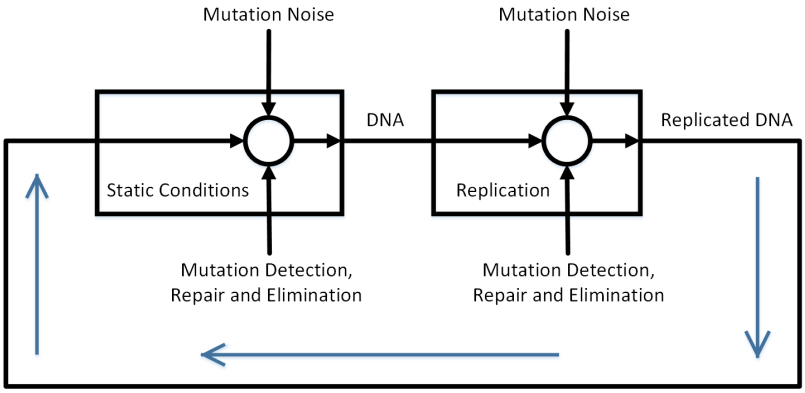

Fig. 6. A systems flow diagram of mutual information loss in a DNA ensemble within a living organism.

repair systems, but a certain percentage will not be eliminated. A systems flow diagram of this scenario is depicted in Fig. 6. DNA actively being transcribed is also more susceptible to mutation (Kim and Jinks-Robertson, 2012), but it is generally believed that the vast majority of mutations arise from replication events or random DNA damage. For this reason, transcription will not be considered as a separate state condition in this analysis.

Assuming that the time spent in the replicative state is comparatively much less than the time in the static state, a general representation of the average rate of mutual DNA information loss takes the form

$$\overline{MIR}_{DNA} = -(k_{rep} r_{rep} p_{noise} + k_{static} r_{mut})(1 - p_{det}) \quad (22)$$

where k_{rep} is the amount of mutual information lost in the average mutation event during replication and k_{static} is the same for static (non-replicating) conditions, r_{rep} is the DNA replication rate, p_{noise} is the probability that a replication event will result in mutation, p_{det} is the probability that a mutation will be detected and eliminated by the cell (assumes similar probability for replicating and non-replicating conditions), and r_{mut} is the rate at which mutations are occurring in non-replicating conditions.

Section 2 - Preserving mtDNA Integrity

The cells of most eukaryotes contain mitochondria, which range in number from several hundred to thousands per cell. Each mitochondrion contains at least one copy of mtDNA. As the primary function of mitochondria is to generate ATP, mitochondrial dysfunction has the potential to produce deleterious downstream effects on every cellular biochemical reaction that requires ATP. Compared to the nuclear genome, the mitochondrial genome is more susceptible to mutation (Larsson, 2010) and these mutations are more likely to cause dysfunction. There are several reasons for this. For one, the mitochondrial genome is replicated during mitobiogenesis, which is required for preservation of a healthy pool of mitochondria (i.e. a low degradation state). Generally speaking, in any given cell a pool of mitochondria will be maintained at relatively steady quantities by a combination of mitochondrial fusion, fission, mitophagy, and mitobiogenesis processes; this results in mtDNA replication rates that are very high

compared to the rate at which nuclear DNA replicates (which, of course, only occurs when cells divide). Due to the imperfect fidelity of replication with DNA polymerase (Zheng et al., 2006) and the vulnerability of the single-stranded mtDNA replicon (Frederico et al., 1990), each replication event involves a period of time where the possibility for a mutation is considerably higher than non-replicating conditions (Kennedy et al., 2013). The microenvironment within a mitochondrion is also particularly harsh compared to other cellular compartments due to the relatively high concentrations of ROS (Wallace, 1999), resulting in larger internal entropy-producing thermodynamic potentials and higher molecular insult rates. Furthermore, as the mitochondrial genome has evolved to be extremely compact, mitochondria are very susceptible to dysfunction resulting from single-base alterations.

Eq. (22) can be applied to mtDNA to help identify factors that could influence the rate at which mutual mtDNA information is lost. Each mtDNA replication event carries an associated probability of resulting in mtDNA mutation ($p_{noise,mtDNA}$). Mutations can also occur when mtDNA are not replicating. Many of these mutated mtDNA molecules will be eliminated or repaired by the cell's mitochondrial quality-control mechanisms, but a certain percentage of these mutations will escape detection (represented by $1 - p_{det,mtDNA}$).

The only known human mtDNA polymerase, DNA polymerase γ, is highly conserved across species as diverse as *Drosophila melanogaster* and *Saccharomyces cerevisiae* (Chan and Copeland, 2009). Nuclear DNA repair pathways are also highly conserved (Gredilla et al., 2010); although mtDNA repair pathways have not been investigated as thoroughly, mitochondria have been found to possess many of the same repair mechanisms and even share some of the nuclear DNA repair enzymes. The GTPases implicated in mitochondrial

fission and fusion are also highly conserved (Ashrafi and Schwarz, 2012). PTEN-induced putative kinase protein 1 (PINK1) and the E3 ubiquitin ligase parkin regulate mitophagy in many metazoans and have homologs across species as diverse as humans and *Drosophila melanogaster* (Cookson, 2012). These similarities suggest that the probability of a mtDNA replication event resulting in a mutation $p_{noise,mtDNA}$ and the probability that a mutated mtDNA molecule will be detected and eliminated or repaired $p_{det,mtDNA}$ are comparable across a wide range of species.

In addition, since the molecular configuration of DNA is conserved, as are the potential reactions that can result in molecular modifications, it follows that the mutual information lost in the average mutation-causing event is relatively constant; i.e. k_{rep} and k_{static} should be similar across species. This leaves the mtDNA replication rate $r_{rep,mtDNA}$ and the static-condition mutation rate $r_{mut,mtDNA}$ as the likely primary factors from Eq. (22) responsible for any variation in the rate of mutual mtDNA information loss between species.

Section 3 - MtDNA Information Loss in Aged Organisms is Primarily the Result of Mutations During Replication

MtDNA mutations increase in an age-dependent manner. High-sensitivity sequencing of human brain tissue from young and old individuals found that most mtDNA point mutations are transition mutations (Kennedy et al., 2011), consistent with replication errors. In addition, 90% of all age-related mutations in mtDNA from human colon are transitions (Greaves et al., 2012). The mtDNA mutation burden in aged *Drosophila melanogaster* is similar to vertebrate levels and also demonstrates a prevalence of transition mutations (Itsara et al., 2014). G:C to T:A transversions, which are typical of oxidative damage, only represented a small percentage of the mutations in these studies.

MtDNA mutation patterns display strand asymmetry consistent with spontaneous cytosine deamination on the lagging strand template during replication (Frederico et al., 1990) in both aged human brain (Kennedy et al., 2011) and aged somatic and germline cells of *Drosophila melanogaster* (Haag-Liautard et al., 2008; Itsara et al., 2014). Mitochondrial mutational spectra produced with purified human DNA polymerase γ accounted for 83% of the mutations found *in vivo* (Zheng et al., 2006). These data strongly suggest that: 1) the majority of mutations in mtDNA result from errors during replication, 2) the rate of mutual mtDNA information loss varies across species but reaches similar levels in aged organisms despite longevity differences, 3) oxidatively-damaged mtDNA is repaired or eliminated with very high efficiency, and 4) oxidatively-damaged mtDNA accounts for only a small percentage of mtDNA mutations occurring with age. Furthermore, these results are inconsistent with theories that implicate ROS levels and the resulting direct oxidative damage to DNA as a primary causative factor in aging.

A logical deduction from this is that mtDNA replication rate is higher in shorter-living animals. Unfortunately, the availability of data to support or refute this assertion is limited. Measuring the mtDNA turnover rate *in vivo* has historically proven difficult, although more recent techniques have overcome some of the issues (Collins et al., 2003). Primary cell cultures are required for deriving accurate mtDNA replication rates *in vitro*. Surprisingly, no studies that quantitate mtDNA replication rates across a range of species have been published.

Mitobiogenesis is required to maintain mitochondrial component quality. Reducing the rate of mitobiogenesis excessively will compromise mitochondrial performance since less negative entropy will be produced to counteract degradative internal entropy production

and, as a result, a shift to a higher degradation state will occur. Yet mitobiogenesis incorporates mtDNA replication, so a reduction in mitobiogenesis will also generate reductions in the replication rate of mtDNA $r_{rep,mtDNA}$. Thus, although reduced mitobiogenesis could negatively impact mitochondrial performance, provided that the rate of mutation during non-replicating conditions $r_{mut,mtDNA}$ does not drastically increase, reduced mitobiogenesis will lead to a lower rate of mutual mtDNA information loss per Eq. (22).

On the other hand, a higher mitobiogenesis rate will increase the amount of negative entropy available to offset degradative internal entropy production affecting mitochondrial components (other than mtDNA), effectively lowering the degradation state in those components. However, this will also raise the mtDNA replication rate $k_{rep,mtDNA}$ and generate increased exposure of mtDNA to the high thermodynamic-stress conditions experienced during replication—resulting in an increase in the rate of mutual mtDNA information loss.

Preservation of youthful mitochondrial homeostasis requires that the rate of negative entropy production from mitobiogenesis equals or exceeds the rate of degradative internal entropy produced within the mitochondrial network when in a youthful degradation state. If the rate of degradative internal entropy production within mitochondria varies between species, then the rate of mitobiogenesis required to preserve youthful homeostasis in mitochondrial components is likely to also vary. In addition, differences in the intrinsic mitochondrial degradation state between species could affect the rate of mitobiogenesis. This suggests that variations in the rate of mutual mtDNA information loss between species

are likely due to either differences in the rate of degradative internal entropy production within mitochondria or different mitochondrial degradation states.

Section 4 - A Closer Look at Mitochondrial Configurations and Membrane Composition

In order to preserve youthful cellular homeostasis, mitobiogenesis must occur at a rate sufficient to sustain mitochondrial component quality at youthful levels by producing negative entropy to offset degradative internal entropy production. Yet since mitobiogenesis encompasses mtDNA replication, which accelerates losses in mutual mtDNA information, forfeiture of youthful mitochondrial homeostasis is not only inevitable but must occur after a period of time dictated, at least in part, by the rate of mitobiogenesis. How then might this rate differ by species, and why?

An examination of cellular metabolic demands provides some clues. Across species, whole-organism basal metabolic rate scales allometrically with body mass: $BMR \propto M_b^f$. Kleiber (1932) estimated f to be 3/4 for the basal metabolisms of mammals and birds. This same value was found to hold for most multicellular organisms, including many other animals (Peters, 1986) and plants (Niklas, 1994).[7] When expressed per unit body mass, resting oxygen consumption scales proportionally with $M_b^{-1/4}$. In other words, mass-specific BMR decreases by approximately 16% across species for every doubling of body mass. The inverse correlation between relative oxygen consumption and body mass has been verified in isolated hepatocytes from mammals (Porter and Brand, 1995) and birds (Else, 2004) as well as in mammalian liver slices (Couture and Hulbert, 1995). Porter and

[7] The universal value of f is contentious. Scientists are largely divided into two camps: one arguing for 2/3 and the other for 3/4 (White and Seymour, 2005).

Brand (1995) found a 5.5-fold decrease in hepatocyte oxygen consumption for every 12,500-fold increase in body mass and concluded that this was due to a decrease in the intrinsic metabolic activity of the cell, not increased cell volume.

Therefore, on average, cells from smaller species have increased oxygen consumption and ATP turnover rates compared to cells from larger organisms. As a result, cells from smaller species place greater energetic demands on their mitochondrial networks. It has been known for some time that mitochondrial count correlates with mass-specific changes in tissue metabolic rate (Smith, 1956). However, the differences in mitochondrial number per cell cannot fully explain the variation in respiration rate with body mass (Porter and Brand, 1995).

Increasing the mitochondrial inner membrane surface area per unit volume of mitochondrial matrix allows for additional transmembrane-localized oxidative phosphorylation enzymatic machinery in the same volume of space. Organisms with higher ATP demands may benefit from increased membrane density. Indeed, a significant negative correlation has been found between mitochondrial inner membrane surface area per unit volume of matrix and body mass. In a study involving mammalian hepatocytes, membranes were as dense as 555 cm^2 per μL of matrix in mice while, on the other end of the spectrum, horse hepatocytes contained only 170 cm^2 membrane surface area per μL of matrix (Porter et al., 1996).

Mitochondrial membrane phospholipid composition also differs widely across species, specifically in fatty acid composition (Daum, 1985). The fatty acid composition of mitochondrial membranes in tissues was found to correlate with body size, with smaller mammals having more polyunsaturated mitochondrial membranes than larger mammals

(Porter et al., 1996). The "membrane pacemaker hypothesis of metabolism" (Hulbert and Else, 1999), and subsequently the "membrane pacemaker theory of aging" (Hulbert, 2003), were developed from these and other observations linking not only mitochondrial but overall tissue membrane composition to metabolic rate, body mass, and longevity. Hulbert (2003) suggested that changes in membrane fatty acid composition can make membranes more prone to oxidation, resulting in an increase in reactive molecules that can damage cellular molecules and impact longevity.

Why does membrane fatty acid composition vary allometrically? Some light was shed on this question when the molecular activity of transmembrane proteins were examined in different membrane compositions. The cytoplasmic membrane-localized sodium pump ($Na^+ \cdot K^+$-ATPase) varies in molecular activity from approximately 8,000 ATP/min in mammals compared to 2,500 ATP/min in ectotherms (all data taken at 37°C) (Else et al., 1996). Cytoplasmic membrane crossover studies demonstrated that the activity of ectothermic sodium pumps increased significantly when transferred to mammalian membranes, while mammalian sodium pump activity was attenuated in ectothermic membranes (Else and Wu, 1999).

It was hypothesized that the higher sodium pump activities seen in endotherms were due to influences from surrounding lipids, with polyunsaturated membranes promoting increased molecular activity compared to membranes with more monounsaturated membranes. Hulbert and Else (1999) proposed a mechanism by which this may occur: The lateral diffusion coefficient of lipids within a membrane bilayer is greater than that of transmembrane proteins by two orders of magnitude (Storch and Kleinfeld, 1985). As such, membrane proteins are continuously colliding with membrane lipids. The kinetic energy

exchanged during these collisions is believed to be critical in facilitating membrane protein function. The acyl chains of saturated and monounsaturated fatty acids are more flexible than polyunsaturated fatty acids. Therefore, a collision involving a lipid containing polyunsaturated fatty acids is expected to transfer more energy to membrane proteins and result in increased molecular activity of the protein than a collision with a lipid containing only highly saturated fats. Of the fatty acids found in membrane lipids, docosahexanoic acid (DHA or 22:6 n-3) contains the largest number of evenly spaced double bonds but is also particularly susceptible to peroxidation. DHA has been referred to as the "acme" of polyunsaturates and may serve as a membrane "energizer" (Hulbert and Else, 1999). Sodium pump molecular activity correlates with membrane DHA concentration in both ectotherms (Turner et al., 2005) and endotherms (Turner et al., 2003).

Peroxidation index is a measure of the susceptibility of membrane lipids to peroxidation and is closely tied to fatty acid unsaturation. The peroxidation index of mitochondrial phospholipids, predominantly driven by DHA content, negatively correlates with MLSP (Pamplona et al., 1998). Importantly, the same trend line holds for both mammals and birds (Hulbert et al., 2007). In addition, mitochondrial membrane remodeling resulting from various levels of caloric restriction in mice produced changes in peroxidation index and MLSP that fit the same trend line (Faulks et al., 2006; Hulbert, 2008).

In addition to the negative allometry of metabolic rate, body mass positively correlates with MLSP (Austad, 2005; Calder, 1984; de Magalhães et al., 2007). The discussed findings suggest that smaller organisms with reduced longevity may utilize membranes with more polyunsaturated membranes—largely dictated by DHA content—in order to

increase the rate of work that can be performed by each transmembrane protein molecule and, as discussed in Section 6, to satisfy functional requirements largely specified by recognized allometric relationships that characterize fitness optimization across species. A downside of polyunsaturated fatty acids is their susceptibility to oxidative damage and contribution towards increased free radical generation. In other words, polyunsaturated fatty acids are less resistant to molecular alterations resulting from the thermodynamic forces of their environment; the presence of higher levels of polyunsaturated fatty acids will lead to increased rates of degradative internal entropy production within mitochondria and will necessitate that mitobiogenesis rates be increased to maintain a given mitochondrial degradation state.

Section 5 - Identifying Longevity Determinants

In his "membrane pacemaker theory of aging", Hulbert (2005) proposed that membrane lipid peroxidation influences the cellular levels of ROS, resulting oxidative stress and consequently longevity. He posited that this feedback effect is variable and determined by the membrane fatty acid composition. Hulbert further suggested that this results in accumulated damage to proteins, genetic material and membrane lipids over an individual's life—finally reaching a tipping point where antioxidant defenses are exceeded and youthful homeostasis can no longer be sustained.

The argument for membrane composition as a longevity determinant is a strong one, even though the exact mechanisms by which a longevity determining effect is exerted have yet to be fully elucidated. However, Hulbert's theory is not in agreement with the negative relationship found between levels of antioxidant defenses and longevity. Species with greater longevity have very low levels of antioxidants (Perez-Campo et al., 1998) and most

mtDNA mutations do not appear to be directly due to oxidative stress (Greaves et al., 2012; Haag-Liautard et al., 2008; Itsara et al., 2014; Kennedy et al., 2011; Zheng et al., 2006). If organisms with more peroxidation-susceptible membranes utilize upregulated antioxidant levels as a countering effect then why do they have reduced longevity? Furthermore, why must youthful homeostasis be lost at all?

I offer an explanation for how a longevity-determining effect could arise from the influence of membrane composition on biomolecular turnover rate, metabolism, and ultimately the rate of loss of mutual DNA information. This concept is depicted in Fig. 7. I postulate that membrane composition, and certain other defining characteristics of an organism, are largely stipulated by an organism's peak biological power density, which has evolved to the level that maximizes fitness in each species. Here the term "peak biological power density" represents the maximum localized volume-specific rate of external work (power per unit volume) that is achievable within an organism. The cells or tissues where this potentiality exists may vary by species (for example, skeletal muscle in some organisms, neurons in others, etc.). "External work", in the context of peak biological power density, refers to the sum of the biomechanical, biochemical and bioelectrical work that is brought to bear on the immediate environment surrounding the localized region where this work originates within an organism. Examples include the mechanical work generated by myocytes, the chemical and electrical work produced by neurons, and the chemical work performed on metabolized products by hepatocytes. External work does not include work that is associated with housekeeping or "overhead" cellular processes such as biomolecular repair and replacement, maintenance of baseline membrane potentials or mitotic cell turnover.

To illustrate the sequence of interactions implicated in this theory, we will consider an arbitrary organism where fitness is maximized by a high level of peak biological power density compared to some reference organism (Fig. 7). A higher level of peak biological power density implies an increase in the maximum potentiality for external work rate per unit volume that is achievable by some cell, or group of cells, within an organism. I postulate that high-output proteins are utilized for realizing this external work in both transmembrane and non-transmembrane locations. To maximize the rate of work attainable from a given volume, the molecule-specific rate of work of the proteins must be as high as possible. One requirement for achieving this is to optimize the structure of the protein for peak work rate, **1** (bold numbers in this section refer to Fig. 7). This is likely to reduce biomolecular durability and resiliency (due to lower selective pressure on these parameters), and protein repair/replacement rate (turnover) may increase as a result. Secondly, the biomolecular performance of the protein pool should be maintained at a high level (i.e. degradation state should be low), **2**. In this way, the contribution from the average protein molecule will be closer to the theoretical maximum. Maintaining low degradation states will increase the rate of protein turnover and lead to a less-than-optimal energetic ROI.

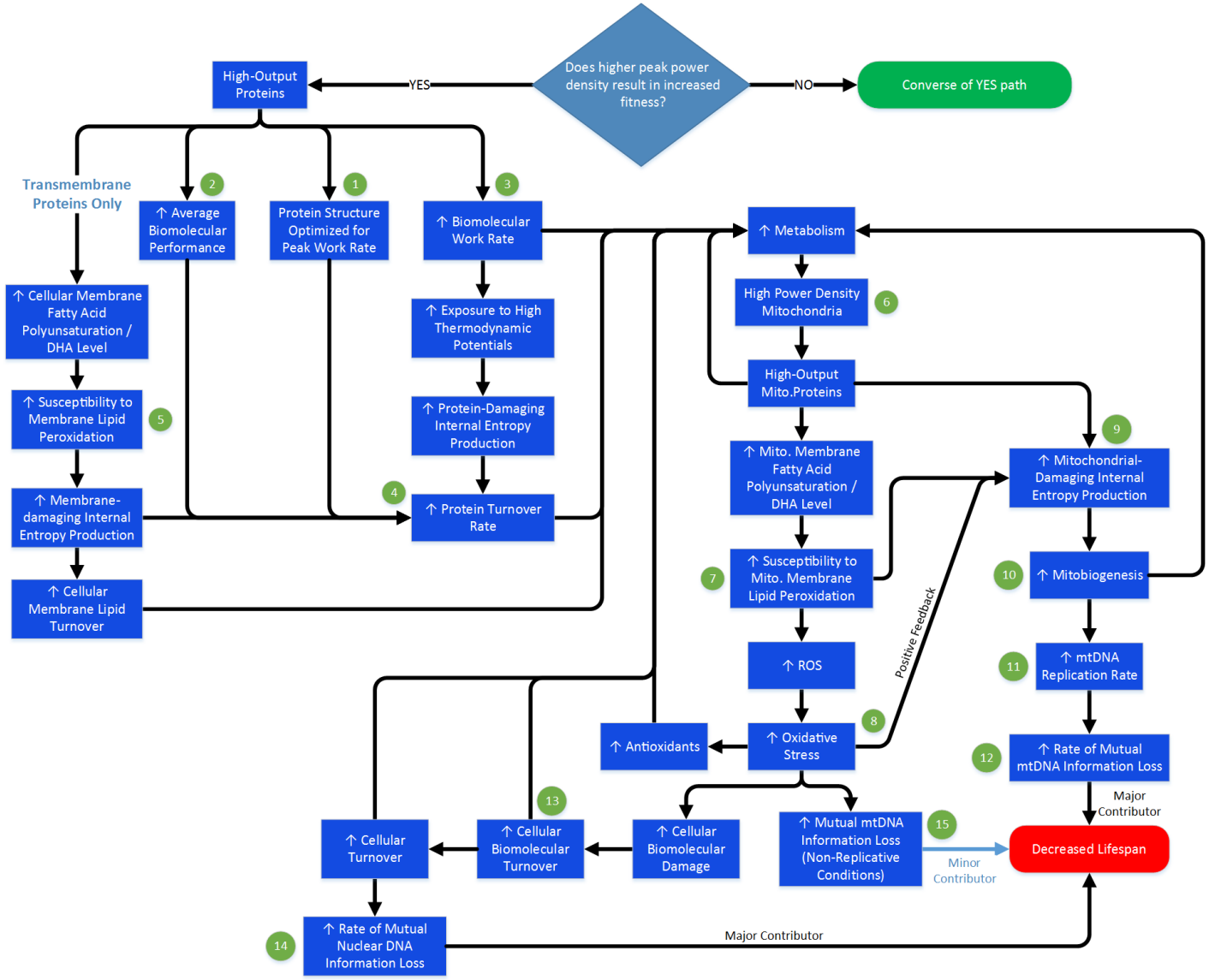

Fig. 7. A theoretical means by which an organism's peak biological power density may influence longevity.

Bold numbers in Section 5 text refer to this figure.

Higher peak biological power density implies the ability to perform work at an increased rate per unit volume somewhere within an organism. It does not mean that the maximum work rate is achieved at all times. On the other hand, if the maximum was never approached then there would be no need to possess this ability in the first place. For these reasons, it is reasonable to expect that high-output proteins are likely to perform work at a higher rate, on average, than proteins from lower peak biological power density configurations, **3**. At a minimum, the cell must have the ability to provide sufficient energetic resources for these high-output proteins even if peaks levels are only attained sporadically. This will equate to a requirement for more usable energy per unit time (i.e. higher ATP turnover) and therefore increased metabolic requirements.

In addition, to achieve a maximal rate of work in a given volume, high-output proteins must spend more time performing work and less time in a resting state. The state of actively performing work involves the transfer of energy and conditions of higher thermodynamic potentials than the static, non-working (resting) state. For these reasons, degradative internal entropy production is likely to be elevated with high-output proteins, resulting in increased protein turnover and further contributing towards an increased metabolic rate, **4**. This is consistent with the increased metabolic rates found in smaller animals and the fact that smaller animals turnover protein at faster rates compared to larger species (as illustrated in Fig. 4).

Transmembrane proteins have increased activity in membranes with lipids that utilize more polyunsaturated fatty acids (increased DHA content) (Else and Wu, 1999; Turner et al., 2003; 2005). It is predictable that configurations that call for a high level of peak biological power density include these type of membranes, which are also more susceptible

to lipid peroxidation, **5**. This contributes towards an elevated rate of membrane-damaging internal entropy production that generates more frequent membrane lipid turnover and further increases in transmembrane protein turnover rate.

The aforementioned metabolic increases generate a need for mitochondrial networks capable of satisfying these high ATP turnover demands. This is realized with high power density mitochondria, **6**, the characteristics of which are outlined in Fig. 8. High-output mitochondrial proteins optimized for maximal ATP production are expected with these configurations. Similar to their cytoplasmic counterparts, high-output mitochondrial proteins will also increase metabolic requirements and are more susceptible to degradation. Increased mitochondrial membrane fatty acid polyunsaturation / DHA levels allow for increased peak ATP output through enhanced transmembrane protein activity but cause the mitochondrial membranes to be more susceptible to lipid peroxidation, **7**. Together with a positive feedback effect from elevated ROS and oxidative stress levels, **8**, this will increase component-damaging internal entropy production within mitochondria, **9**. The combination of elevated mitochondrial membrane polyunsaturation / DHA levels and proteins more susceptible to degradation stipulate that a higher rate of offsetting negative entropy production will be required in order to maintain mitochondrial quality and preserve youthful organismal homeostasis. This need can only be realized through an upregulation of mitobiogenesis, which increases the mitochondrial membrane remodeling and protein turnover rate, **10**, but will coincide with a higher mtDNA replication rate $r_{rep,mtDNA}$, **11**. The rate of mutual mtDNA information loss will increase as a result, **12**. As mtDNA integrity declines, an organism's ability to produce usable energy will become

compromised and worsen progressively. This will generate a downregulation of cellular processes which could largely be responsible for the aging phenotype.

Increased oxidative stress from high power-density mitochondrial configurations is also likely to elevate thermodynamic potentials in cellular proteins, nuclear DNA and other biomolecules—further contributing towards increased metabolic requirements due to the need for additional resources for their repair and replacement, **13**. This and the other aforementioned contributors to increased biomolecular damage and turnover rates could be expected to increase the rate of cellular turnover. The rate of mutual nuclear DNA information loss will be heightened due to elevated replication rates, and this will increase the rate at which viable stem cells are depleted, **14**. Increased oxidative stress may also influence the rate of non-replicative mtDNA damage $r_{mut,mtDNA}$, **15**. However, due to reasons already discussed, this contribution is probably small compared to the effects of an increased replication rate.

The loss of mutual DNA information in the individual is unavoidable. Notably, the logic established here describes how the rate of loss of mutual DNA information may be a function of an organism's peak biological power density requirements, at least in part. As this rate may be critical in determining the amount of time that passes before youthful homeostasis can no longer be sustained, a potential link is herein established between an organism's peak biological power density and longevity; by this token, peak biological power density could be thought of as a high-level longevity determinant.

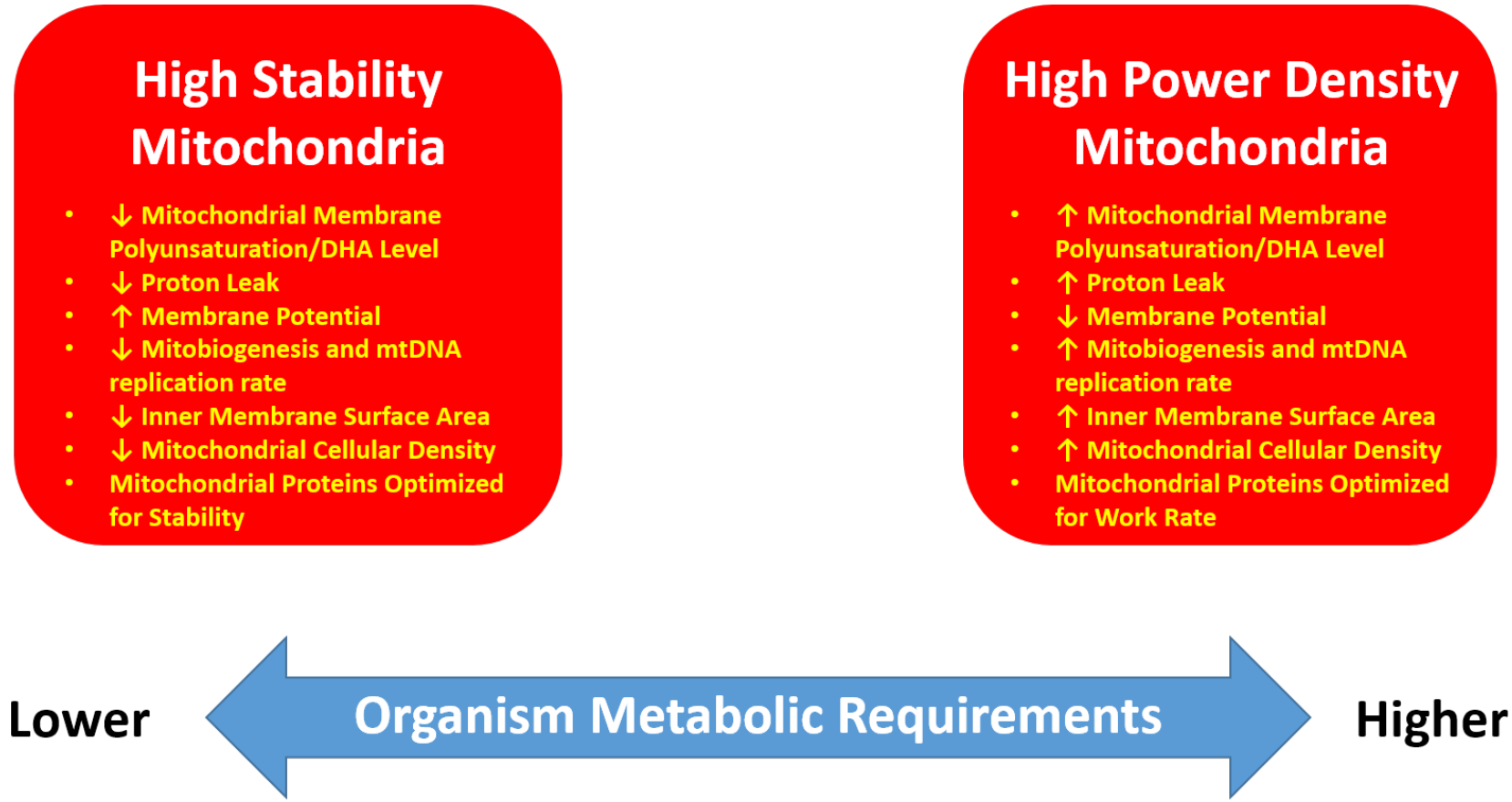

Fig. 8. The characteristics of high stability mitochondria compared to mitochondria optimized for peak biological power density.

The requirements of the organism dictate where a particular species falls within the range of configurations between these two extremes.

A solution for the second half of the naked mole-rat paradox discussed in Chapter 2 Section 2 can now be proposed. Naked mole-rats have limited access to oxygen and as a result they have extremely low metabolic rates. The need to maintain a low metabolism necessitates low-output proteins, as high-output proteins have increased metabolic requirements for a number of reasons (Fig. 7). The situation is therefore the reverse of the high peak biological power density scenario just discussed. Lower metabolism will lead to mitochondria that are better optimized for stability (Fig. 8). Consistent with this notion, naked mole-rats have $1/9^{th}$ the content of DHA in their mitochondrial membranes compared to their similarly-sized cousin the house mouse (Mitchell et al., 2007). Decreased susceptibility to lipid peroxidation will lower the rate of damaging internal entropy production, mitobiogenesis, and reduce the rate at which mutual mtDNA information is lost. Cellular turnover and the rate of mutual nuclear DNA information loss will also decrease. The slower rate of mutual DNA information loss increases the amount of time that passes before transitions from degradation states characteristic of youthful homeostasis will occur. As a result, the naked mole-rat exhibits exceptional longevity for its size. The increased oxidative damage present on biomolecules does not limit longevity as it is not the factor forcing a shift from youthful homeostasis but is merely indicative of the high degradation states that coincide with prioritizing energetic ROI for maximizing evolutionary fitness in very hypoxic conditions. I postulate that the exceptional longevity of the naked mole-rat is primarily a byproduct of the aforementioned requirement for extremely low metabolic rate as opposed to direct selective pressure for extreme longevity.

Section 6 - Allometric Relationships Describe Peak Biological Power Density Trends that Largely Predict Longevity

If peak biological power density is a primary longevity determinant, then how and why does this vary by species? Do variations in peak biological power density align with allometric trends? Some answers to these questions may arise from examining how an organism's mass-specific cost of transport (COT) is driven by certain factors. COT is a measure of the quantity of metabolic energy required to move one unit mass of an organism over one unit distance. In terrestrial animals, COT negatively correlates with body size (Reilly et al., 2007; Strang and Steudel, 1990; Taylor et al., 1982). The reasons for the increased locomotor costs in smaller terrestrial organisms have been discussed in detail elsewhere, including Reilly et al. (2007), and Kilbourne and Hoffman (2013). We will briefly examine some of the more significant causes here. Although the mass-specific metabolic energy consumed per stride remains constant across large and small mammals at the same stride frequency, larger animals require fewer strides to cover an equivalent distance; this at least partly explains the reduction in COT with increasing body size (Heglund and Taylor, 1988; Heglund et al., 1982; Kram and Taylor, 1990). The effect is compounded by the fact that larger mammals have disproportionately longer limbs (positive allometry) (Pontzer, 2007).

In general, smaller animals cannot simply decrease their top speeds to offset the increased COT and preserve a low metabolic rate as they must be able to achieve speeds that are sufficient to evade larger predators. This is demonstrated by the fact that, although top speed does increase with body mass in mammals (Garland, 1982), the allometric scaling factor can only partially counteract the increased COT in smaller mammals. In

other words, the rate of mass-specific metabolic energy consumed by smaller mammals to achieve their top speed is greater than that of larger mammals.

Posture can also significantly affect COT (Biewener, 1989). Smaller terrestrial animals tend to have limbs that are more abducted and flexed during movement (Reilly et al., 2007). Larger animals utilize a more upright posture, which confers a mechanical advantage to anti-gravity muscles. For these reasons, smaller mammals have increased muscular energetic demands for counteracting the flexing moment of the ground reaction force. Additionally, larger animals are able to benefit more from elastic storage because the capacity to store energy in tendons positively correlates with tendon cross-sectional area (Bennett et al., 1986; Biewener and Blickhan, 1988; Biewener et al., 1981). Pendular savings can reduce the metabolic cost of locomotion and become increasingly relevant as body size increases in erect animals—but are insignificant in smaller crouched animals (Reilly et al., 2007).

For the aforementioned reasons, an increase in the peak biological power density of skeletal muscles and supporting organs (heart, lungs, etc.), together with a corresponding increase in the metabolic consumption of the same, is expected in smaller terrestrial animals. As skeletal muscle is the major contributor to non-resting metabolism, it should not be surprising that field metabolic rate scales with negative allometry (Nagy, 2005).

Surface area scales as a function of body mass per the relation $A \propto M_b^{2/3}$. The exponent in this case is less than 1, signifying that the mass-specific capacity for heat exchange decreases as body size increases. Since no thermodynamic process is 100% efficient, a portion of the energy utilized for metabolism is unavoidably converted to heat. The efficiency of the oxidative phosphorylation machinery in mitochondria is highly optimized

and not a function of body mass, as indicated by the fact that ATP turnover per unit of consumed oxygen does not change with body mass in mammals (Porter and Brand, 1995). Therefore, in the absence of other limiters, the maximum sustainable metabolic rate will be lower in larger organisms due to their reduced relative capacity to shed metabolic waste heat. This translates to higher theoretical peak biological power densities in smaller organisms. A converse effect of the surface area to mass ratio is believed to limit the minimum attainable body size of endothermic amniotes: maintenance of a constant body temperature, below a particular body size for a given set of environmental living conditions, will require an increasing proportion of metabolic energy as body size decreases.

Another factor may also contribute to the minimum attainable body size and generate increased metabolic requirements in smaller animals. West and colleagues argued that metabolic rate scaling is constrained by characteristics of the circulatory system (and other fractal networks) that can be explained by principles from fluid dynamics (West et al., 1997; West and Brown, 2005). As vessels become smaller, viscosity causes energy to be dissipated at a substantially increased rate. Additionally, flows become highly damped in smaller vessels and unable to benefit from impedance matching, which can greatly reduce the energy lost due to reflections in larger vessel branch points. These energy-consuming effects play an ever increasing role as body size decreases and narrow vessels predominate. West et al. calculated the minimum mass of a mammal to be ~ 1 gram, based on cardiovascular parameters; this is similar to the mass of the smallest known mammal, the shrew (West et al., 2002). West's concept assumes that the organism utilizes a fractal-like

vascular system, and is not applicable to organisms such as Hydra which exchange nutrients, gases, and waste by simple diffusion.

Although the allometric relationships between BMR and M_b, and longevity and M_b, at the species level are well established and accepted, these describe only general trends; they do not hold true for all species. Clearly, the described allometric relationships are not imposing a strict, specific value for peak biological power density, metabolic rate, or longevity on a species or individual based solely on body mass. Rather, they appear to establish median values (averaged across a range of species) together with upper and lower theoretical bounds on these factors. The optimal compromise between peak biological power density, longevity and body size for a given species must evolve within these general constraints towards the configuration that maximizes species fitness. Deviations from the general relationships should be expected. For example, a species living in an environment with low predatory pressure may receive a fitness benefit from sacrificing peak athletic performance for increased longevity. Suppose that in this case, it is not necessary for the organism to function anywhere near the metabolic limit dictated by its capacity for heat exchange to ensure high rates of survival and fecundity over its lifespan—it receives more fitness benefit from maintaining a reasonable level of fecundity over an increased lifespan than from a marginal decrease in predation over a shorter lifespan. Another example of an expected significant deviation from the median are situations where organisms utilize a specific behavioral tactic or enhanced cognitive capabilities to increase their survival odds in lieu of maximizing peak biological power density. Humans are the ultimate embodiment of such a strategy.

Although BMR correlates with longevity across a wide range of organisms, no significant correlation remains in either eutherians or birds after correcting for body mass and phylogeny (de Magalhães et al., 2007). One possible explanation for this can be derived from the fact that peak biological power density, which may be a primary high-level longevity determinant, need not correlate exactly with BMR. BMR measures the amount of energy used while an organisms is at rest. Field metabolic rate (FMR), which also scales allometrically with M_b, takes into account BMR as well as thermoregulation and activity costs. Even within the same class, FMR allometric scaling slopes are frequently different from BMR slopes (Nagy, 2005). FMR will correlate more closely with peak biological power density than BMR will because FMR values always exceed BMR and thus are closer to peak sustainable metabolic levels (which is a better measure of peak biological power density). Even so, FMR still represents a time average of metabolism; organisms that exhibit short periods of very high metabolic activity (and hence possess higher peak biological power density) could have similar FMRs to organisms that have much lower peak biological power density but less average variation in metabolic rate, and vice-versa. This offers a reasonable explanation for how peak biological power density can still be a longevity determinant and correlate with BMR across species and within distinct phylogenetic groups, even if BMR does not correlate with longevity after correcting for body mass and phylogeny.

Birds have higher BMRs than mammals, yet they live on average approximately three times as long as similar-sized mammals. Many of the same arguments just mentioned could help explain this discrepancy. Of course, the thermal physiology of mammals and birds is vastly different and this could contribute to the variation in longevity as a function of BMR.

As pointed out earlier and in agreement with the notion that peak biological power density is a primary longevity determinant, a common trend line predicts MLSP as a function of mitochondrial membrane peroxidation index for both birds and mammals (Hulbert et al., 2007).

These generalized allometric relationships also do not hold universally when examining the individuals with a species. For example, larger individuals in some species, such as dogs (Speakman et al., 2003) tend to have shorter lives than smaller individuals. This may be in part because longevity determinants have evolved, and are genetically engrained, at the species level; in other words, the genetic elements that specify peak biological power density, membrane composition, biomolecular turnover rates, stem cell reserve levels, and other factors that contribute towards resisting (or promoting) permanent thermodynamically-induced changes in biocomponents subject to irreversible losses are mostly preset within the genome of a species and do not vary significantly as a function of body size. It is not surprising that significant deviations from the median body size would result in a compromised individual—and that this would include decreased longevity.

Chapter 8 - Longevity Optimization

With sufficient time, the loss of mutual DNA information must lead to reduced viability in individual organisms. Mitochondrial energy production efficiency will be compromised as a result of loss of mitochondrial mutual DNA information, while losses in nuclear DNA are expected to eventually result in a mosaic of random cellular dysfunction.

Once mitochondrial dysfunction has progressed to the point that resource deficits prevent the funding of all cellular processes at youthful levels and/or genetic redundancies are no longer able to sufficiently compensate for other losses in genetic fidelity, an aged phenotype must begin to take shape. It is reasonable to expect that the optimal allocation of resources for preserving maximal survival and fecundity in an aged individual would be different than the configuration used in young adulthood when adequate resources are available to fully fund all cellular processes. Factors most critical to immediate survival are of highest priority to the individual. Therefore, a genotype optimized for an aging individual could be predicted to increasingly deprioritize less vital processes and biocomponents as useable energetic resource availability decreases and dysfunction increases so that more critical biocomponents are preserved in states that are adequate to sustain life and maximize survival potential and fecundity. Eventually, a state will be reached where even vital factors cannot be adequately sustained and the individual's overall condition becomes unconducive to continued life.

Could an anti-aging strategy such as the one described above exist in multicellular organisms? A large number of genetic elements regulating pathways that appear to be related to longevity have been identified (ENCODE Project Consortium et al., 2007). Many

scientists believe that these pathways are largely responsible for stipulating the presence of aging and for modulating the rate of aging between species (Austad, 2009; Holliday, 2010; Kirkwood, 2005; Vijg and Campisi, 2008). A proposed complementary hypothesis is that longer-living species have evolved to contain superior mechanisms and/or biomolecules for retarding senescence; some scientists believe that incorporation of these changes into shorter-living organisms could lead to delayed senescence in these other organisms as well.

I submit here an alternative theory proposing that a major function of the putative aging pathways is the optimization of the process of aging to maximize individual longevity and fecundity, and that this is an evolved response. Contained within these pathways, genetic elements that I term "longevity optimizers" work together to elicit a balanced response to the unavoidable progression towards increasing levels of irreversible biomolecular fidelity loss.

To my knowledge, this concept has not been previously discussed or proposed in published literature. There are several likely reasons for this. Firstly, it is not generally acknowledged that the aging of an individual is unavoidable, regardless of genotype. Many popular aging theories (e.g. antagonistic pleiotropy, mutation accumulation, and disposable soma) utilize evolutionary concepts to justify the existence of aging in the individual and do not incorporate fundamental physical law or approach the problem in a multidisciplinary fashion. These theories claim that aging is not unavoidable but rather that it exists because it projects beneficial effects on species fitness in other ways (antagonistic pleiotropy, disposable soma) or that there is insufficient evolutionary pressure to eradicate aging (mutation accumulation). If biological aging is not mandated by fundamental physical law, then there is no need for mechanisms or strategies to resist and optimize it.

Here, rationale and evidence has been provided for why biological aging is in fact an inevitable consequence of fundamental physical law that cannot be overcome by evolution. If this is the case, then it is reasonable to propose the existence of evolved mechanisms to resist and optimize an organism's susceptibility to these effects in order to maximize fitness. For reasons explained in detail in the following sections, I believe that the argument is strong that such mechanisms exist.

A counterargument is that aging optimizations are unlikely to evolve because selective pressures begin to decrease once an individual has reached the age of reproductive maturity. However, as the potential for loss of mutual DNA information begins at conception—not at reproductive maturity—this phenomenon must be suitably combatted at all life stages. Even if selective pressures were entirely absent past the age of reproductive maturity, in order to maximize fitness an individual organism would require strategies for preventing the loss of mutual DNA information from reaching excessive levels and to best handle the mutual DNA information loss that has occurred at all life stages up to this age.

Section 1 - Selective Pressures Favor Genotypes that Attenuate Increases in Mortality and Losses in Fecundity Occurring After Reproductive Maturity

Germline mutations are only rarely beneficial to the organism. Similarly, we can confidently state that, in the absence of compensating mechanisms, any somatic mutation or other form of irreversible degradation to a necessary biocomponent (biomolecule, cell, tissue, etc.) will nearly always impact an individual's instantaneous mortality rate and/or fecundity negatively or, at best, neutrally. Therefore, the integrative effect of the systemic

degradation occurring with age must eventually result in negative repercussions for the individual.

In any aging individual organism, those biocomponents that are susceptible to irreversible fidelity losses will be the first biocomponents to incur shifts from their youthful homeostatic states; for most organisms with at least moderate longevity this is likely to be DNA molecules. The continual loss of mutual DNA information must eventually force shifts in the degradation state of other biocomponents. The magnitude of any deleterious impact on individual instantaneous mortality rate and fecundity due to an increase in the degradation state of a biocomponent will vary depending on the function of the biocomponent and the extent of the shift in degradation state.

What are some potential biological responses for minimizing the negative repercussions of unavoidable fidelity loss with age? One such strategy for maximizing survival rate and fecundity in these conditions is a genotype that prioritizes minimizing the degradation state, or that reduces the failure likelihood, of biocomponents most critical to these parameters. We will examine whether such a strategy would be evolutionarily favored.

Hamilton (1966) exploited the Euler-Lotka equation (Euler, 1767; Fisher, 1930; Lotka and Sharpe, 1911) to derive a measure of fitness r from age-specific survival and fecundity rates.

$$\int_0^\infty e^{-rx} l(x) m(x) dx = 1 \qquad (23)$$

Here $l(x)$ represents survival up to age x and $m(x)$ is fecundity at age x. Using a similar framework, Fisher (1930) introduced the concept of age-specific reproductive value $v(x)$ with the following relation

$$v(x) = \int_x^{\infty} e^{-r(y-x)} \frac{l(y)}{l(x)} m(y) dy \qquad (24)$$

Fisher (1930) described reproductive value as a measure of the contribution of individuals of age x to the future ancestry of a population and stated that (p.27) "the direct action of natural selection must be proportional to this contribution". In other words, genotypes that maximize reproductive value for a given age will be favored by selection over those that produce a lower $v(x)$—thus maximizing fitness. Fisher also discussed why reproductive value typically increases from birth before reaching an apex and then declining at more advanced ages. He demonstrated this trend with human population data.

Let us examine some plots of reproductive value with age for a hypothetical organism with slightly different genotypes. Assume that in this organism, $m(x)$ peaks near reproductive maturity and declines after this age. Also assume that mortality increases from this point forward, accelerating the rate at which $l(x)$ is decreasing with age. We will assume that irreversible fidelity loss is the primary driver of these reductions in $l(x)$ and $m(x)$, aside from a baseline constant mortality rate. In Fig. 9a, the red curve depicts a reproductive value curve for this organism with a genotype that does not incorporate any elements for optimizing fecundity and/or survival in response to irreversible losses in fidelity. If the same values for survival and fecundity up to the age of reproductive maturity are used but losses in $l(x)$ and $m(x)$ occurring after this age are attenuated, peak reproductive value will increase, occur at a later age, and reproductive value will be maintained longer (Fig. 9a, blue curve). Due to the positive contribution to reproductive

value, genes/genotypes that attenuate the described pattern of losses in $l(x)$ and/or $m(x)$ will be evolutionarily favored (i.e. they will increase fitness), provided they do not negatively influence early reproductive value. Therefore, if genes that attenuate reductions in $l(x)$ and $m(x)$ occurring after reproductive maturity due to irreversible fidelity loss exist, then it is likely that these genes will be selected for and incorporated into an organism's genome.

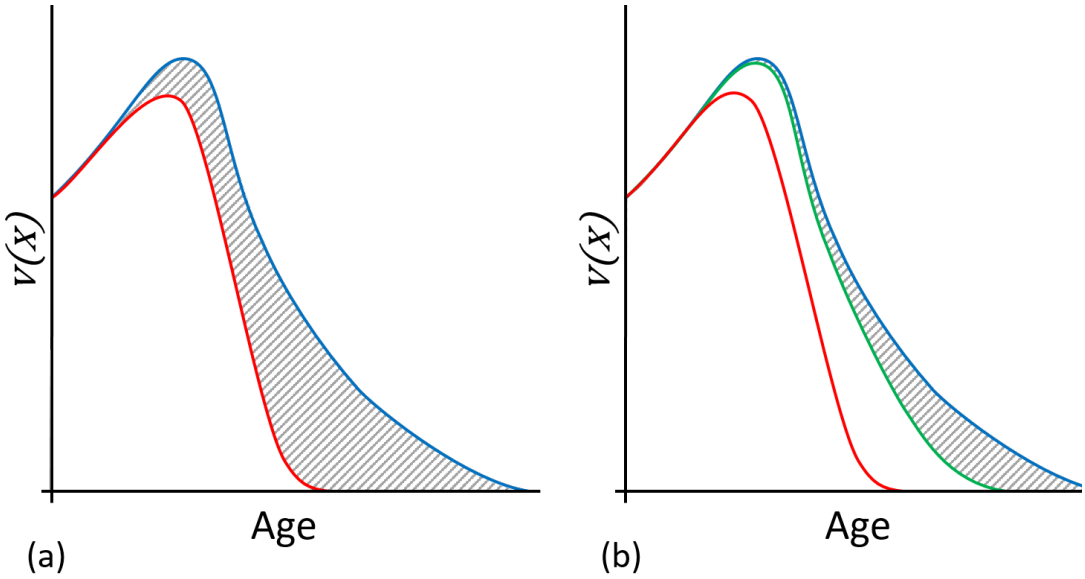

Fig. 9. Two scenarios of reproductive value curves for a hypothetical organism.

(a) Optimization (blue curve) of the organismal response to irreversible losses in fidelity (as detailed in text) will provide a fitness advantage compared to a genotype lacking longevity optimizers (red curve), due to the increase in reproductive value depicted by the grey shaded region. (b) Variations on optimization. Three genotypes are illustrated: no longevity optimization (red curve), optimal longevity optimization (blue), and partial longevity optimization (green). All curves were modeled according to parameters described in text and using Eqs. (23) and (24). Curves depict calculated trends.

Section 2 - Deterioration Management Strategies

It is illogical for an organism to have evolved such that fecundity or mortality are negatively affected (at ages where selective pressure is still above some minimal threshold) due to the disproportionate deterioration, or increased likelihood of failure, of one or a

small number of vital biocomponents. As demonstrated in the previous section, selection would favor genotypes that avoid susceptibility to the catastrophic failure of a small number of weak links.

I propose that through evolution, organisms have developed cellular mechanisms and pathways for managing the irreversible, and inevitable, losses of fidelity afflicting an aging individual in a progressive and dynamic manner. Biocomponents most susceptible to degradation effects, and most critical to survival and fecundity, are prioritized. To illustrate this concept, two terms will be utilized: "managed deterioration" and "unmanaged deterioration".

With unmanaged deterioration, the degradation of critical singular biocomponents would occur at a rate proportional to the biocomponent's susceptibility to irreversible fidelity loss due to internal entropy production, or the direct and indirect effects of degradation present in other components (Fig. 10, left). Regardless of their importance to instantaneous mortality rate or fecundity, the most susceptible components would reach failure levels first—leading to premature reductions in survival probability and fecundity—while other components could still remain at relatively high performance levels (i.e. low degradation states).

In managed deterioration, longevity optimization genes could modulate the rate of deterioration of different biocomponents so that biocomponents of similar importance degrade at comparable rates and/or reach their failure threshold at equivalent ages. Critical biocomponents would be prioritized. Thus, the age at which any one biocomponent reaches a level that compromises fecundity or survival probability is delayed—effectively

increasing longevity and overall fitness (Fig. 10, right). This could be accomplished by several means, including:

1. Reallocation of resources, at the cellular level and higher, as usable energetic resource availability becomes compromised to prioritize those biocomponents most important to preserving reproductive value.
2. Adjustment of microenvironmental conditions to decrease the thermodynamic potentials on more vital biocomponents and thereby lower the rate of damage-inflicting internal entropy production.
3. Reduce biocomponent turnover rates to delay the clonal expansion of irreversibly compromised biocomponents (effectively reduces the rate of mutual information loss).
4. Alter physiology such that stresses on more vital biocomponents are reduced and maintained below their operating limits, resulting in a decreased likelihood of failure of biocomponents most critical to preserving fecundity and mitigating increases in mortality.

One possible example of items (2) and (3) is the way by which mutual mtDNA information loss may be attenuated by controlled decreases in mitochondrial fusion and fission in aging individuals. This can be demonstrated by examining the "Mitochondrial Infectious Damage Adaption" (MIDA) model proposed by Figge et al. (2012). Using a probabilistic modelling approach, they showed that the decrease in mitochondrial fusion and fission rates seen with increasing age preserves average mitochondrial quality and delays the age at which mitochondrial quality drops below the minimal level required for cell viability. In short, the age-linked reduction of mitochondrial fusion and fission rates

may attenuate mutual mtDNA information loss by reducing the exposure of mtDNA molecules to the high thermodynamic stress conditions encountered during replication and delaying the spread of parasitic mutated mtDNA molecules.

A downside to decelerating mitochondrial fusion/fission rates is that these processes are integral to mitophagy (Twig et al., 2008; Youle and Narendra, 2011). Mitophagy serves to remove the mitochondrial mutants that are detectable (Kowald and Kirkwood, 2011) but is also believed to be critical in preserving the quality (low degradation state) of mitochondrial components by segregating deteriorated components, such as lipids and protein, into mitochondria that will be targeted for destruction. Therefore, a reduction in fusion/fission rates increases the load of ROS products and otherwise damaged mitochondrial components, compromising overall mitochondrial quality (i.e. increasing mitochondrial degradation state). The combination of reduced mitochondrial fusion/fission and the loss of mutual mtDNA information results in mitochondria in aged organisms that produce less usable energy (Yaniv et al., 2013).

Since mutual mtDNA information loss is inevitable, preserving a constant mitochondrial fusion/fission rate will still result in the eventual loss of mitochondrial quality. However, Figge et al. (2012) demonstrated that decelerating mitochondrial dynamics actually preserves mitochondrial quality and extends the limit on longevity implied by mitochondrial dysfunction; this is evidently because the resulting reduction in the rate of mutual mtDNA information loss is more critical to preservation of reproductive value than the tradeoff of increased degradation state in other mitochondrial biocomponents. In the context of the current discussion, the genes responsible for realizing this strategy would be considered longevity optimizers.

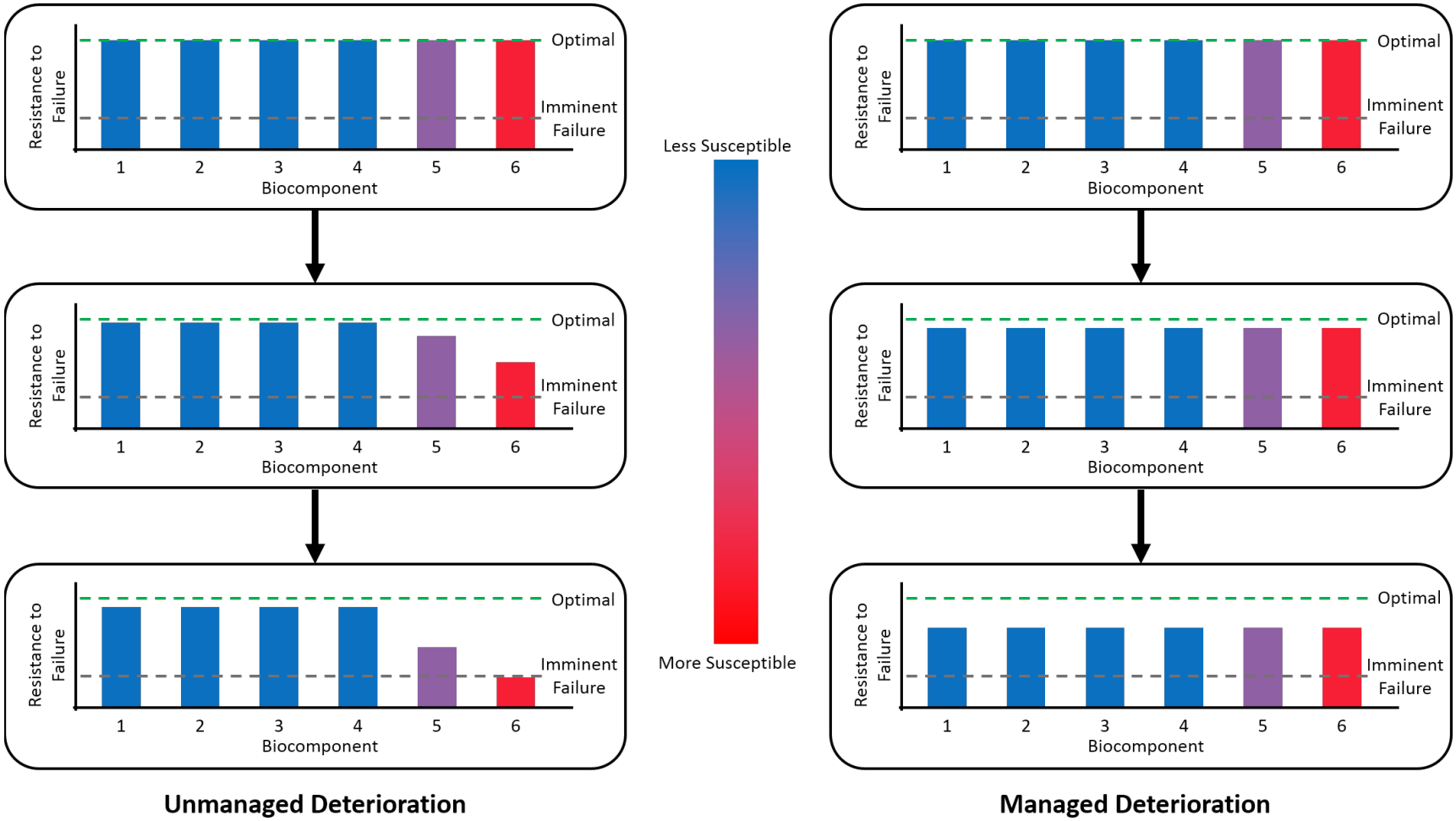

Fig. 10. Demonstration of unmanaged (left) and managed (right) deterioration strategies.

(Fig. 10 cont'd) A group of arbitrary biocomponents, equally vital to an organism's fecundity/survival, are depicted. Three ages are considered: Top—Young Adult, Center—Middle-Age, Bottom—Elderly. 'Red' indicates that a biocomponent is very susceptible to irreversible degradation (which could be due to direct and/or indirect effects), while 'blue' signifies that a biocomponent has very little or no susceptibility to irreversible degradation. The vertical axis depicts how resistant a biocomponent is to failing, given its current degradation state. In unmanaged deterioration, biocomponents will approach imminent failure at a rate proportional to their susceptibility to the effects of irreversible fidelity loss. Biocomponents most susceptible to irreversible degradation will reach failure levels first and the organism will die prematurely. With managed deterioration, longevity optimization genes produce adjustments in the aging individual which partially offset decreases in resistance to failure of the most vital and susceptible biocomponents (details in main text). By not allowing any one vital factor to reach the imminent failure state at an earlier age than others, managed deterioration strategies may enhance longevity and increase fecundity.

Skeletal muscle mass has been shown to decrease substantially with age (Grounds, 1998). The loss of muscle mass with age is generally regarded as a purely undesirable physical manifestation of aging. Along this line of thinking, a safe and effective therapeutic intervention capable of preventing or attenuating age-related skeletal muscle mass loss is commonly viewed as something that would be desirable and beneficial for the health of the elderly. For example, a substantial body of evidence suggests that the loss of function in satellite cells is a proximal cause of age-related muscle mass loss (Carlson and Conboy, 2007; Sousa-Victor et al., 2014) and interventions have been proposed to "correct" this deficiency (Carlson and Conboy, 2007; Dumont et al., 2015; García-Prat et al., 2013; Sousa-Victor et al., 2014; 2015).

I propose that an alternative path of reasoning should be considered for explaining this, and perhaps other, age-linked traits. Given that cardiac output declines significantly with age in humans (Brandfonbrener et al., 1955) and is rooted in functional deficits at the cardiomyocyte level (Guo and Ren, 2006), a reduction of skeletal muscle mass will lower the stresses on an age-compromised heart by reducing the volume of blood in the body and decreasing the contractile forces required to circulate the blood. This raises the possibility that a decrease of skeletal muscle mass with age is a beneficial, evolved response—or at

least a tolerated condition—which reduces cardiovascular stress and lowers the mortality risk of cardiac events. This is one example of how age-dependent physiological alterations could decrease the likelihood of failure of more critical biocomponents in light of inevitable losses in fidelity, as proposed in item (4) from the above list, and serve to extend longevity. To be clear, this hypothesis is not intended to explain extreme muscle wasting outside of normal age-related trends, which is undoubtedly a genuine pathological condition. In addition, there are certainly a number of undesirable aspects of age-related skeletal muscle dysfunction. The concept being put forth is the idea that age-dependent physiological alterations, even those that at first glance appear purely detrimental, may actually serve a purpose in establishing an optimally balanced configuration in the face of inevitable, and progressively increasing, fidelity loss in the individual.

It is prohibitively difficult to directly establish that the altered age-dependent expression of one gene represents an evolutionarily established tradeoff with some other gene(s) that extends longevity, as suggested by item (1). The reason for this is the sheer number of genes, which renders establishment of any correlation a highly multifactorial problem. However, beyond the evolutionary argument for their existence, there is other evidence suggesting that mechanisms of this type may exist—specifically, features of the proteomic, gene expression, and epigenetic signatures that have been found to characterize aging individuals.

A meta-analysis of gene expression profiles from mice, rats and humans revealed a characteristic age-associated pattern of changes in expression of specific genes (de Magalhães et al., 2009). These differential expressions were consistent across all three species and across multiple tissue types examined. Specific biological processes and

functions were associated with this meta-signature. Lysosomal genes were one group found to be overexpressed with age. This could represent an adaptive mechanism for counteracting the increased degradation state in proteins (since, due to reductions in usable energetic cellular resources, protein turnover is reduced with age). A result of decreased protein turnover is that a greater proportion of proteins may degrade to the extent that they are not effectively ubiquitinated or processed by proteasomes and must be recycled by other means, i.e. by lysosomes. Although the energetic resources dedicated to increased lysosomal expression could have been allocated to lessening the severity of the general reduction in protein turnover, it may be that age-dependent lysosomal overexpression optimizes the overall protein degradation state based on energetic resource availability and that this represents the best compromise for maximizing reproductive value. A proteomic analysis of human fibroblasts from healthy adult female donors from 3 age groups (young: 20-30 years; middle-aged: 40-50; older: 60-70) revealed 43 proteins with age-associated abundance changes (Waldera-Lupa et al., 2014). Interestingly, this included two proteasome subunits that were significantly down-regulated and two heat shock proteins that were up-regulated. This further supports the possibility that age-linked responses have evolved that minimize protein degradation state via optimization of resource allocation.

Epigenetic studies have also demonstrated the presence of characteristic aging signatures. DNA methylation expression patterns have been shown to change across the human lifespan in line with chronological age (Bell et al., 2012; Bocklandt et al., 2011; Boks et al., 2009; Christensen et al., 2009; Christiansen et al., 2015; Florath et al., 2013; Garagnani et al., 2012; Gentilini et al., 2012; Hannum et al., 2013; Heyn et al., 2012; Horvath, 2013; McClay et al., 2013; Rakyan et al., 2010). Predictors have also been

developed that can reliably estimate the age of human cells from any human tissue type based on epigenomic DNA methylation profiles (Hannum et al., 2013; Horvath, 2013). One of these predictors has also been demonstrated to be applicable to chimpanzees, although less so to gorillas (Horvath, 2013). Importantly, a significant correlation was also observed between cell passage number and predicted age in both induced pluripotent and embryonic stem cells. This supports the notion that age-related epigenetic signatures do not simply represent accumulated regulatory dysfunction, but that at least some component of this signature represents a progressive and dynamic response to the loss of mutual DNA information—possibly in part through a telomere-related mechanism. Furthermore, a number of characteristic age-related epigenetic changes have been found to be tissue-type dependent (Christensen et al., 2009; Thompson et al., 2010), supporting the hypothesis that longevity optimization may extend to the tissue-level.

In sum, the above findings support the feasibility of the notion that an age-associated reallocation of resources indeed occurs and is not limited to the cellular level but functions with some degree of tissue specificity (item 1 from above list). These findings also further support the existence of items (2), (3), and (4).

Section 3 - Longevity Optimization Strategies from Early Adulthood May Serve as Templates for Those Used in Later Life

The theory advanced here proposes that selective pressures have led to the evolution of genetic optimizations that attenuate the rate of loss of mutual DNA information (and other irreversible fidelity losses) and the detrimental effects of these losses in aging individuals. There can be little doubt that in the face of inevitable, irreversible and progressive fidelity loss, a diverse array of intermediate configurations would be required to realize optimal aging during all stages of life. As compromised biomolecules reach non-trivial levels even

during early adulthood (Ben-Zvi et al., 2009; Greaves et al., 2014), it is reasonable to propose that longevity optimizers have evolved to incorporate complex modulatory strategies to ensure optimal adjustments to the corresponding overall state of an aging individual.

This suggests that evolved, early adult-life longevity optimization pathways may serve as the basis for at least some of a late-life longevity optimization strategy. It could be largely through the extrapolation of these early adult-life mechanisms that the maximal lifespan of an organism is able to extend well beyond the age of peak reproductive value, particularly in species such as humans where older individuals are kept in protected environments. The use of pre-existing genes and pathways as a basis for later-life optimizations may also explain how genetic elements could evolve to a highly optimized state for relatively advanced ages, even though selective pressure decreases with age (Hamilton, 1966; Medawar, 1952; Williams, 1957). If genes and pathways for early adult-life longevity optimization were already present within an organism's genome, the extension of these strategies for late-life longevity optimization may require considerably less selective pressure.

Since selective pressure does decrease with age, it would likely still require an extremely long time for very late-life longevity optimizations to evolve to fully maximize longevity extension potential. Therefore, it could be predicted that longevity optimization in any given organism will be somewhat below ideal. This concept is illustrated in Fig. 9b. Utilizing a hypothetical organism with survival and fecundity parameters similar to those described in Section 1, it can be shown that a genotype lacking any longevity optimization will exhibit a relatively steep drop in reproductive value with progressing age after the age

of peak reproductive value (red curve). Incorporating longevity optimizer genes capable of maximally attenuating losses in fecundity, and increases in mortality, with age into the same organism will preserve higher reproductive values into later ages (blue curve). Now suppose that longevity optimization is close to ideal for ages near peak fecundity but becomes progressively less ideal as age increases and selective pressure decreases; this would result in a reproductive value curve between the two described extremes (green curve). I propose that this last curve is representative of the evolved state of the typical metazoan. The gray shaded region thus represents the "intervention potential"—the maximal gains in reproductive value attainable by further genetic longevity optimizations or through artificial manipulation of individuals (i.e. drugs and therapies, excluding therapies that replenish mutual DNA information). Although beyond the scope of the current discussion, by examining statistics of proportionate mortality by pathological condition and other population data, it may be possible to predict the ideal longevity optimization curve for a particular organism (blue curve in Fig. 9b).

Section 4 - Entropy-Driven Managed Deterioration in Further Detail

It is theorized here that metazoans have evolved to make compensatory adjustments as individuals age so as to minimize the deleterious effects of thermodynamic phenomena on reproductive value—resulting in survival, for the moment, but nonetheless unable to avoid an ever-increasing negative phenotype. These longevity optimizers may protect the biocomponents of an organism at all levels (biomolecules, cells, tissues, and organs) that are most critical to immediate survival and fecundity by sacrificing other aspects of health, leading to a diverse "spread the misery" phenotype. In essence, the diversity of the biocomponents affected during aging and the relatively high degree of conservation of the

aging phenotype across taxa may be largely manifestations of these compromises. A more detailed depiction of this theory links further aspects of the aging process (Fig. 11).

MtDNA mutations are ubiquitous in aged mammals (Wallace, 1999), equating to the loss of mutual mtDNA information with age. The described theory incorporates the concept that these losses, resulting from the effects of the second law, are a driving force towards the deceleration of mitochondrial fusion/fission, **1** (bold numbers in this section refer to Fig. 11)—mitigating, but unable to prevent, further losses in mutual mtDNA information. This deceleration is metered (Figge et al., 2012) in response to an ever-increasing systemic mutational load (Cao et al., 2001; Kennedy et al., 2013; Kraytsberg et al., 2006). As an individual ages, losses in mutual mtDNA information and reduced fusion/fission rates lead to elevated levels of mitochondrial ROS products and compromised mitochondrial components (increased degradation state), **2**. This reduces the peak amount of usable cellular energy (ATP) that a mitochondrion from an aged individual can produce (Yaniv et al., 2013), **3**. This deficit becomes progressively worse with age.

Once mitochondrial dysfunction exceeds a threshold, youthful homeostasis can no longer be preserved. A shortage of sufficient ATP to fund all cellular processes at youthful levels results in the aforementioned reallocation of resources and physiological alterations, **4**. I propose that these adjustments have evolved, are balanced and adaptive, and are largely signified by the epigenetic state of a cell—which has been found to have distinctive signatures for different ages (Bell et al., 2012; Bocklandt et al., 2011; Boks et al., 2009; Christensen et al., 2009; Christiansen et al., 2015; Day et al., 2013; Florath et al., 2013; Gentilini et al., 2012; Hannum et al., 2013; Heyn et al., 2012; Horvath, 2013; McClay et al., 2013; Rakyan et al., 2010; Thompson et al., 2010). The resulting age-dependent

epigenetic signatures should not be confused with epimutations, where distribution is mostly random (Heyn et al., 2012).

Protein production is slowed in the cells of an aging animal (Ben-Zvi et al., 2009) and fewer resources are dedicated to maintaining the proteome (Douglas and Dillin, 2010; Hwang et al., 2007). These mandatory energy-conserving events reduce the ability of cells to counter the degradative effects of internal entropy production and to preserve youthful biomolecular homeostasis, leading to a continuous but slowly accelerating increase in biocomponent degradation states, **5**. This is exemplified by the increased levels of damaged, misfolded and polymerized proteins seen with age (Balch et al., 2008). Since ATP is also required to help protect the nuclear and mitochondrial genomes from permanent losses, nuclear and mitochondrial DNA integrity is gradually further compromised as usable energy becomes more scarce, **6**, as demonstrated by higher sustained levels of unrepaired damage (Bailey et al., 2004; Wallace, 1999). This increases the probability of sustaining further permanent losses in mutual DNA information.

Losses in mutual nuclear DNA information with age contribute to increased cell-to-cell stochasticity in gene expression (Bahar et al., 2006) and clonal mosaicism (Lodato et al., 2015), causing average cellular performance to decrease. The loss of mutual DNA information will also decrease stem cell viability and consume stem cell reserves, in addition to generating losses in the number and viability of nonmitotic somatic cells, **7**.

Dysfunctional telomeres can activate the DNA damage response pathway, engaging tumor protein p53 and leading to promotion of apoptosis or replicative senescence (Deng et al., 2008). Telomere attrition is upregulated in aged cells (Passos et al., 2007). This is an evolved mechanism, distinct from the length reduction that occurs during replication,

believed to partially offset the increased likelihood of developing cancerous mutations in age-compromised cells (Campisi, 2005), **8**. This adaptive response involves the preferential degradation of telomeric DNA in conditions of increased mitochondrial superoxide production (Passos et al., 2007; Petersen et al., 1998; Zglinicki, 2002), as occurs with aging.

Epigenome maintenance is downregulated in aged mammals (Cencioni et al., 2013). As internal entropy production will continue to result in insults to the once tightly-regulated epigenome and fewer resources are dedicated to its maintenance, the number of unrepaired spontaneous epigenome mutations will increase with age (Chambers et al., 2007), **9**. This, combined with the downregulation of conventional DNA damage repair mechanisms (Beerman et al., 2014; Zhang et al., 2010), contributes to an ever-increasing risk of developing cancer (Hansen et al., 2011), as seen with advancing age (American Cancer Society, 2013).

Inevitably, the result of cellular component-level degradation will be compromised cellular performance, **10**—albeit less overall performance loss than if the damage had not been apportioned. This loss in cellular performance will lead to a concomitant loss in performance of the macro structures that they constitute: tissues, **11**, organs and the overall organism. Cells will also be compromised in their ability to perform specialized functions—leading to inflammation, compromised immune function and increased susceptibility to disease.

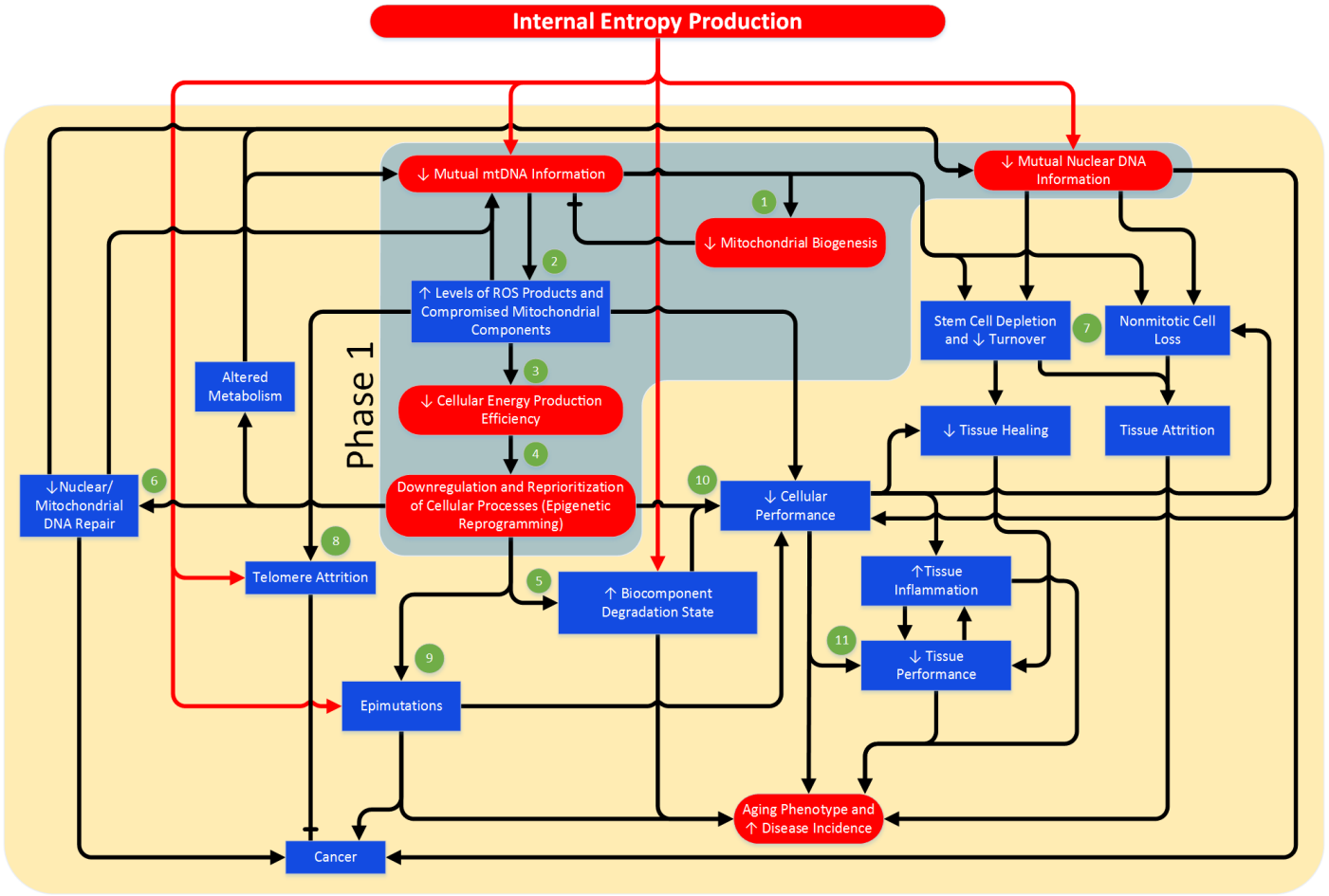

Fig. 11. A more detailed look at the higher-level interactions implicated in this theory during the progression of the aging phenotype.

The red lines are used to highlight where the degradative effects of internal entropy production are exerted. Bold numbers in Chapter 8 text refer to this figure.

Chapter 9 - Connecting the Dots

Section 1 - Differentiating between Longevity Determinants and Longevity Optimizers

It is proposed here that two groups of factors contribute to the intrinsic longevity of a species: 1) longevity determinants and 2) longevity optimizers. The first term has been utilized in previous literature but the definition used here is somewhat different. It is important to differentiate between these distinct, but occasionally overlapping, groups. Longevity determinants are defined as factors that directly or indirectly specify or influence the basal rate of loss of fidelity in any biocomponent (biomolecule, organ, tissue, etc.) susceptible to irreversible fidelity loss (such as DNA). This is accomplished either by manipulation of the magnitude of the thermodynamic forces affecting these structures, the level of redundancy, replication rate, or by influencing the ability of said biocomponents to resist the thermodynamic forces present in their microenvironments. The genetic arrangements that ultimately determine an organism's basal longevity are driven by fundamental physical law and evolutionary factors, and are further contingent on the exact environment and environmental interaction factors in which the species exists (Fig. 12). Every genetic factor that specifies a phenotypic characteristic that influences the basal rate of aging can be viewed as a longevity determinant, as can the phenotypic characteristics themselves. Some of the macro-level characteristics that may be classified as longevity determinants are peak biological power density, physical size, athletic ability, and metabolic rate. At the micro-level, longevity determinants may include: stem cell reserves, membrane composition, biomolecular performance, biomolecular stability, degree of

genetic redundancy within DNA molecules, and the thermodynamic potentials on biocomponents subject to irreversible fidelity loss. Environmental determinants of species basal longevity include temperature/climate, resource availability (food, oxygen, etc.), predation pressure and other factors that mandate tradeoffs between fecundity/mortality and longevity. Survival strategies, and behavior in general, can also influence basal longevity by providing competitive advantages that result in reduced negative repercussions associated with characteristics that serve a role in longevity determination.

A number of the relationships between longevity determinants and basal longevity across species can be represented with simple mathematic formulae. For example, the general relationships between longevity and body mass, and longevity and metabolic rate, are well characterized. At the micro-level, relationships between membrane composition and longevity are well known. Due to the fact that no single factor alone determines longevity in an organism, it is not surprising that these relationships are unable to hold invariably across taxa.

In contrast to a longevity determinant, a longevity optimizer is any genetic element that increases basal longevity by contributing towards an effect that generally becomes progressively more dominant over an organism's lifespan and effectively delays the severity, or rate of progression, of the aged phenotype. As an individual ages, longevity optimizers reallocate resources and alter physiology such that the organism's overall state maximizes instantaneous survival rate and fecundity at all ages. In summary, longevity determinants define an organism's basal longevity while longevity optimizers seek to further maximize longevity through dynamic adjustments during the aging process which ultimately serve to balance the aging phenotype.

Typically, the putative "aging pathways/genes"[8] have been branded as such because they were found to contain genetic elements which, when altered, modulated longevity in some model organism (often of low complexity, e.g. fruit fly or nematode) or produced a distinct effect on a characteristic(s) typically associated with the aging phenotype. The problem with this method of identifying aging pathways/genes is that it fails to incorporate, and does little to elucidate, many of the high-level factors that are likely involved in the determination of organismal longevity. Observations of singular connections between genetic elements and particular phenotypes demonstrates only that the gene is responsible for modulating those characteristics—it should not imply that the gene is responsible for aging, nor does it necessarily reveal anything about the aging process.

I posit that the current catalog of putative aging pathways/genes fails to include a large number of genetic elements involved in determining longevity; even worse, this has directed research focus away from the high-level factors that are truly important. For example, physical size implies physiological limits on peak biological power density and metabolism that must be balanced with other factors affecting longevity. Yet, despite this and the clear allometry of longevity across species, the genetic elements specifying physical size, and aspects of physiology related to physical size, are not generally considered to be longevity determinants. The logic commonly utilized to identify so-called aging pathways/genes diverts attention from more overriding principles that may help to

---

[8] As I subscribe to the belief that aging is a chance-driven catabolic process rather than a genetically-engrained behavior (Hayflick, 2007a; 2007b), I view the terms "aging pathways" and "aging genes" as misnomers. I use these terms here only to make reference to current literature. "Longevity determinants" and "longevity optimizers" are more appropriate terms for these factors, and this is used when referring to concepts discussed in this paper.

explain the differences in longevity between species and instead focuses on individual components—obfuscating the true relevance of any particular factor to the overall process of aging. For these reasons, I believe that the current putative aging pathways/genes represent, at best, a grossly incomplete set of the factors truly relevant to longevity determination.

The framework proposed here attempts to establish a hierarchy to aid in the identification and categorization of the actors involved in the determination of species longevity. Longevity determinants are considered separately from the forces that drive aging (fundamental physical law and evolutionary theory) (Fig. 12). The subdivision of longevity determinants into genotypic, phenotypic, and environmental elements allows for a clearer depiction of the interplay between the drivers and these different factors. Longevity optimizers are classified into a separate group as well. Although these elements also affect longevity (they could be thought of as "secondary" longevity determinants), considering the factors specifying basal longevity separately from those that dynamically optimize the aging process brings further conceptual clarity to the theory of aging presented here.

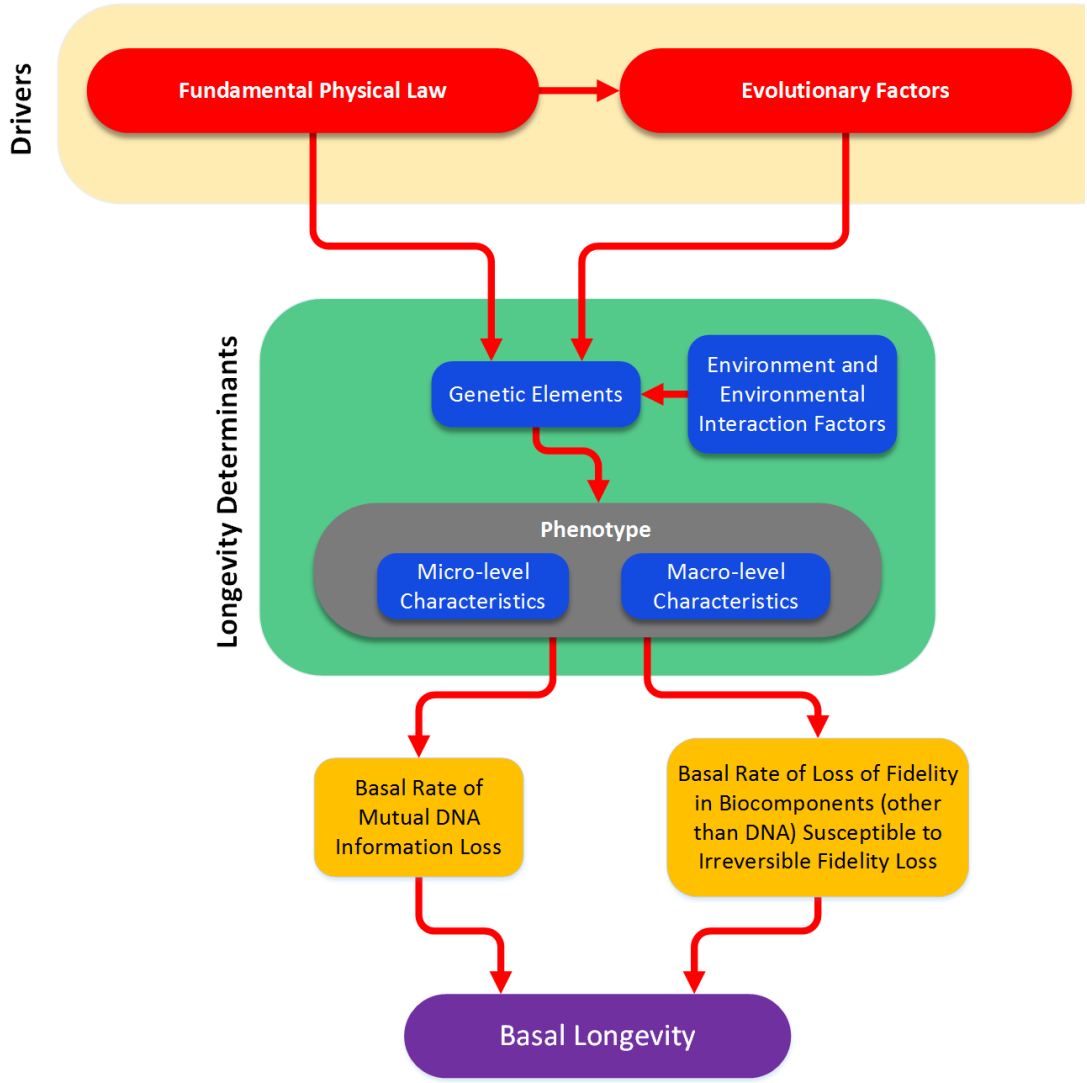

Fig. 12. The proposed relationship between longevity determinants, the root causes of aging (explained by fundamental physical law and evolutionary theory) and basal longevity in multicellular organisms.

Section 2 - The Number of Genetic Elements Serving as Longevity Determinants/Optimizers Likely Correlates Positively with Organismal Complexity

It follows from the previous discussion that highly complex organisms would be expected to possess a larger number of longevity determinants and optimizers compared to less complex organisms. The reasons for this are fairly intuitive and can be explained by considering the characteristics implicated in increasing organismal complexity. Complex organisms are likely to have more cell and tissue types and to have increased specialization in these structures. Cellular interactions are more numerous and more sophisticated. Signaling pathways and their associated biomolecules, though often highly conserved, may utilize additional component derivatives to increase complexity. Due to this sophistication, more complex organisms will tend to have an increased number of opportunities for problems to occur. Complex organisms require additional "protective" mechanisms to temper this increase in vulnerability, further contributing to increased organismal complexity.

As an individual ages, functional deficits will eventually become unavoidable. The repair and replacement of biocomponents less vital to survival or preservation of fecundity may be deprioritized before more vital biocomponents. To minimize the severity of the aging phenotype in an older individual, alterations in resource allocation must be continuous and dynamic, and other physiological adjustments must also occur to effectively prioritize the functionality of those biocomponents most critical to survival. For these reasons, even simple organisms could conceivably display a relatively high level of sophistication in their longevity optimization pathways.

In organisms with a greater number of biocomponents and potential interactions, additional corrective factors must exist to manage these elements and provide an ideal configuration during all phases of aging. Furthermore, these adjustment mechanisms must also allow for a variable and dynamic response, in accordance with an organism's current state of degradation. This logic suggests that the number of longevity determinants and optimizers should, in general, positively correlate with organismal complexity across species. The FOXO subfamily of forkhead transcriptions factors is a core player in one such conserved pathway that is implicated in longevity, but shows variation in its sophistication (Calnan and Brunet, 2008). While invertebrates have only one *FoxO* gene, there are four *FoxO* family members in mammals, each with distinct but occasionally overlapping functions. *Sirtuins* are another gene family implicated in longevity determination that demonstrate significantly greater diversification in mammals compared to invertebrates.

If there are indeed a greater number of longevity determinants and optimizers in more complex organisms, then it follows that significant longevity increases in complex organisms would require manipulation of a multitude of longevity determinants and, likely, alterations to longevity optimization pathways. On the other hand, this may explain how the longevity of simple organisms might benefit significantly from manipulation of only one or a few longevity determinants. Examination of conserved pathways known to be related to longevity support this hypothesis. In invertebrates, insulin-like growth factor 1 (IGF-1) and insulin bind to a single receptor, whereas in mammals distinct receptors are used for IGF-1 and insulin. Specific mutations in this receptor can reduce metabolism and greatly increase longevity in *Caenorhabditis elegans* (Kenyon et al., 1993; Kenyon, 2010)

while longevity increases in the more complex *Drosophila melanogaster* are much lower (Tatar et al., 2001). Manipulation of the IGF-1 and insulin pathways in mice imparts only a modest increase in longevity (Blüher et al., 2003; Selman et al., 2008). These observations illustrate the relationship between organismal complexity and the increasingly multifactorial nature of longevity determination.

Section 3 - The Rigidity of Longevity

Beyond the supposition that significant longevity increases in more complex organisms are likely to require manipulation of considerably more elements than in simpler organisms, physiological barriers also constrain the longevity possibilities. It may be possible to assess the plasticity, or rigidity, of longevity for a particular species by these two factors: complexity and physiology. Selective pressures have led to highly optimized physiology, based on compromises between other factors affecting fitness (peak biological power density, physical size, etc.). Consider the potential implications of lowering the mass-specific metabolic rate of a mouse to $1/8^{th}$ its normal rate (approximately that of a human). The physiology of a murine heart is appropriate for the level of performance of the individual murine cardiomyocytes that it is comprised of and for the demands of a mouse body. Reducing the metabolic rate by such a large amount would likely mandate a loss in the peak biological power density of cardiomyocytes. These cardiomyocytes would be less able to generate the contractile forces necessary to counter the energy dissipation inherent to the murine circulatory system and hence blood circulation may be insufficient for sustaining life. Only with fundamental changes to the configuration of the vasculature, which would require additional genomic alterations, could this energy dissipation factor be reduced. Yet, even with a configuration optimized for efficiency over performance, viable

metabolic rates will be constrained to those values capable of satisfying certain physical requirements. Governing models derived from principles of fluid dynamics have been proposed (West et al., 1997; West and Brown, 2005) that provide an example of this type of phenomenon. Although the circulatory system is perhaps the easiest example to conceptualize, there are many other potential negative physiological implications of manipulating singular longevity determinants such as metabolism. A number of other tissues would be similarly affected in this scenario, such as the liver and brain. This logic also offers an additional reason for why the aforementioned metabolic manipulations found to increase longevity in simple model organisms do not translate well to more complex organisms. While such modifications are well tolerated by organisms such as *Caenorhabditis elegans*, which evidently remain viable at greatly reduced metabolic rates, comparable changes to metabolic rate in mammals are likely to render the organism nonviable. It should also be noted that, even in *Caenorhabditis elegans*, reducing metabolic rate via genetic manipulation likely lowers fitness. This fitness cost would explain why *Caenorhabditis elegans* has not evolved to incorporate such changes in their genome; the tradeoff between increased longevity and other factors affecting fitness is not sufficient to select for these changes.

For these reasons, I hypothesize that longevity exhibits a degree of rigidity that increases with organismal complexity and is also closely tied to physiology. If accurate, this highlights the naivety of longevity extension efforts to identify and manipulate genes that could significantly increase human longevity without compromising health or performance, and the futility of attempting to use simple "model" organisms such as *Caenorhabditis elegans* as the vehicle for such efforts.

Chapter 10 - Summary and Conclusions

Aging is the greatest risk factor for severe pathology. Yet, most "aging research" is focused on age-associated pathologies, rather than the fundamental biology of aging (Hayflick, 2000; 2007b). Because of this, and despite the fact that a number of pathways related to longevity have been identified and elucidated, it could be strongly argued that scientists today know little more about the true reasons for aging than was known 50 years ago. This is exemplified by the lack of any consensus theory of aging. Even worse, despite the continued accumulation of serious anomalies challenging common aging theories, the scientific community remains complacent. The multitude of aging theories, the discontinuities between them, and the failure of the scientific community to agree on the root causes of aging, while disappointing, represents a clear opportunity to revisit this problem with a multidisciplinary and somewhat radical approach.

In many aging theories proposed during the last half century, evolutionary theory has been relied on heavily, and often singularly, to explain aging. Yet, an evolutionary-based model of senescence that does not incorporate, or at least consider, more fundamental physical law (e.g. physics) is incomplete. Previous attempts to undermine the relevance and importance of thermodynamics in aging (Mitteldorf, 2010) are misguided, as they fail to recognize and accept the impact of the second law on mutual information flow within an organism. Nonequilibrium thermodynamic theory stipulates that biomolecules will suffer degradative insults with time. DNA molecules cannot escape the inevitability that some of these insults will result in changes to the genetic sequence. As it is not possible to select for only neutral or advantageous configurations in the individual, the loss of mutual

DNA information requires that the viability of an individual must eventually decrease after some period of time unless the individual dies first. The species is also susceptible to the loss of mutual DNA information but through selection is able to preserve species fitness. In any case, mutual DNA information cannot be retained indefinitely in either the species or in individuals.

Although evolutionary theory predicts that senescence will arise inevitably due to declining selective pressure with age (Hamilton, 1966), this is redundant for aging to occur. Furthermore, blanket acceptance of declining selective pressure as the sole cause of aging is a logical fallacy (converse error). The rate at which mutual DNA information is lost in an individual can clearly be impacted by factors that otherwise affect species fitness. This is most easily conceptualized by examining the flow of genetic information through the individual cells of an organism and considering those factors that may increase or decrease the probability of an irreversible insult occurring to a DNA molecule. The predicted effect of some of these factors (many of which can be described by allometric trends) on the rate of mutual DNA information loss suggests the presence of a negative correlation between the rate of mutual DNA information loss and longevity. For this reason, it is reasonable to propose that the loss of mutual DNA information may be a more critical determinant of longevity than declining selective pressure in many organisms.

Living organisms are nonequilibrium systems. As such, they are constantly producing internal entropy which leads to biomolecular degradation. This degradation must be continually countered in order to prevent structure from quickly deteriorating to a nonviable state. It is not possible to attain ideal biomolecular performance (a degradation state of zero) in any population of biomolecules. The degradation state of a biomolecular

ensemble is determined in part by the rate at which degraded molecules are replaced and damage is repaired. Biomolecular degradation state also depends on how well biomolecules resist thermodynamic potentials and the magnitude of the potentials themselves—as stipulated by biomolecular structure, the microenvironment and the time distribution between the high thermodynamic potential "active" molecular state and the resting state. These parameters are specified by an organism's genotype and may vary considerably between organisms.

Aging is perceived to commence when an individual is no longer able to maintain a youthful steady state—although individuals actually begin to lose mutual DNA information at conception. Biomolecular and cellular turnover rate alone cannot explain why youthful steady-state homeostasis is lost. An obvious vulnerability lies in any biocomponent that lacks renewal capacity. Given the short half-life of most biomolecules other than DNA, those that can be expressed are unlikely to be the vulnerable factors in organisms with at least moderate longevity. As DNA molecules are the information-containing biomolecules encoding all other biomolecules, the absolute integrity of the information in DNA molecules would have to be retained universally within an individual to avoid a shift from the existing steady state. This, of course, is not possible. Cellular pooling (via stem cells) increases DNA information redundancy and must be scaled appropriately within an organism to ensure that mutual DNA information is preserved for a sufficiently long period of time and at adequate levels to satisfy the longevity requirements of the organism. With age, undersized stem-cell pools would result in progenitor cells that prematurely reach the Hayflick limit (Hayflick and Moorhead, 1961) and/or stem cells with excessive losses in mutual DNA information.

Increased biomolecular activity results in a higher rate of loss of mutual DNA information due to increased exposure of DNA molecules to the high thermodynamic stress conditions of replication and an increased rate of clonal expansion of compromised DNA molecules. This affects intracellular pools of mtDNA, as well as the fidelity of nuclear DNA. The loss of mutual DNA information will consume redundancy until a pathological phenotype is unavoidable. There are fitness tradeoffs associated with the establishment and preservation of information redundancy. Organisms must establish a balance such that their internal entropy management strategy is sufficient to preserve mutual DNA information for an adequate period of time—to meet the longevity requirements of the organism—but not so burdensome as to lower fitness. This balance is, of course, represented by a species' evolved genotype.

It is an interesting observation that organisms with shorter longevity expend more energy on biomolecular repair and replacement. Although this is the precise opposite of what the disposable soma theory of aging would predict, it is, in fact, quite expected and straightforward to explain. Internal entropy production is higher in organisms with shorter longevity due to their increased peak biological power density; this necessitates a greater rate of negative entropy production, which is represented by upregulated biomolecular repair and replacement. A consequence of the increased metabolic activity required to achieve this is that higher thermodynamic stress is placed on DNA molecules (largely through increased replication rates)—resulting in an increase in the rate of loss of mutual DNA information and reduced longevity. The establishment of a link between peak biological power density, metabolism, and longevity may help to explain the existence of many of the species longevity trends that have been found to describe metazoans. The basic

premise of the disposable soma theory is thus fatally flawed and should be rejected—longevity is not positively correlated with the proportion of energy directed towards repair and replacement, but rather is likely largely determined by an organism's overall entropy management strategy.

Longevity determinants are encoded within the genome; however, genes are not the only longevity determinants. The phenotypic characteristics represented by those genetic elements should also be considered longevity determinants. Phenotype is contingent on the environment and environmental interaction factors, and is constrained, defined, and driven by fundamental physical law and evolutionary factors (Fig. 12). The relationship between these drivers and phenotype is the fundamental core of a theoretical framework that may help to explain why organisms age and why longevity varies between species as it does. This thinking is quite a departure from the current mainstream approach, which focuses on establishing direct relationships between particular genes and their observable effects on the aging phenotype—leading to short-sighted conclusions of cause and effect that reveal very little of the true essence of organismal aging.

I propose that the putative aging pathways are also involved in molding the progression of the aging phenotype. As mutual DNA information loss escalates to the point where youthful homeostasis can no longer be preserved, longevity optimizers adjust the configuration of an organism to lessen the effects of irreversible fidelity loss on the viability of the individual. While longevity optimizers may be an important component of an organism's entropy management strategy, it is useful to view these factors as separate from the primary longevity determinants because their mode of action is distinct.

If managed deterioration, as described here, is a true component of the aging process, then there is little doubt that scientists are drawing some incorrect conclusions from studies focused on manipulation of the aging phenotype. The *retrospective* approach taken by most scientists to demystifying aging, where the end results are studied and one attempts to work backwards to establish causality, has virtually no chance of success. Manipulation of many of the genetic elements implicated in longevity can indeed alter certain aspects of the aging phenotype. Yet, the complexity of the aging phenotype and the many intercorrelations between longevity determinants and optimizers make it very difficult to draw meaningful inferences towards the true causes of aging, absent a solid theoretical framework of the aging process. Instead, this approach will lead to incorrect presumptions regarding the culpability of a particular factor as a root-level longevity determinant or "cause" of aging. A *prospective* approach is required to both recognize the possibility of the presence of managed deterioration and to understand and properly interpret experimental results involving longevity determinants and optimizers.

While evolutionary theory alone cannot explain aging, neither can other theories that approach this problem from a singular field of study—a multidisciplinary approach is required. The theoretical framework discussed here utilizes concepts from physics, information theory, as well as evolutionary theory. This theory differs from most others in that it does not ask, "what could possibly go wrong?" but rather, "what will inevitably go wrong and why?" While the theory put forth here is well supported by the findings of others in diverse fields, it is admittedly not devoid of speculative components. Additional data, such as the species differences in mitobiogenesis rates, would bring better clarity to

important questions that remain and would be very helpful in refining the argument presented here.

Experimental Supplement - Engineering of a Mitochondrial-Targeted Proteoliposome Nanocarrier for the Treatment of Mitochondrial Disease

Section 1 - Objectives

An effective gene therapy for diseases associated with virtually any mutation in the mtDNA requires technology to deliver complete, healthy mitochondrial genomes to the mitochondrial matrix in order to shift the level of heteroplasmy below the threshold which typifies the presence of a disease phenotype. An injectable, systemic therapy is proposed which takes the form of a nanocarrier loaded with mtDNA and is capable of crossing the plasma membrane of most cell types. Following translocation into the cytoplasm, the proposed vehicle will fuse with both the outer mitochondrial membrane (OMM) and the inner mitochondrial membrane (IMM) to deliver a mtDNA payload. Where possible, a system that mimics the natural mechanisms used by cells for these processes is desirable.

The initial steps towards realizing the first challenge in creating such a vehicle, the development of a proteoliposome nanocarrier that will recognize and fuse specifically with the OMM, are described herein. Realization of the completed construct is a multiyear project requiring large commitments in both personnel and monetary resources. The objective of this experimental study was to make progress towards establishing the feasibility of the primary concept.

Section 2 - Rationale

Since its inception in the late 1980's, the field of mitochondrial medicine has progressed rapidly (Dunn and Pinkert, 2012; Irwin et al., 2013; Wallace, 2010). Molecular

mechanisms are unraveling for a host of mutations in the nuclear DNA and mtDNA that negatively impact mitochondrial function. Although the vast majority of mitochondrial proteins are nuclear-encoded, 13 polypeptides (all of which are subunits of mitochondrial respiratory chain enzymes) are encoded by the ~16.5 kb closed circular mitochondrial genome. Mutations occur at higher frequency in mtDNA than in the nuclear genome, and affect not only protein genes but also mitochondrial tRNAs and rRNAs. Mutations in mtDNA generally influence cellular ATP production and manifest preferentially in tissues with high bioenergetic requirements, such as nerve, muscle, heart, liver, kidney and endocrine. The gradual accumulation of somatic mtDNA mutations has been implicated in the overall aging phenotype and in many diseases, including Alzheimer's and Parkinson's. None of the well-established technologies for altering the nuclear genome of laboratory animals readily adapt to mitochondrial genetic engineering.

There are a number of significant hurdles that must be overcome in order to manipulate mitochondrial genetics in a meaningful way. The mitochondrial genome is effectively sequestered within two lipid bilayers: the outer mitochondrial membrane (OMM) and the inner mitochondrial membrane (IMM), making access to the mtDNA difficult. In addition, homologous recombination of mtDNA is poorly understood (Mbantenkhu et al., 2011) and generally considered to be a rare event, making integration of foreign DNA unlikely. While the nuclear genome exists as a single, diploid copy in most cells, and nuclear genes behave according to the laws of classical Mendelian genetics (excluding epigenetic influences), characteristics of the mtDNA more closely adhere to principles of population genetics. Cells contain hundreds to thousands of copies of mtDNA and mutations in mitochondrial genes are typically heteroplasmic, i.e. they exist alongside wild-type mtDNA within the

cell. The proportion of mutated mtDNA is critical to the manifestation of mitochondrial disease—exceeding the so-called "threshold level" of heteroplasmy (~70% for many mtDNA mutations) can cause a cell to rapidly degenerate from normal to a disease phenotype. The critical factor influencing the approach described here is that this threshold phenomenon can potentially be exploited. Changing the balance between wild-type and mutated mtDNA by just a small fraction could achieve a dramatic therapeutic benefit (Bacman et al., 2011; Comte et al., 2012; Desquiret-Dumas et al., 2012; Smith and Lightowlers, 2010).

To date, strategies to deliver engineered gene constructs to compensate for mtDNA mutations have focused mainly on utilizing existing mitochondrial protein and RNA import pathways. While feasible, this approach has limited utility (Wang et al., 2012). Ectopic expression of engineered gene constructs to correct deficiencies caused by defective mtDNA-encoded proteins has shown progress, most notably with expression of a mitochondrial-targeted electron transport chain (ETC) complex I subunit ND4 in the treatment of a mouse model of Leber's Hereditary Optic Neuropathy (LHON) (Guy et al., 2009; 2002). However, these approaches are inherently limited as the pathways that they exploit are intended for translocation of molecules significantly smaller than a mitochondrial genome packaged as a nucleoid (~70nm), and size constraints have become readily apparent. Furthermore, as these strategies do not introduce mtDNA, heteroplasmy levels are unaffected and mutation loads may continue to increase unhindered. A new paradigm is needed: a mitochondrial gene therapy strategy that is both long-lasting and has the potential to treat virtually any type of mtDNA mutation by *in vivo* delivery of entire mitochondrial genomes.

Proposed here is a set of discrete functional components that can be integrated into a single nanocarrier to enable passage across the plasma membrane followed by fusion with both the OMM and the IMM to achieve effective payload delivery to the mitochondrial matrix. This nanocarrier will consist of an outer liposomal "shell" formulated to take advantage of recent *in vivo* delivery optimization efforts (Allen and Cullis, 2013), containing concentric inner proteoliposomes designed for OMM fusion and IMM fusion (see Fig. 13). Confronted with the potential pitfalls that may be encountered at each step of the development of such a vehicle, one must solve the individual challenges in isolation. Although the ultimate goal of this research is to deliver functional mitochondrial genomes packaged as nucleoids to the mitochondrial matrix complete, the initial project will focus specifically on development of a proteoliposome nanocarrier that will fuse with the OMM. The challenges of passing through the plasma membrane (while avoiding endosomal entrapment) and fusion with the IMM can only be meaningfully addressed with a vehicle that has first been shown to effectively fuse with the OMM.

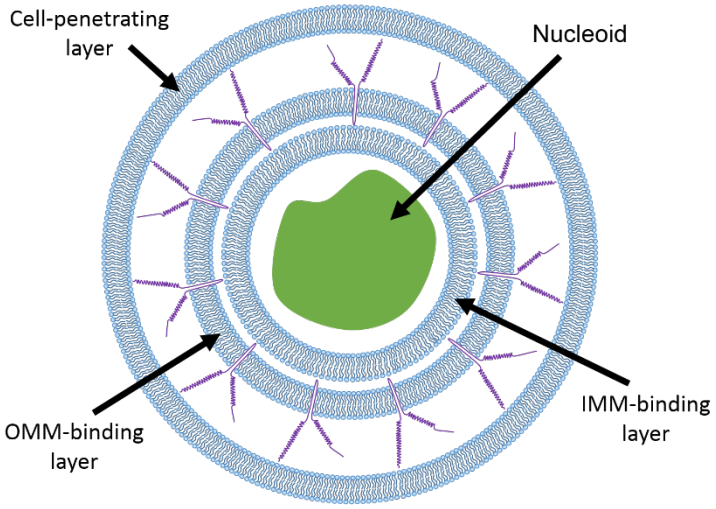

Fig. 13. Proposed mitochondrial genome delivery nanocarrier

Section 3 - Innovation

Current treatments for human mtDNA diseases are palliative. A comprehensive approach—targeted delivery of complete mitochondrial genomes to the mitochondrial matrix in order to shift heteroplasmy below the threshold level—is lacking. Ectopic expression of a mitochondrial-encoded protein (in the cytoplasm or stably integrated into the nuclear genome) with mitochondrial signaling sequences appended may work in some instances. However, it is unclear if such an approach would have any value in treating some of the most devastating mtDNA diseases, such as MELAS (Mitochondrial Encephalopathy with Lactic Acidosis and Stroke-like episodes) and MERRF (Myoclonus Epilepsy with Ragged Red Fibers) which are caused by mutations in mitochondrial tRNAs. The most notable gene therapy success story to date used adeno-associated virus (AAV) with a mitochondrial targeting peptide fused to the viral VP2 capsid protein to deliver a wild-type *ND4* gene to mitochondria, achieving rescue in a mouse model of LHON (Yu et al., 2012). The major shortcoming of this approach is the limited effective duration of the transfected gene and the requirement for regular treatments with the AAV vector to keep the disease phenotype in check. In addition, AAV can accommodate only up to ~5 kb of foreign DNA, making it an unlikely candidate to carry the complete ~16.5 kb mitochondrial genome. Recently, a liposome-based vehicle, the DF-MITO-Porter, was used to putatively deliver DNAse I to the mitochondrial matrix (Yamada et al., 2012); however, the mechanism by which this nanocarrier achieved fusion with the IMM was not addressed and it is doubtful that this vehicle, as designed, actually fused with the IMM. The approach proposed here is clearly innovative, calling for development of a mitochondrial-targeted proteoliposome nanocarrier capable of delivering whole mitochondrial genome nucleoids through the

plasma membrane, across both the OMM and IMM, and into the mitochondrial matrix—ultimately in living organisms, including human patients. Proposing to create such a mitochondrial gene therapy technology is clearly ambitious; however, the initial efforts focus specifically on construction of a synthetic proteoliposome utilizing a mitofusin-based OMM fusion mechanism to deliver a fluorescent marker to mitochondria in a cell-free microplate-based assay.

Section 4 - Experimental Plan

The first objective is to explore the feasibility of exploiting the mitochondrial fusion pathway for the purpose of delivering mitochondrial genetic material to living cells. This will be demonstrated by utilizing a synthesized mitochondria-like unilamellar liposomal

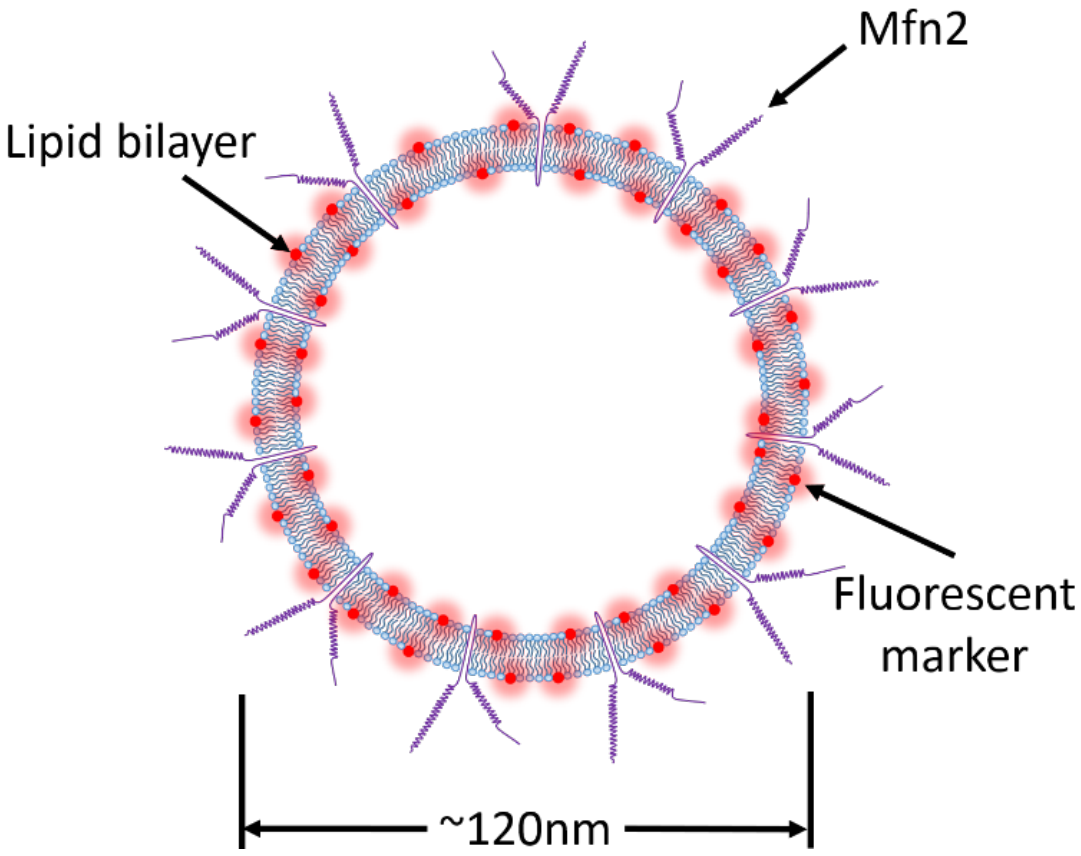

Fig. 14. Mfn2 proteoliposome

nanocarrier incorporating transmembrane mitofusin for delivery of a lipophilic fluorescent dye to the mitochondrial OMM *in vitro* (see Fig. 14). The membrane composition of the proteoliposome nanocarrier will be formulated and synthesized to closely approximate the lipid composition of the OMM. The lipophilic, non-exchangeable fluorescent dye DiD (Invitrogen/Life Technologies) will be used for labeling proteoliposomes (red fluorescence, excitation 644nm, emission 663nm). Mitochondria for this *in vitro* cell-free assay will be purified from a 32D Clone 3 (ATCC CRL-11346) suspension cell line stably transfected with *pAcGFP1-Mito* plasmid (Clontech), a plasmid that encodes for mitochondrial-targeted green fluorescent protein (GFP). To detect and measure liposome-mitochondria fusion events, flow cytometry will be used to quantitate double-labeled (GFP/DiD) mitochondria vs. single-labeled (GFP) mitochondria (Fig. 15).

While a mitochondrion might be observed as a discreet entity at a frozen time point within the cell (e.g., in an electron micrograph), a more accurate description evokes a

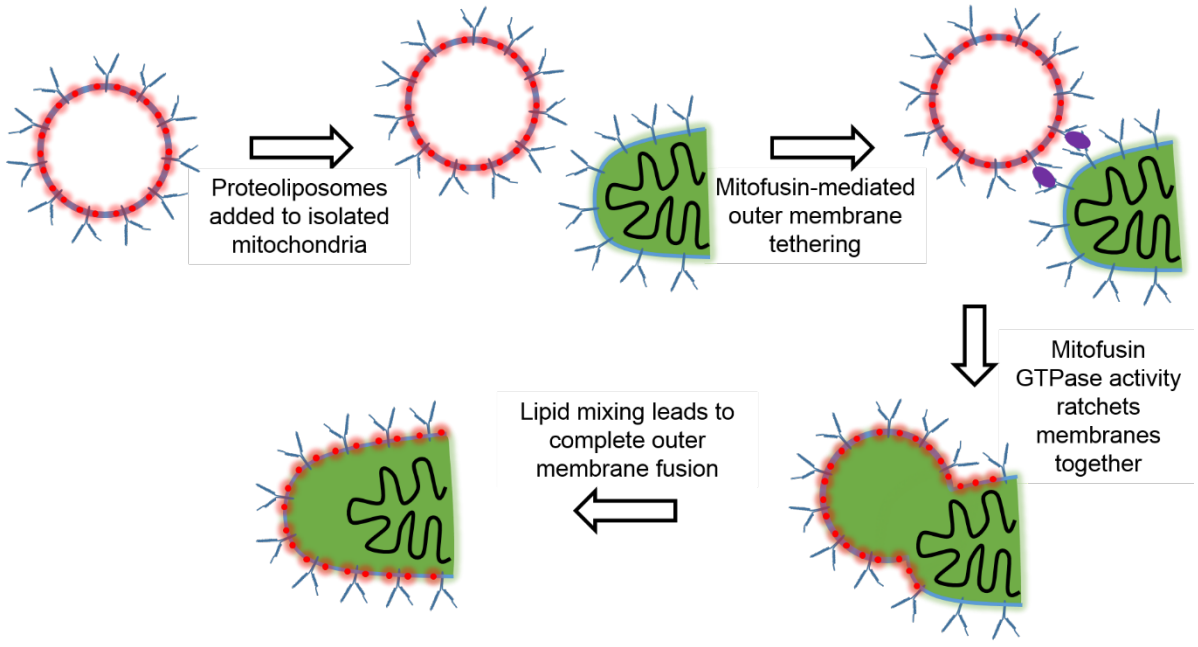

Fig. 15. Sequence of events for in vitro fusion of DiD-labeled Mfn2 proteoliposome construct with mitochondrion from 32D pAcGFP1-Mito cell line

dynamic mitochondrial network in which individual mitochondria are constantly joining together (fusion) and splitting apart (fission). During these synergistic processes, worn-out, compromised mitochondrial components, both membrane and protein, are selectively sequestered into organelles that are targeted for orderly destruction by mitophagy (Chan, 2012).

Mitochondrial fusion is a multistep, sequential process that begins with organelle tethering followed by OMM, and finally IMM, fusion (Detmer and Chan, 2007). In mammals, fusion of the OMMs of adjacent mitochondria is mediated by a pair of transmembrane GTPase proteins called mitofusin 1 (Mfn1) and mitofusin 2 (Mfn2). The mitofusins are the only conserved OMM proteins known to mediate OMM fusion (Santel et al., 2003). Mfn1 (84 kDa) and Mfn2 (86 kDa) have similar functional domains and demonstrate strong sequence homology (Rojo et al., 2002; Santel and Fuller, 2001). On the carboxy-terminal end, both mitofusins contain a GTPase domain and a heptad-repeat domain identified as HR1 (Fig. 17). The amino-terminal end consists of a second heptad-repeat domain, HR2, and a transmembrane domain (TM). Both amino- and carboxy-terminals are exposed to the cytosol. During fusion, the HR2 domains of mitofusins on adjacent mitochondria interact in an anti-parallel manner and facilitate mitochondrial tethering. For fusion to occur, mitofusin must be present on the OMM of both mitochondria. The GTPase domain is activated following a

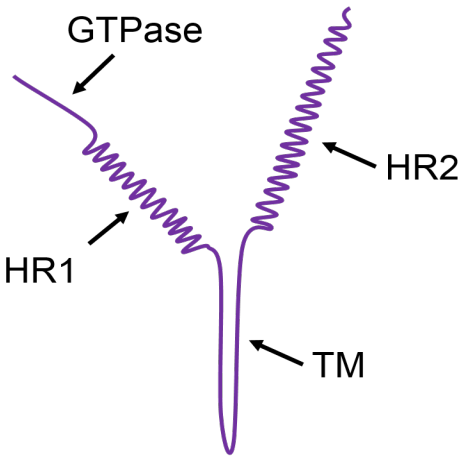

Fig. 16. Mitofusin 1/2 domain structure

tethering event and serves to effectively 'ratchet' the mitochondria together. Mitochondria of cultured murine embryonic fibroblasts (MEF) lacking both Mfn1 and Mfn2 (mitofusin double knockout, "Mfn DKO"), display a fragmented morphology and decreased cellular respiration (Koshiba et al., 2004). Expression of Mfn1 or Mfn2 alone proved sufficient for restoring normal mitochondrial morphology (Huang et al., 2011; Koshiba et al., 2004). This suggests that the incorporation of both mitofusins is not mandatory to generate a functional synthetic mitochondrial proteoliposome and hence, for the initial proposed experiments, Mfn2 will be used alone. However, as the expression of Mfn1 and Mfn2 varies by tissue type, for *in vivo* applications it is likely that both mitofusins will be necessary for effective delivery; the optimal relative proportions of each will need to be determined for maximal effectiveness. Admittedly, the choice between Mfn1 and Mfn2 for these experiments was somewhat arbitrary as both are highly conserved and the functional differences between the two have not been fully elucidated. However, more literature has been published on Mfn2, in particular with regard to HR1/HR2 domain interactions (Huang et al., 2011). Based on these and other studies (Chen and Dorn, 2013), potential mutation sites have been identified on Mfn2 that could enhance fusion efficiency.

Initial liposome composition will consist of: 51% phosphatidylcholine (PC), 11% phosphatidylinositol (PI), 33% phosphatidylethanolamine (PE) and 5% cardiolipin (CL). This composition closely replicates the composition of the OMM (Ardail et al., 1990). Trace components that are unlikely to be critical for fusion will be omitted in initial experiments. To visualize fusion of this construct with GFP-labelled mitochondria *in vitro*, a lipophilic red fluorescent membrane dye (DiD) will be incorporated into the proteoliposomes. Flow cytometry will be used to detect liposomal-mitochondrial fusion

(i.e., green/red double-labeled mitochondria). The initial liposome diameter will be ~100-200nm. This is an adequate size to accommodate a mitochondrial nucleoid (Kukat et al., 2011). It is also within the normal distribution of mitochondrial diameter, and is small enough that its use in an *in vivo* delivery system is feasible.

Section 5 - Production of soluble Mfn2 recombinant protein

One of the most challenging aspects of this project is producing soluble, full-length Mfn2 protein. There are no published reports of any mitofusins having been successfully produced in soluble, sufficiently pure form. As Mfn2 is a transmembrane protein, protein solubility was a serious concern. Although some difficulties were anticipated, the efforts required to produce soluble Mfn2 were beyond initial expectations. Since it was unknown what expression conditions could be used to produce soluble Mfn2, initial experiments began with conventional protein expression conditions. In short, the first expressions utilized verified murine Mfn2 cDNA transferred into a standard expression plasmid (pET-30, Novagen) via the ligation-independent cloning (LIC) method, followed by expression in the BL21(DE3) *E. coli* expression strain at 37°C with expression induction initiated by isopropyl β-D-1-thiogalactopyranoside (IPTG).

Approach # 1 - Expression of Mfn2/pET-30 in BL21(DE3)

Amplification of Murine Mfn2 cDNA

Murine Mfn2 cDNA from the Mammalian Gene Collection database was procured from Invitrogen. The cDNA is supplied packaged into the pCMV-SPORT6 vector, expressed in DH10B TonA *E. coli*, and in glycerol stocks. 90 μL each of 1:10, 1:100, and 1:1000 dilutions of the Mfn2 glycerol stocks were streaked onto separate LB agar plates supplemented with 100 μg/mL ampicillin and incubated overnight at 37°C. 4 colonies from the 1:100 plate were used to inoculate separate tubes containing 5ml LB broth with 100

μg/mL ampicillin. After overnight incubation at 37°C, mini-preps (Promega Wizard) were performed on all four cultures. DNA mass concentrations and plasmid purity were assessed via agarose gel electrophoresis of restriction digested (EcoRV) product. Plasmid samples at the appropriate concentrations were sent to Operon for sequencing. Verified plasmid stocks were utilized as the Mfn2 cDNA source for the creation of all future Mfn2 expression plasmids.

Generation of Mfn2/pET-30 Expression Plasmid

Mfn2 plasmid DNA was diluted to 15 ng/μL. Insert cDNA was amplified via PCR using Mfn2-specific LIC forward and reverse primers and a high-fidelity DNA polymerase (Phusion Hot Start Flex, New England Biolabs). The PCR product was purified using a QIAquick PCR Purification Kit. DNA was eluted from purification columns with 50 μL of elution buffer containing 10 mM Tris-HCl, pH 8.5. Agarose gel electrophoresis was used to verify insert length and purity, and to estimate mass concentration.

The pET-30 LIC protein expression vector (Novagen) was chosen for initial Mfn2 expression experiments. Purified Mfn2 insert was treated with T4 DNA polymerase per the manufacturer protocol. The insert was then annealed to the pre-ligated pET-30 vector supplied with the vector kit. NovaBlue Giga Singles (Novagen) were transformed separately with either annealed Mfn2/pET-30 product or one of 3 control vectors. Following a short incubation period (60 min) at 37°C and 250 RPM, samples from each culture were steaked onto LB agar plates containing appropriate antibiotics (either 30 μg/ml kanamycin or 100 μg/ml ampicillin, depending on plasmid). Plates were incubated overnight at 37°C. Three Mfn2/pET-30 colonies were picked and transferred to 500 μL of LB broth with 30 μg/mL kanamycin for a 1 hour incubation at 37°C and 250 RPM. One

half of each culture was then used to inoculate two tubes each containing 5 mL LB broth and 30 μg/mL kanamycin. Following overnight incubation at 37°C and 250 RPM, samples of each colony with 10% glycerol were aliquoted and stored at -80°C. Mini-prep plasmid isolations (Promega Wizard) were performed on the remainder of each culture sample. Purified plasmid samples were sent to Operon for sequencing. The vector insert was sequenced using 4 primers in each direction, spaced to provide thorough coverage. Sequence results demonstrated that all samples matched the expected sequence.

Protein Expression

BL21(DE3) competent cells were transformed with Mfn2/pET-30 plasmid DNA and streaked onto LB agar plates with 30 μg/ml kanamycin. After overnight incubation at 37°C, colonies were picked and used to inoculate 5 mL of LB medium with 30 μg/mL kanamycin. Cultures were incubated at 37°C and 250 RPM until OD600 readings reached 0.6. Transformed expression cultures were aliquoted into freezer vials with 10% glycerol for future experiments and stored at -80°C.

Pipette scrapings from frozen Mfn2/pET-30 BL21(DE3) samples were used to inoculate 3 mL of LB broth with 30 μg/mL kanamycin. Cultures were incubated at 37°C and 250 RPM until OD600 readings reached 0.6. This culture was then used to inoculate 100 mL of LB broth with 30 μg/mL kanamycin, and allowed to incubate again until OD600 reached 0.6. The 100 mL culture was then split in half. One of the 50 mL cultures was induced with 400 μM IPTG while the other was left uninduced. Incubation was allowed to continue until a 1:5 dilution of culture produced an OD600 of ~0.6.

Protein Localization Assessment of Mfn2 Protein

Insoluble expressed protein frequently collects into inclusion bodies when expressions are performed in *E. coli*. For this reason, assessment of protein in the total cell, soluble

cytoplasmic, and insoluble cytoplasmic fractions was conducted for determining whether the protein of interest was being expressed and the proportion that was soluble. Protein localization was performed by following the general procedure outlined in the Novagen pET system manual (pages 18-24). Cell lysis was accomplished with BugBuster Protein Extraction Reagent (Novagen) and rLysozyme (Novagen). The individual fractions were loaded onto 10% SDS-PAGE gels and run at 150 V. Sypro Orange fluorescent dye (Molecular Probes) was used to visual protein bands on a UV transilluminator. A band corresponding to the expected molecular weight of Mfn2 (86kDa) was clearly visible in the total cell and insoluble fractions, while not present in the control expression (Fig. 17). It was determined that the vast majority of the expressed protein was localized to the insoluble cytoplasmic fraction (i.e. in inclusion bodies).

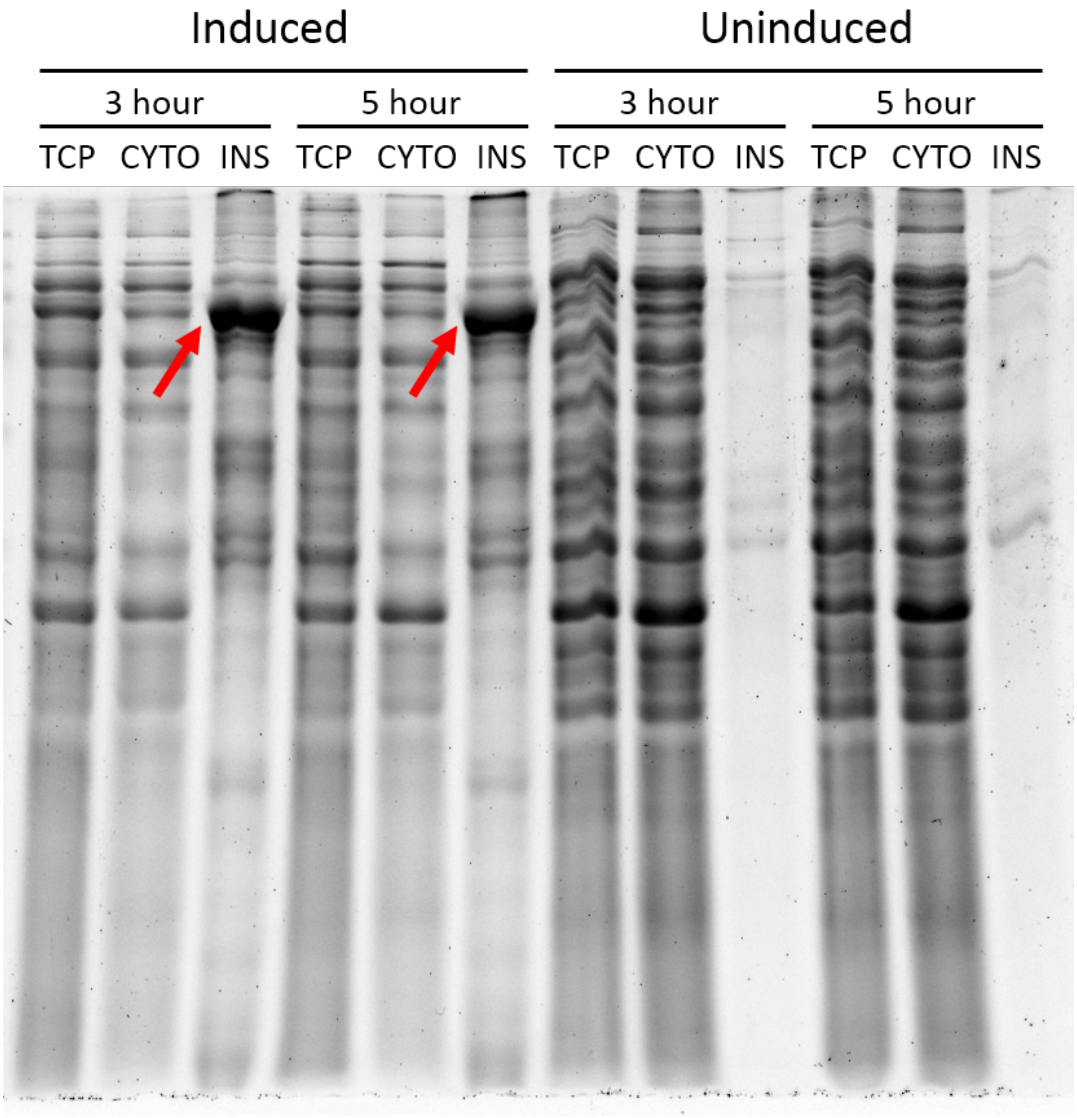

Fig. 17. SDS-PAGE of cell fractions from Mfn2/pET-30 expressions in BL21(DE3) at 37°C.

Samples were taken after 3 hours and 5 hours of incubation. Induced culture was treated with 400 μM IPTG. Arrow points to expressed Mfn2. Position corresponds to expected size of 86kDa.

Approach # 2 - A GFP-tagged Mfn2 variant (Mfn2/pLIC-eGFP) and a Titratable Promoter Expression System

The expression of soluble Mfn2 protein from with Mfn2/pET-30 plasmid in BL21(DE3) at 37°C was unsuccessful. Several changes were made to increase the likelihood of expressing soluble protein. Mfn2 cDNA was transferred to a different plasmid, pLIC-eGFP (Cormier et al., 2009), which is similar to the previous pET-30 vector but incorporates a C-terminal, TEV-cleavable eGFP tag. The eGFP allows for easy quantification of successful folding of the protein as eGFP should not fluoresce unless this portion of the protein is properly folded, which is contingent on the successful folding of the expressed protein (Drew et al., 2005). The eGFP moiety is also known to increase the solubility of protein fusions.

Mfn2/pLIC-eGFP plasmid clones were created using LIC in a similar fashion as previously discussed and established in NovaBlue cells. All plasmids were sequence verified before use.

An *E. coli* cell line with a titratable induction system, Lemo21(DE3) (New England BioLabs), was used to assist in optimizing expression conditions. Inclusion body formation can be alleviated in many cases by fine tuning T7 expression and this often helps to solubilize membrane proteins (Wagner et al., 2008). Titrating the concentration of L-rhamnose in the culture alters the rate of expression, with higher concentrations being more inhibitory.

Protein expression of Mfn2: Mfn2/pLIC-eGFP in Lemo21(DE3)

The addition of the eGFP tag to the expressed protein provided a means to quantitate the amount of correctly folded eGFP tag in the protein fusions by measuring fluorescence. Whole-cell eGFP fluorescence has found to correlate well with the amount of purifiable

active membrane protein product (Drew et al., 2005). To assess various culture conditions, 100 µL of each culture were placed into separate wells in a 96-well plate and fluorescence (488nm excitation, 512nm emission) was measured with an Infinite M200 plate reader (Tecan). Expression experiments were performed at 37°C, 30°C, and 25°C. Seven L-rhamnose concentrations, ranging from 0 to 1000 µM, were tested at each temperature. Every experiment also included two uninduced controls, one without L-rhamnose and the other with 2000 µM L-rhamnose. All experiments were performed in duplicate (at a minimum) and on different days.

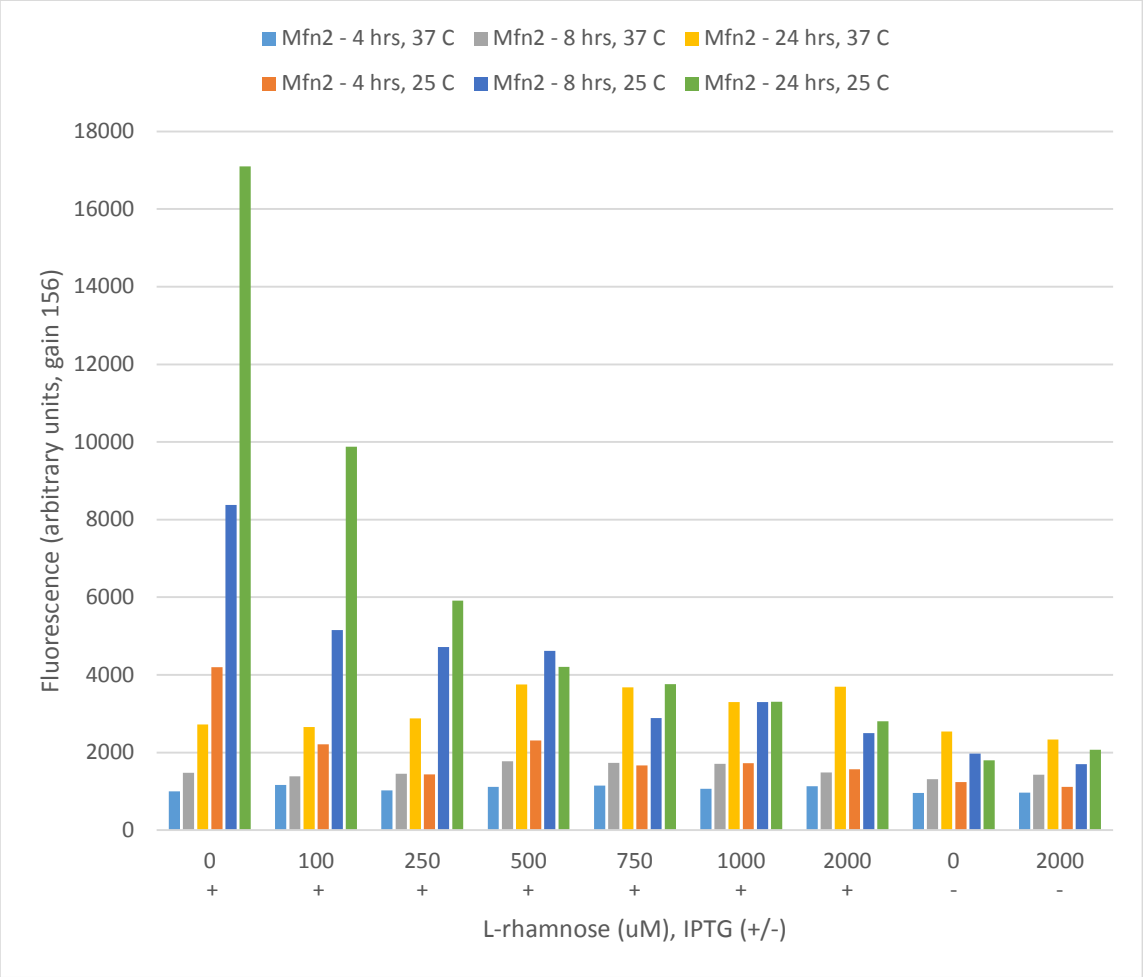

Fig. 18. Mfn2/pLIC-eGFP whole-cell fluorescence in Lemo21(DE3) under various culture conditions

Very low levels of fluorescence were present in expressions cultured at 37°C, regardless of L-rhamnose concentration (Fig. 18). Fluorescence signal increased dramatically as culture temperature was reduced, with maximal fluorescence occurring with 25°C incubations (30°C incubations not shown). The fluorescence of cultures incubated at 25°C was much higher after 24 hours of incubation then after 4 and 8 hours.

The titratable T7 promoter system did not prove to be useful. Maximal fluorescence occurred when no L-rhamnose was present. The Mfn2/pLIC-eGFP construct was next tested in BL21(DE3) at 37°C and 25°C culture temperatures. This revealed that BL21(DE3) was as effective as Lemo21(DE3) in producing maximal fluorescence and that low culture temperature and extended culture time were the most critical parameters for maximizing the fluorescence signal in these expressions (Fig. 19).

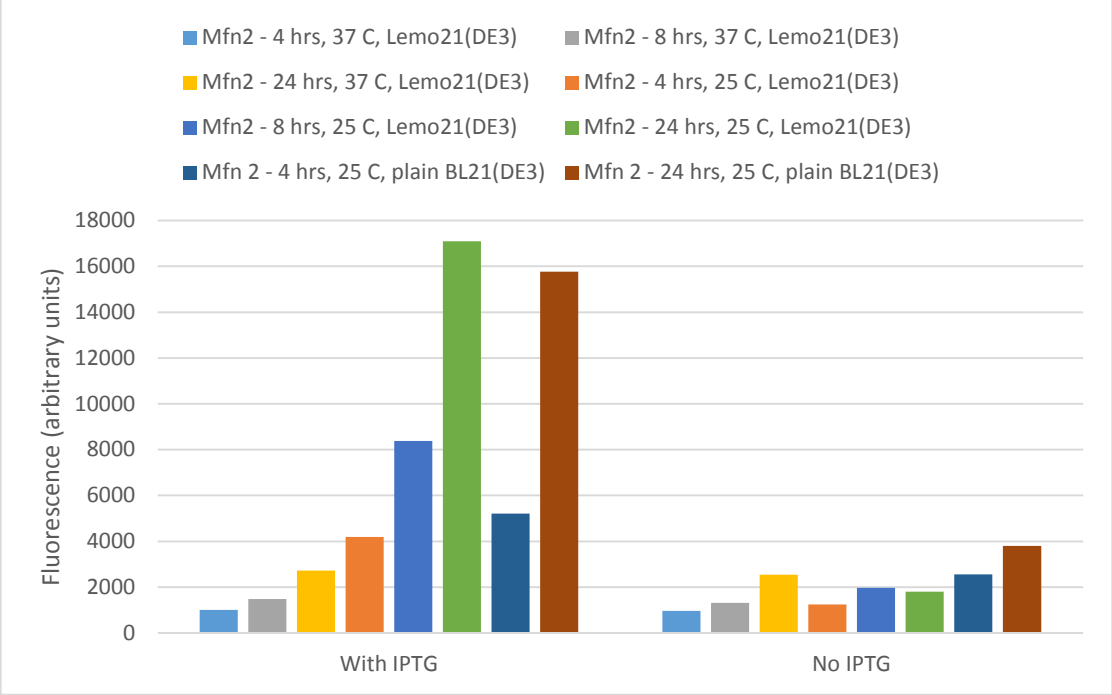

Fig. 19. Expression of Mfn2/pLIC-eGFP in Lemo21(DE3) versus BL21(DE3) at two culture temperatures

Assessing the True Solubility of Mfn2-eGFP Protein

Mfn2/pLIC-eGFP was used to transform BL21(DE3) as previously discussed, followed by protein expression with culture conditions of 25°C, 250 RPM and incubation for 24 hours after induction with 400 μM IPTG. After expression, cultures were centrifuged for 15 minutes at 6200g and 4°C. Supernatant was removed and the cell pellet was resuspended in 100 mL of ice-cold *E. coli* lysis buffer (50 mM sodium phosphate, pH 7.5, 500 mM NaCl) per gram of cell pellet. Centrifugation was repeated and supernatant was decanted again. The cell pellet was then resuspended in 2 mL of ice-cold lysis buffer per gram of cell pellet. Washed cells not immediately further processed were snap frozen in liquid nitrogen and stored at -80°C.

Washed cells were treated with rLysoszme (Novagen) at a concentration of 45-60 KU per gram of cell paste. Protease inhibitors (Protease Inhibitor Cocktail Set VII, EMD Millipore) were also included (1 mL / 10 g cells). Cells were then sonicated (550 Sonic Dismembrator, Fisher Scientic) with a 1/16" titanium probe (#4417, Qsonica, LLC) at a power setting of 7 for 3 minutes. Lysed cells were cleared by centrifuging at 15,000g for 20 minutes. Optimal sonication settings were determined by varying sonication parameters and assessing the fluorescence of the cleared supernatant (data not shown). All processing steps were performed with material on ice or at 4°C.

The fluorescence of the cleared supernatant was only approximately $1/20^{th}$ that of the total fluorescence of the washed cells prior to lysis. This suggested that the majority of the Mfn2-eGFP fusion protein is not membrane bound and is insoluble. Various combinations of reducing agents, salts, buffers, buffer strengths, and pH were used in an attempt to

improve the proportion of recovered fluorescence. None of these changes were effective in significantly increasing the amount of fluorescence in the cleared supernatant.

Expressions were repeated in Lemo21(DE3) cells with various levels of L-rhamnose to control the speed of expression. The hypothesis was that slowing down expression might increase the amount of soluble protein, even if the amount of total whole-cell fluorescence decreased. Although the level of fluorescence in the cleared supernatant in proportion to fluorescence of the lysed cells increased dramatically with 100 μM L-rhamnose, the fluorescence of the lysed cells when cultured with 100 μM L-rhamnose was much lower compared to expressions without L-rhamnose (Table 2 and Fig. 20).

Table 2. Fluorescence of lysed versus soluble (lysed and cleared) cells

L-rhamnose (uM)	0	100	250	500	750	1000	2000
IPTG (+/-)	+	+	+	+	+	+	+
Sol.	3025	3572	2242	2401	1950	2029	1953
Lysed	43796	12632	8055	6283	5686	5081	3890

The amount of fluorescence that remained in the soluble fraction of the lysed cells was far below expectations and was contradictory to published literature, which claim that the GFP moiety of a membrane protein-GFP fusion will only fluoresce if the protein has integrated into the cytoplasmic membrane and is properly folded (Drew et al., 2005; 2006). Clearly, this was not the situation in this case as the vast majority of the fluorescing protein was in the pellet following the low-speed centrifugation of the lysed cells. Although it was clear that the yield of soluble protein would be low at best with this approach, attempts were made to collect the membrane fractions of the lysate and detergent solubilize the membranes to determine if any measurable amount of soluble protein could be produced. Lemo21(DE3) cells with 100 μM L-rhamnose were used for these experiments.

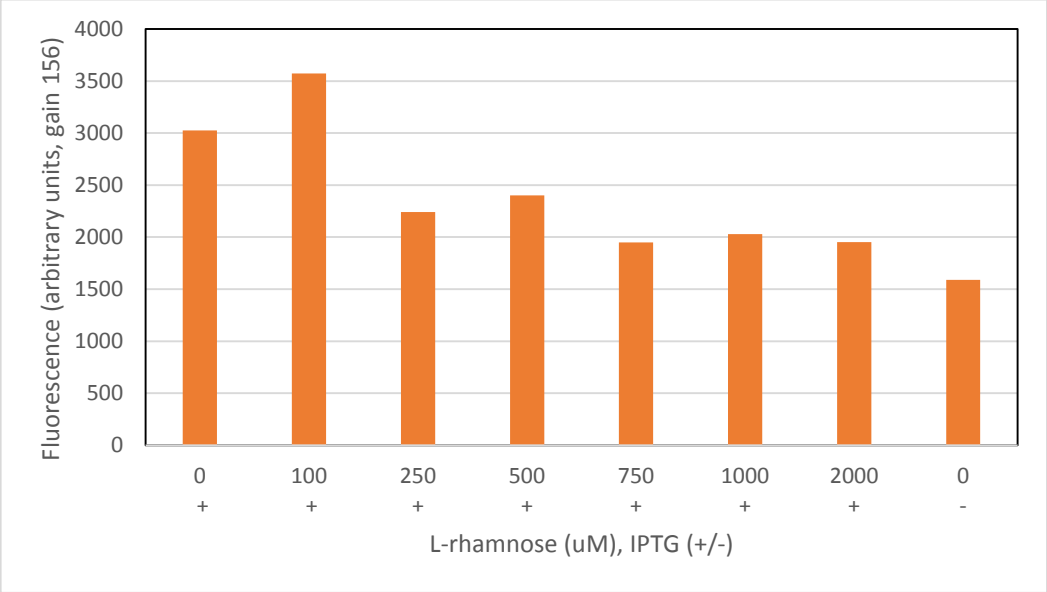

Fig. 20. Mfn2/pLIC-eGFP - Fluorescence of cleared cells with varying concentrations of L-rhamnose

Isolation of Membrane Fractions

Membrane fractions from the cleared lysates of protein expressions were collected per Drew et al. (2006). In brief, cleared lysates were centrifuged at 150,000g for 45 minutes at 4°C. Supernatant was then removed and the pellets (membranes) were resuspended in lysis buffer to the initial volume using a 21-gauge needle and a 10 mL syringe. The high-speed centrifugation was repeated and membranes were resuspended again in the same manner.

Detergent Solubilization Screen

Various detergents commonly utilized for membrane protein solubilization were screened to assess their effectiveness in exchanging membrane lipids with detergent molecules. The detergents tested were: lauryl maltose neopentyl glycol (LMNG), octyl glucose neoptenyl glycol (OGNG), CHAPS, Cymal-5, and n-Dodecyl β-D-maltopyranoside (DDM), all from Anatrace, Inc. Membranes were diluted 3-fold in lysis buffer with 1% of each detergent. Samples were allowed to incubate for 1 hour at 25°C on a rotary mixer and then centrifuged at 150,000g for 1 hour at 4°C. Supernatants were

collected and pellets were resuspended in an equal volume of lysis buffer. Fluorescence measurements suggested that Cymal-5 and DDM were most effective at solubilizing Mfn2-eGFP protein. DDM was used going forward as it is the most commonly used detergent for membrane protein solubilization.

Western Blot Assessment of Mfn2 Protein Oligomerization/Aggregation State

The aggregation state, fragmentation and relative quantity of Mfn2 (pET-30) and Mfn2-eGFP protein were assessed using both Mfn2 and His monoclonal antibodies (Cell Signaling) in standard western blotting assays. Blots were scanned using a C-DiGit blot scanner (LiCor). Although low levels of Mfn2 protein were detected in the cleared lysates and detergent-solubilized membrane samples, no detectable amount of the monomer form of Mfn2 was present in either (Fig. 21). Interestingly, Mfn2 monomer appeared to be the major form of the protein expressed. Yet, this protein was not soluble and remained in the pellet after lysis and low-speed centrifugation. The primary Mfn2 oligomer remaining in the cleared lysate and detergent-solubilized membrane samples was likely an Mfn2 dimer, as suggested by the weight of the band, although this could not be verified. Various additives (reducing agents, glycerol) were tried, and salt and detergent concentrations were varied in an unsuccessful attempt to produce detergent-solubilized Mfn2 monomer.

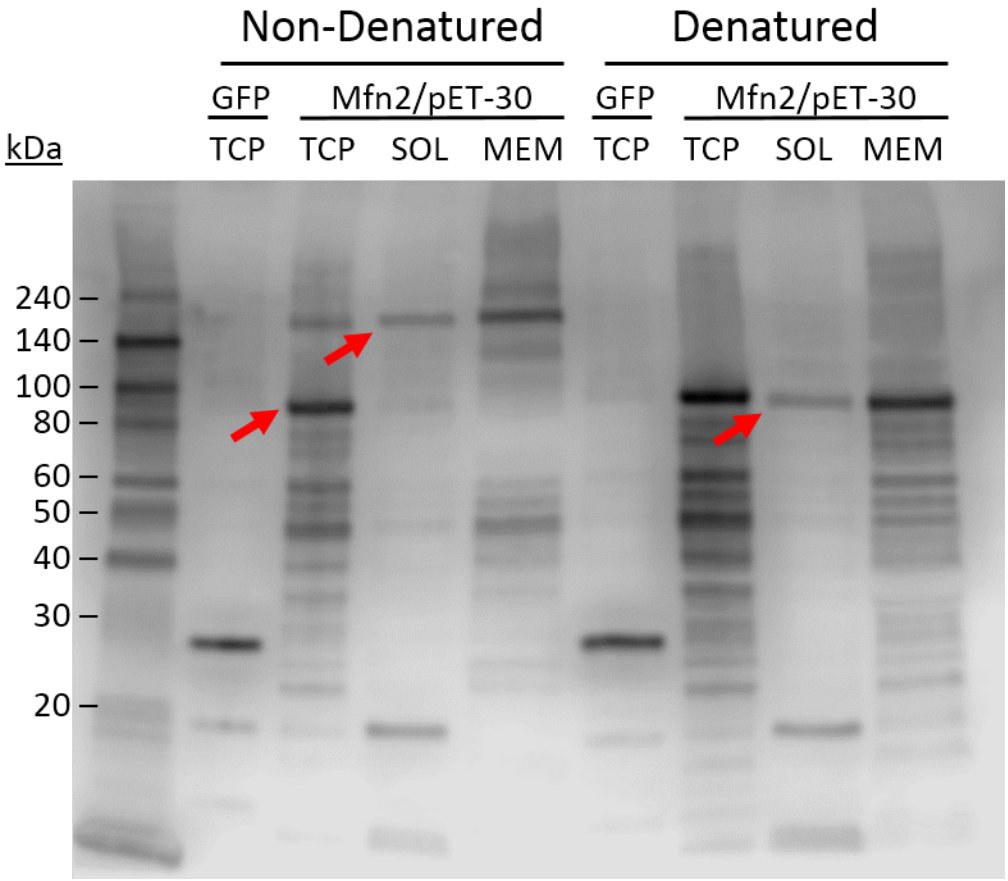

Fig. 21. Anti-His western blot of denatured and non-denatured Mfn2/pET-30 expressions

"Non-denatured" samples were incubated at 37°C for 5 mins prior to loading on gel, while "denatured" samples were incubated at 95°C for 5 mins. GFP was produced using the pLIC-eGFP plasmid without a fusion protein insert. TCP – total cell protein. SOL – soluble fraction after lysis. MEM – detergent (DDM) solubilized membranes. Results shown are typical for both His and Mfn2 mAbs and both Mfn2/pET-30 and Mfn2-eGFP expressions.

Approach # 3 – Cell Free Protein Synthesis (*E. coli*)

Since attempts to produce soluble Mfn2 protein in whole cell *E. coli* were unsuccessful, cell-free protein synthesis (CFPS) was considered. A major advantage of CFPS is that detergents and other additives can be included in the reaction during protein expression, and this often allows for the successful expression of difficult to express membrane proteins (Isaksson et al., 2012). An *E. coli* based CFPS system was determined to be the best first choice as this is the most widely used system type and Mfn2 does not require any post-translational modifications or have any disulfide linkages that would necessitate the use of mammalian or insect cells.

To test the feasibility of this approach, a commercial CFPS kit (PURExpress InVitro, New England Biolabs) was used for initial experiments. Reactions were assembled according to the kit manufacturer's recommended protocol. The size of the individual reactions were 28 μL. Separate reactions with the Mfn2/pET-30 plasmid used either 1% Brij-58, 0.1% DDM, or no detergent. The reactions were incubated for 2 hours at 37°C in an iCycle thermal cycler (Bio-Rad). 16 μL of the reactions were placed in separate tubes and centrifuged for 20 minutes at 13,000g, 25°C. Total reaction and soluble (supernatant) fractions were visualized by SDS-PAGE. Mfn2 protein was detected in all reactions containing Mfn2/pET-30 (Fig. 22a) at the expected monomer weight of ~86kDa. Mfn2 was also detected in the soluble fractions of the reactions incorporating Brij-58 or DDM. Band intensity was highest with DDM. These results suggested that *E. coli* CFPS could be used to successfully express soluble Mfn2 in monomer form.

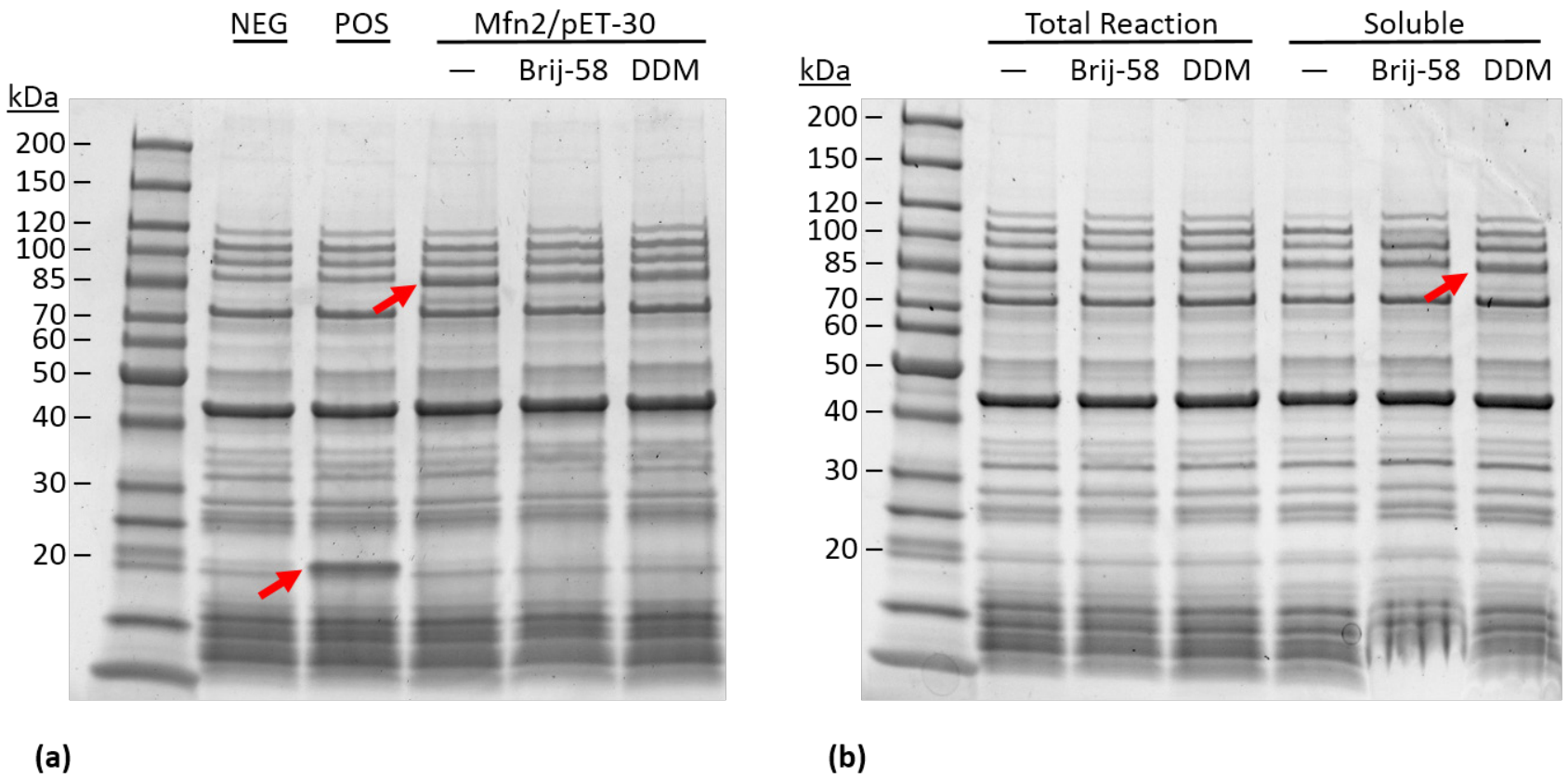

Fig. 22. SDS-PAGE results from cell-free protein synthesis trials

(a) Analysis of total reactions. Mfn2/pET-30 was expressed in the presence of 1% (w/v) Brij-58, 0.1% DDM, or (—) no detergent. NEG – negative control, no plasmid added. POS – positive control plasmid expressing DHFR (dihydrofolate reductase), MW 18kDa. (b) Comparison of total reaction and soluble fractions after 20 min at 13,000g, 25°C. All samples from (a) and (b) are non-denatured (samples incubated at 37°C for 5 minutes prior to gel loading).

Development of an In-House Cell-free Protein Synthesis System

Commercial *E. coli* CFPS systems are prohibitively expensive, costing approximating $1000 per mL of reaction with estimated yields of 10-500 μg of protein per mL of reaction. As a reasonably priced method of generating (at least) milligram quantities of Mfn2 is required, it was necessary to develop a CFPS system that could be assembled in-house. This could effectively lower the cost to ~$10 per mL of reaction.

I developed a batch-style *E. coli* CFPS system for our laboratory based on published systems and production techniques, specifically Kim et al. (2006), Isaksson et al. (2012), Li et al. (1999), Pedersen et al. (2011), Torizawa et al. (2004), and Yang et al. (2012). Some of the major components produced in the lab include:

- T7RNAP: From pAR1219 plasmid expressed in BL21(DE3). Purified in-house on an Akta Explorer 10 FPLC system using an anion-exchange column (HiPrep DEAE FF 16/10, GE Life Sciences).
- S12 cell extract: derived from Rosetta2 cells (Novagen)
- Amino acid mix, nucleotide solution, magnesium acetate solution, creatine kinase solution, creatine phosphate solution, and salt solution were all assembled/produced in-house.

The reaction concentrations of the various components in the final system are listed in Table 3. Detailed methods are included in Appendix 1. Reactions were assembled on ice and aliquoted into separate wells of a 96-well plate (TPP Cat. No. 92696) at 100 μL per well. Reaction plates were incubated on a temperature-regulating plate shaker (Thermomixer R, Eppendorf) set at 800 RPM. Completed reactions were pooled into appropriately sized tubes and kept at 4°C during future processing steps.

Table 3. CFPS reaction concentrations

	Reaction Conc.	
S12 Extract	30	% (v/v)
10mg/mL Creatine Kinase Solution	125	µg/mL
T7RNAP	100	µg/mL
DNA template	15	µg/mL
L-Glutamine	4	mM
L-Serine	2	mM
Amino Acids (except L-glutamine and L-Serine)	1	mM
Adenosine 5'-Triphosphate Disodium Salt (ATP)	1.1	mM
Cytidine 5'-Monophosphate Disodium Salt (CMP)	0.85	mM
Guanosine 5'-Monophosphate Disodium Salt (GMP)	0.85	mM
Uridine 5'-Monophosphate Disodium Salt (UMP)	0.85	mM
Creatine Phosphate	61.3	mM
tRNAs	175	µg/mL
cAMP	0.64	mM
Folinic acid	68	µM
Magnesium Acetate Solution	10-20	mM
L-Glutamic acid potassium salt monohydrate	230	mM
L-Glutamic acid ammonium salt	27.44	mM
Malic acid	4.4	mM
2-oxoglutaric acid	1.9	mM
Succinic acid	1.5	mM
Hepes-KOH, pH 7.5	52.5	mM
DTT	1.7	mM
Complete EDTA-free Protease Inhibitor	1	x
RNase inhibitor	40	U/mL
Detergent (DDM/Brij-58)	varies	%
IPTG	400	µM

Approximately three months were required to optimize the system for good yield. This was complicated by the fact that a French press was not available, which is the recommended equipment to use for cell lysis in the preparation of S12 cell extract. Sonication was used instead and this required many rounds of optimization as the expression yields were highly sensitive to the power level and duration of sonication. The pLIC-eGFP plasmid (no insert) was used to express GFP, which could be monitored by

fluorescence to assess expression yields during system optimization. Final yields were 300-400 times higher than that of the earliest in-house CFPS reactions (as determined by fluorescence readings). Following optimization, the characteristic green hue of eGFP could be easily seen with the naked eye in completed reactions. The fluorescence of eGFP reactions placed on a UV transilluminator and imaged with a 590nm bandpass filter were intense (Fig. 23).

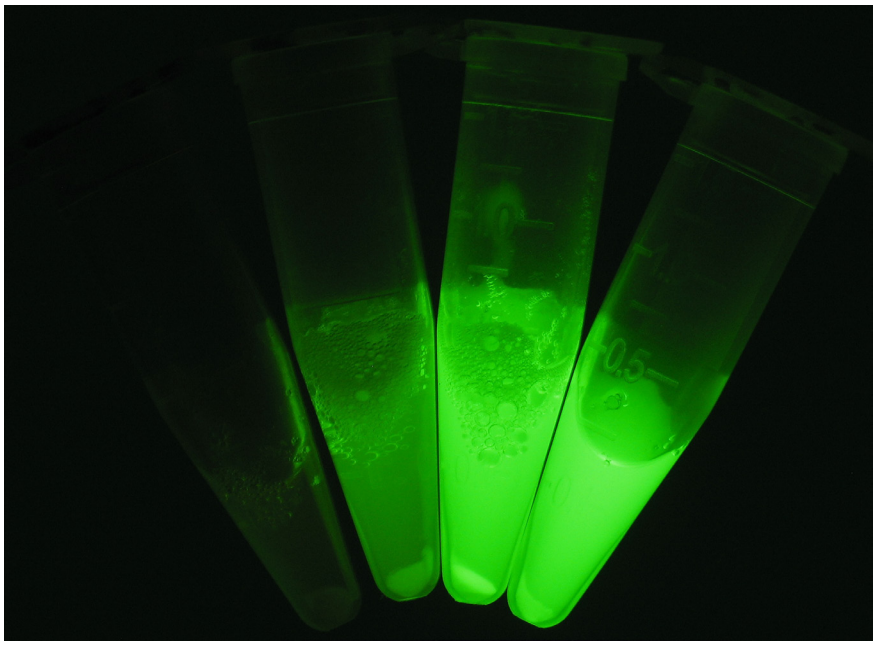

Fig. 23. eGFP fluorescence after CFPS optimization

Pooled CFPS reactions. From left to right: control (no plasmid), pLIC-eGFP with 8mM magnesium acetate [$Mg(OAc)_2$], pLIC-eGFP with 10mM $Mg(OAc)_2$ and pLIC-eGFP with 12mM $Mg(OAc)_2$.

After the core CFPS system was optimized, the expression conditions (time, temperature, and detergent type and concentration) that maximized solubility and yield of Mfn2 was determined. The greatest amount of soluble Mfn2 was expressed when the reaction temperature was 25°C (30°C and 37°C were also tested). A reaction time of 2.5 hours was determined to be optimal (expression slowed significantly after 2 hours). Incorporating Brij-58 into the reaction at a concentration of 1.5% (w/v) resulted in the best

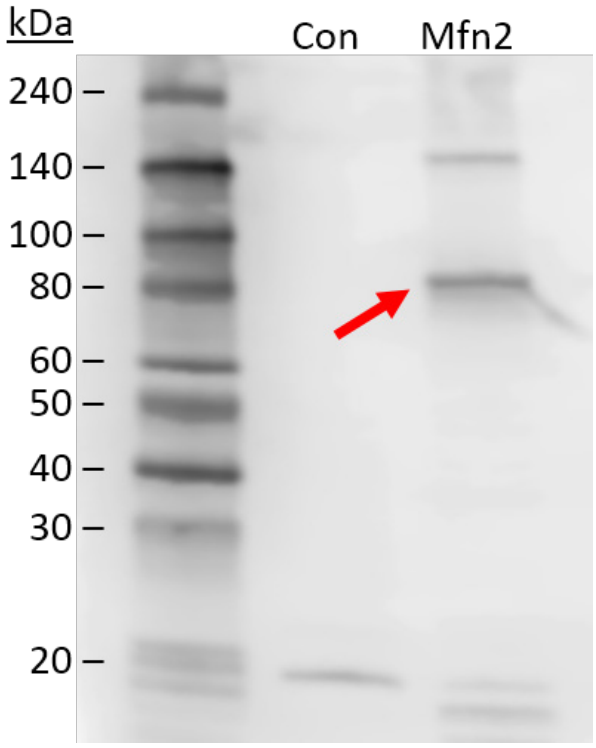

Fig. 24. Anti-Mfn2 western blot of Mfn2 expression with optimized in-house CFPS system

CFPS reactions were centrifuged for 20 minutes at 13,000g, 25°C and loaded onto gel. Con – CFPS expression with no expression plasmid.

Mfn2 solubility. Western blot analysis confirmed that the major Mfn2 product from the reactions was soluble monomers (Fig. 24). This was a significant step forward compared to earlier results that used whole-cell expressions and in which no Mfn2 monomer was detectable in the soluble lysed fraction. Using CFPS and the appropriate reaction conditions, soluble Mfn2 can be expressed in sufficient quantities for the downstream requirements of subsequent steps in this project and can be produced at a reasonable cost.

Summary of Mfn2 Expression Studies

Mfn2 proved challenging to express in soluble form. Beyond the fact that Mfn2 is a transmembrane protein, which usually increases the difficulty of expressing soluble and biologically-active protein, the HR2 domain of Mfn2 molecules can interact with the same domain on other Mfn2 molecules. This interaction may not be easy to reverse once it occurs.

Expression of Mfn2 protein in whole-cell *E. coli* under standard expression conditions resulted in Mfn2 aggregating into inclusion bodies. Lowering the culture temperature from

37°C to 25°C was the primary factor responsible for maximizing fluorescence in Mfn2-eGFP fusions expressed by whole-cell *E. coli*. Unexpectedly, the bulk of this fusion product remained in the pellet after low-speed centrifugation, indicating that it was still insoluble. The small proportion of Mfn2 that could be detergent solubilized from isolated *E. coli* membranes was not in a monomer state. Judging by the position of the band on the western blots, the primary band was likely an Mfn2 dimer. I hypothesize that the HR2 domains on membrane-inserted Mfn2 molecules interact irreversibly during whole-cell expression, resulting in dimers.

By providing a means for detergents and other additives to be present during expression, CFPS was successfully used to produce soluble Mfn2 monomer. Although this required the extreme measure of developing and optimizing a CFPS system for the laboratory, this system can now be utilized to produce soluble Mfn2 protein for the next steps of this project and may also prove to be valuable to other laboratories for production of membrane proteins.

Section 6 - Future Work

With the ability to express soluble Mfn2 protein, the only step remaining to produce usable Mfn2 for downstream experiments is to purify the protein. This is likely to be a multistep chromatography procedure. After this, the following steps are proposed:

Production of Proteoliposomes

Synthesis of liposomes: Liposomal formulations will be prepared from commercially available phospholipids (Avanti Polar Lipids, Alabaster, AL). Different liposome formulations will be prepared by the thin-film hydration method (Arnold, et al, 2005). In brief, the components of the lipid delivery system will be dissolved in chloroform, transferred to a round bottom flask, and secured in a rotary evaporator (Büchi, R-210). The chloroform will be evaporated under vacuum at a temperature greater than the phase transition (T_m) of the primary lipid. The dry film will be hydrated with an aqueous buffer, freeze/thawed (liquid nitrogen/water bath) and passed through an extruder (Lipex Biomembranes) containing 0.1-0.2 μm polycarbonate filters to achieve a uniform particle size (100-200 nm). The vesicles will be sequentially dialyzed overnight in a sterile saline (isotonic) solution to remove residual buffer at 4°C. The size of each formulation will be determined by dynamic light scattering (DLS) in triplicate. Liposome size, shape and unilamellarity will be further accessed with electron microscopy. The preformed vesicles will be used immediately or stored protected from light, refrigerated, and purged with nitrogen until use.

Incorporation of protein into liposomes: Mfn2 protein will be reconstituted into liposomes using the GRecon method developed by Althoff (2012).

Preparation of sucrose gradient: Two solutions will be prepared. For the first solution, Triton X-100 will be added to the liposomes in an equal amount (w/w) of detergent to

lipids. After a brief incubation at room temperature, sucrose and cyclodextrin will be added to the solution and dissolved by gently mixing. The second solution will consist of a lower concentration of sucrose. An equal volume of the second solution is layered on top of the first in an ultracentrifuge tube. The tube is sealed with caps to expel all air and the gradient is formed by tilted-tube rotation (Coombs and Watts, 1985).

Protein reconstitution: Purified, detergent-solubilized Mfn2 protein at the appropriate concentration will be added to the sucrose gradient solution described above and centrifuged at 150,000g for 18 hours. Opaque liposome bands will be collected with a syringe and diluted in detergent-free buffer. Proteoliposomes will be pelleted using ultracentrifugation, followed by resuspension in a small volume of buffer. To remove traces of detergent, the solution will be incubated overnight with Bio-Beads SM-2 (Bio-Rad).

Incorporation of fluorescent marker: DiD fluorescent membrane label (Life Technologies) will be dissolved, added to the proteoliposome solution and allowed to incubate at room temperature in the dark. Unincorporated marker will be removed through repeated centrifugation and washing steps. Fluorescence confocal microscopy and flow cytometry will be used to verify the presence and intensity of membrane fluorescence.

Verification of liposome physical characteristics: SDS-PAGE will be used to verify incorporation of Mfn2 into liposomes. Liposome size and morphology (electron microscopy), and fluorescence (confocal microscopy and flow cytometry) will also be verified.

Demonstration of Fusion of the Proteoliposome Nanocarrier with Isolated Mitochondria *in vitro*

Translocation of the plasma membrane is an unavoidable, and often troublesome, requirement in cell delivery. A standardized cell-free assay system for measuring fusion of proteoliposomes and mitochondria is proposed. This approach has several notable advantages over using a cell-transfection agent or incorporation of transfection-promoting properties into the proteoliposome. For one, this approach delineates the requirements of cell membrane transfer and OMM merging capability. This allows the focus of this study to be on optimizing the proteoliposome to the requirements of membrane fusion, without introducing components that could interfere with merging. This approach also has the advantage of obviating a concern regarding endosomal escape issues that could quarantine a large population of the proteoliposomes. Furthermore, this will enable high-throughput screenings to be performed and for quantitative data comparing a variety of constructs and *in vitro* conditions to be obtained.

The proposed cell-free fusion assay is an adaptation of a published cell-free mitochondrial fusion assay (Schauss et al., 2010). This assay utilizes two populations of mitochondria isolated from separate cell lines, each engineered to express one half of a split Venus and Renilla luciferase marker protein, a so-called "bimolecular complementation assay", for quantitation of mitochondrial fusion. The assay proposed for this project will use similar buffering and energizing conditions, including the use of a cytosolic fraction for incorporation of cell signaling pathways. The assay differs in that the proteoliposome construct will substitute for one of the mitochondrial populations. Additionally, a lipophilic fluorescent dye (DiD, Invitrogen/ Life Technologies) will be used for labeling the membrane of these liposomes (the split Venus/Renilla luciferase marker

will be omitted). Flow cytometry will be used to detect double-labeled mitochondria, representing liposomal-mitochondrial fusion events. Initial fusion assays will utilize DiD-labelled (red; Ex644/Em663nm) liposomes and GFP-labeled mitochondria (green; Ex395/Em509nm) purified from a 32D cell line stably transfected to express mitochondrial-targeted GFP by differential centrifugation, which yields spherical mitochondrial "vesicles" approximately 500nm in diameter (see Fig. 15). For flow cytometry, gating (if necessary) of 100-120nm liposomes should be easily accomplished.

Optimization of OMM fusion by targeted Mfn2 mutation and refinement of liposome properties.

After establishing and quantifying fusion activity, lipid composition and overall proteoliposome diameter will be modified to determine potential effects on fusion. In separate experiments, Mfn2 mutations will be introduced at specific sites that could potentially regulate fusion efficiency. Variations in molar ratio of transmembrane-incorporated Mfn2 will also be explored.

Optimizing lipid composition for fusion: Initial lipid composition will be based on OMM compositional analysis studies: 51% PC, 11% PI, 33% PE and 5% CL (Ardail et al., 1990). However, it is possible that the local lipid composition at the site of fusion is different than the overall OMM composition that has been reported. Phospholipids PC and PI are cylindrically shaped and have nearly equivalent diameters along their length, which allows molecular packing and promotes bilayer formation (Osman et al., 2011). Unlike PC and PI, PE and CL are more conical in shape and do not form bilayers. However, the tendency for PE and CL to form hexagonal phases is likely to be important for the fusion process as it creates tension in the membranes (van den Brink-van der Laan et al., 2004). In bacteria, PE and CL laterally segregate into distinct domains but little is known about

the lateral distribution of phospholipids in mitochondrial membranes (Osman et al., 2011). It has been suggested that the spatial distribution of phospholipids is important for mitochondrial fusion (Osman et al., 2011). The ability of the conically shaped lipids to more readily conform to rearrangements suggests that the local concentrations of these lipids are likely higher at the points of fusion. Therefore, the relative amounts of these lipids will be varied in the construct to determine the effect of these changes on fusion.

Optimize proteoliposome size for fusion: The effects of varying the liposome diameter on fusion will be determined by repeating fusion experiments with liposome constructs of both larger and smaller diameter than in initial experiments (100-200 nm).

Mfn2 mitophagy-related mutations: PINK1 (PTEN-induced putative kinase protein 1) is a mitochondrial-targeted serine-threonine protein kinase. PINK1 phosphorylates Mfn2 in response to mitochondrial depolarization causing ubiquitination of Mfn2 by the E3 ubiquitin ligase Parkin, ultimately leading to mitophagy (Chen and Dorn, 2013). PINK1-Mfn2 activity is attenuated through mitochondrial membrane potential-induced import of PINK1 and its subsequent degradation within the intermembrane space (Jin et al., 2010; Narendra et al., 2010). Although Mfn2 is present in the proposed proteoliposome vehicle, the molecular machinery for interacting with mitochondrial-targeting proteins is not. To rule out interactions with PINK1 leading to proteoliposome autophagy, a mutated form of Mfn2 that cannot be phosphorylated by PINK1 (Chen and Dorn, 2013) will be produced, which will include mutating Thr^{111} and Ser^{442} to alanine residues.

Mfn2 mutations to improve binding efficiency: Based on a review of recent literature, several mutations have been identified that could impact fusion rates in these experiments. Huang and colleagues (2011) found that the heptad-repeat regions (HR1 and HR2) of Mfn2

interact with each other (see Fig. 16). Furthermore, an interaction between Mfn2 and the fission dynamin-like protein DLP1 was revealed. DLP1 resides mostly in the cytosol but can become associated with the OMM surface and mediate fission through direct interactions with the mitochondrial membrane (Pitts et al., 1999; Smirnova et al., 2001; Yoon et al., 2001). Fusion is inhibited when the HR1 and HR2 domains of Mfn2 are associated with each another. In contrast, the association of DLP1 with Mfn2 promotes fusion. Huang found that two lys>pro mutations in the HR1 domain were able to individually disrupt the interaction between the HR1 and HR2 domains, thereby eliminating the fusion inhibitory effect of the HR1/HR2 interaction. Using Mfn DKO MEFs, Huang demonstrated that expression of Mfn2 containing either mutation was capable of restoring tubular mitochondrial morphology more so than transfection with non-mutated Mfn2, suggesting increased fusion. It is proposed that similar mutations be produced for use with the proposed vehicle and that the impact on proteoliposome fusion be evaluated.

References

Ahima, R.S. (2009). Connecting obesity, aging and diabetes. Nat Med *15*, 996–997.

Allen, T.M., and Cullis, P.R. (2013). Liposomal drug delivery systems: from concept to clinical applications. Adv Drug Deliv Rev *65*, 36–48.

Althoff, T., Davies, K.M., Schulze, S., Joos, F., and Kühlbrandt, W. (2012). GRecon: A Method for the Lipid Reconstitution of Membrane Proteins. Angew Chem Int Ed *51*, 8343–8347.

American Cancer Society (2013). Cancer Facts and Figures 2013 (Atlanta: American Cancer Society).

Andziak, B., and Buffenstein, R. (2006). Disparate patterns of age-related changes in lipid peroxidation in long-lived naked mole-rats and shorter-lived mice. Aging Cell *5*, 525–532.

Andziak, B., O'Connor, T.P., Qi, W., DeWaal, E.M., Pierce, A., Chaudhuri, A.R., Van Remmen, H., and Buffenstein, R. (2006). High oxidative damage levels in the longest-living rodent, the naked mole-rat. Aging Cell *5*, 463–471.

Andziak, B., O'Connor, T.P., and Buffenstein, R. (2005). Antioxidants do not explain the disparate longevity between mice and the longest-living rodent, the naked mole-rat. Mech Ageing Dev *126*, 1206–1212.

Ardail, D., Privat, J.P., Egret-Charlier, M., Levrat, C., and al, E. (1990). Mitochondrial contact sites. Lipid composition and dynamics. J Biol Chem *265*.

Arias-Gonzalez, J.R. (2012). Entropy involved in fidelity of DNA replication. PLoS ONE *7*, e42272.

Ashrafi, G., and Schwarz, T.L. (2012). The pathways of mitophagy for quality control and clearance of mitochondria. Cell Death Differ *20*, 31–42.

Austad, S.N. (2005). Diverse aging rates in metazoans: targets for functional genomics. Mech Ageing Dev *126*, 43–49.

Austad, S.N. (2009). Comparative biology of aging. J Gerontol a Biol Sci Med Sci *64*, 199–201.

Bacman, S.R., Williams, S.L., Duan, D., and Moraes, C.T. (2011). Manipulation of mtDNA heteroplasmy in all striated muscles of newborn mice by AAV9-mediated delivery of a mitochondria-targeted restriction endonuclease. Gene Ther *19*, 1101–1106.

Bahar, R., Hartmann, C.H., Rodriguez, K.A., Denny, A.D., Busuttil, R.A., Dollé, M.E.T., Calder, R.B., Chisholm, G.B., Pollock, B.H., Klein, C.A., et al. (2006). Increased cell-to-cell variation in gene expression in ageing mouse heart. Nature *441*, 1011–1014.

Bailey, K.J., Maslov, A.Y., and Pruitt, S.C. (2004). Accumulation of mutations and somatic selection in aging neural stem/progenitor cells. Aging Cell *3*, 391–397.

Bailly, A., and Gartner, A. (2013). Germ cell apoptosis and DNA damage responses. Adv Exp Med Biol *757*, 249–276.

Balch, W.E., Morimoto, R.I., Dillin, A., and Kelly, J.W. (2008). Adapting Proteostasis for Disease Intervention. Science *319*, 916–919.

Baum, D.A., Futuyma, D.J., Hoekstra, H.E., Lenski, R.E., Moore, A.J., Peichel, C.L., Schluter, D., and Whitlock, M.C. (2013). The Princeton Guide to Evolution (Princeton University Press).

Beerman, I., Seita, J., Inlay, M.A., Weissman, I.L., and Rossi, D.J. (2014). Quiescent Hematopoietic Stem Cells Accumulate DNA Damage during Aging that Is Repaired upon Entry into Cell Cycle. Stem Cell *15*, 37–50.

Bell, J.T., Tsai, P.-C., Yang, T.-P., Pidsley, R., Nisbet, J., Glass, D., Mangino, M., Zhai, G., Zhang, F., Valdes, A., et al. (2012). Epigenome-wide scans identify differentially methylated regions for age and age-related phenotypes in a healthy ageing population. PLoS Genetics *8*, e1002629.

Ben-Zvi, A., Miller, E.A., and Morimoto, R.I. (2009). Collapse of proteostasis represents an early molecular event in Caenorhabditis elegans aging. Proc Natl Acad Sci USA *106*, 14914–14919.

Bennett, M.B., Ker, R.F., Dimery, N.J., and Alexander, R. (1986). Mechanical properties of various mammalian tendons. J Zool (London) *209*, 537–548.

Biewener, A.A. (1989). Scaling body support in mammals: limb posture and muscle mechanics. Science *245*, 45–48.

Biewener, A.A., and Blickhan, R. (1988). Kangaroo rat locomotion: design for elastic energy storage or acceleration? J Exp Biol *140*, 243–255.

Biewener, A., Alexander, R.M., and Heglund, N.C. (1981). Elastic energy storage in the hopping of kangaroo rats (Dipodomys spectabilis). J Zool (London) *195*, 369–383.

Blüher, M., Kahn, B.B., and Kahn, C.R. (2003). Extended Longevity in Mice Lacking the Insulin Receptor in Adipose Tissue. Science *299*, 572–574.

Bocklandt, S., Lin, W., Sehl, M.E., Sánchez, F.J., Sinsheimer, J.S., Horvath, S., and Vilain, E. (2011). Epigenetic Predictor of Age. PLoS ONE *6*, e14821.

Boks, M.P., Derks, E.M., Weisenberger, D.J., Strengman, E., Janson, E., Sommer, I.E., Kahn, R.S., and Ophoff, R.A. (2009). The relationship of DNA methylation with age, gender and genotype in twins and healthy controls. PLoS ONE *4*, e6767.

Bradshaw, S.D., and Bradshaw, F.J. (2009). Measurement of the rate of protein turnover and synthesis in the marsupial Honey possum (Tarsipes rostratus). J Comp Physiol B *179*, 183–192.

Brandfonbrener, M., Landowne, M., and Shock, N.W. (1955). Changes in Cardiac Output with Age. Circulation *12*, 557.

Brinster, R.L., and Troike, D.E. (1979). Requirements for blastocyst development in vitro. J Anim Sci *49 Suppl 2*, 26–34.

Calder, W.A. (1984). Size, Function, and Life History (Harvard University Press).

Calnan, D.R., and Brunet, A. (2008). The FoxO code. Oncogene *27*, 2276–2288.

Campisi, J. (2005). Senescent Cells, Tumor Suppression, and Organismal Aging: Good Citizens, Bad Neighbors. Cell *120*, 513–522.

Cao, Z., Wanagat, J., McKiernan, S.H., and Aiken, J.M. (2001). Mitochondrial DNA deletion mutations are concomitant with ragged red regions of individual, aged muscle fibers: analysis by laser-capture microdissection. Nucleic Acids Res *29*, 4502–4508.

Carlson, M.E., and Conboy, I.M. (2007). Loss of stem cell regenerative capacity within aged niches. Aging Cell *6*, 371–382.

Cencioni, C., Spallotta, F., Martelli, F., Valente, S., Mai, A., Zeiher, A., and Gaetano, C. (2013). Oxidative Stress and Epigenetic Regulation in Ageing and Age-Related Diseases. IJMS *14*, 17643–17663.

Chambers, S.M., Shaw, C.A., Gatza, C., Fisk, C.J., Donehower, L.A., and Goodell, M.A. (2007). Aging Hematopoietic Stem Cells Decline in Function and Exhibit Epigenetic Dysregulation. PLoS Biol *5*, e201.

Chan, D.C. (2012). Fusion and Fission: Interlinked Processes Critical for Mitochondrial Health. Annu Rev Genet *46*, 265–287.

Chan, S.S.L., and Copeland, W.C. (2009). DNA polymerase gamma and mitochondrial disease: Understanding the consequence of *POLG* mutations. Biochim Biophys Acta *1787*, 312–319.

Chen, Y., and Dorn, G.W. (2013). PINK1-phosphorylated mitofusin 2 is a Parkin receptor for culling damaged mitochondria. Science *340*.

Christensen, B.C., Houseman, E.A., Marsit, C.J., Zheng, S., Wrensch, M.R., Wiemels, J.L., Nelson, H.H., Karagas, M.R., Padbury, J.F., Bueno, R., et al. (2009). Aging and environmental exposures alter tissue-specific DNA methylation dependent upon CpG island context. PLoS Genetics *5*, e1000602.

Christiansen, L., Lenart, A., Tan, Q., Vaupel, J.W., Aviv, A., McGue, M., and Christensen, K. (2015). DNA methylation age is associated with mortality in a longitudinal Danish twin study. Aging Cell *15*, 149–154.

Collins, M.L., Eng, S., Hoh, R., and Hellerstein, M.K. (2003). Measurement of mitochondrial DNA synthesis in vivo using a stable isotope-mass spectrometric technique. J Appl Physiol *94*, 2203–2211.

Comte, C., Tonin, Y., Heckel-Mager, A.M., Boucheham, A., Smirnov, A., Aure, K., Lombes, A., Martin, R.P., Entelis, N., and Tarassov, I. (2012). Mitochondrial targeting of recombinant RNAs modulates the level of a heteroplasmic mutation in human mitochondrial DNA associated with Kearns Sayre Syndrome. Nucleic Acids Res *41*, 418–433.

Cookson, M.R. (2012). Parkinsonism due to mutations in PINK1, parkin, and DJ-1 and oxidative stress and mitochondrial pathways. Cold Spring Harb Perspect Med *2*, a009415.

Coombs, D.H., and Watts, N.R.M. (1985). Generating sucrose gradients in three minutes by tilted tube rotation. Anal Biochem *148*, 254–259.

Cormier, C.Y., Mohr, S.E., Zuo, D., Hu, Y., Rolfs, A., Kramer, J., Taycher, E., Kelley, F., Fiacco, M., Turnbull, G., et al. (2009). Protein Structure Initiative Material Repository: an open shared public resource of structural genomics plasmids for the biological community. Nucleic Acids Res *38*, D743–D749.

Couture, P., and Hulbert, A.J. (1995). Membrane fatty acid composition of tissues is related to body mass of mammals. J Membr Biol *148*, 27–39.

Daum, G. (1985). Lipids of mitochondria. Biochemica Et Biophysica Acta *822*, 1–42.

Day, K., Waite, L.L., Thalacker-Mercer, A., West, A., Bamman, M.M., Brooks, J.D., Myers, R.M., and Absher, D. (2013). Differential DNA methylation with age displays both common and dynamic features across human tissues that are influenced by CpG landscape. Genome Biol *14*, R102.

De Baets, G., Reumers, J., Delgado Blanco, J., Dopazo, J., Schymkowitz, J., and Rousseau, F. (2011). An Evolutionary Trade-Off between Protein Turnover Rate and Protein Aggregation Favors a Higher Aggregation Propensity in Fast Degrading Proteins. PLoS Comp Biol *7*, e1002090.

De Bont, R., and van Larebeke, N. (2004). Endogenous DNA damage in humans: a review of quantitative data. Mutagenesis *19*, 169–185.

Delaney, M.A., Ward, J.M., Walsh, T.F., Chinnadurai, S.K., Kerns, K., Kinsel, M.J., and Treuting, P.M. (2016). Initial Case Reports of Cancer in Naked Mole-rats (Heterocephalus glaber). Vet Pathol.

Demirel, Y. (2014a). Nonequilibrium thermodynamics: transport and rate processes in physical, chemical and biological systems (Elsevier).

Demirel, Y. (2014b). Information in Biological Systems and the Fluctuation Theorem. Entropy *16*, 1931–1948.

Deng, Y., Chan, S.S., and Chang, S. (2008). Telomere dysfunction and tumour suppression: the senescence connection. Nat Rev Cancer *8*, 450–458.

Desquiret-Dumas, V., Gueguen, N., Barth, M., Chevrollier, A., Hancock, S., Wallace, D.C., Amati-Bonneau, P., Henrion, D., Bonneau, D., Reynier, P., et al. (2012). Biochimica et Biophysica Acta. Biochim Biophys Acta *1822*, 1019–1029.

Detmer, S.A., and Chan, D.C. (2007). Functions and dysfunctions of mitochondrial dynamics. Nat Rev Mol Cell Biol *8*, 870–879.

Douglas, P.M., and Dillin, A. (2010). Protein homeostasis and aging in neurodegeneration. J Cell Biol *190*, 719–729.

Drew, D., Lerch, M., Kunji, E., Slotboom, D.-J., and de Gier, J.-W. (2006). Optimization of membrane protein overexpression and purification using GFP fusions. Nat Meth *3*, 303–313.

Drew, D., Slotboom, D.-J., Friso, G., Reda, T., Genevaux, P., Rapp, M., Meindl-Beinker, N.M., Lambert, W., Lerch, M., Daley, D.O., et al. (2005). A scalable, GFP-based pipeline for membrane protein overexpression screening and purification. Protein Science *14*, 2011–2017.

Dumont, N.A., Wang, Y.X., and Rudnicki, M.A. (2015). Intrinsic and extrinsic mechanisms regulating satellite cell function. Development *142*, 1572–1581.

Dunn, D.A., and Pinkert, C.A. (2012). Nuclear Expression of a Mitochondrial DNA Gene: Mitochondrial Targeting of Allotopically Expressed Mutant ATP6 in Transgenic Mice. J Biomed Biotechnol *2012*, 1–7.

ENCODE Project Consortium, Birney, E., Stamatoyannopoulos, J.A., Dutta, A., Guigó, R., Gingeras, T.R., Margulies, E.H., Weng, Z., Snyder, M., Dermitzakis, E.T., et al. (2007). Identification and analysis of functional elements in 1% of the human genome by the ENCODE pilot project. Nature *447*, 799–816.

Ellouze, S., Augustin, S., Bouaita, A., Bonnet, C., Simonutti, M., Forster, V., Picaud, S., Sahel, J.-A., and Corral-Debrinski, M. (2008). Optimized Allotopic Expression of the Human Mitochondrial ND4 Prevents Blindness in a Rat Model of Mitochondrial Dysfunction. Am J Hum Genet *83*, 373–387.

Else, P.L. (2004). Respiration rate of hepatocytes varies with body mass in birds. J Exp Biol *207*, 2305–2311.

Else, P.L., and Wu, B.J. (1999). What role for membranes in determining the higher sodium pump molecular activity of mammals compared to ectotherms? J Comp Physiol B, Biochem Syst Environ Physiol *169*, 296–302.

Else, P.L., Windmill, D.J., and Markus, V. (1996). Molecular activity of sodium pumps in endotherms and ectotherms. Am J Physiol *271*, R1287–1294.

Euler, L. (1767). Recherches générales sur la mortalité et la multiplication du genre humain. In Memoires De L'academie Des Sciences De Berlin, pp. 144–164.

Everett, A.W., Taylor, R.R., and Sparrow, M.P. (1977). Protein synthesis during right-ventricular hypertrophy after pulmonary-artery stenosis in the dog. Biochem J *166*, 315–321.

Eyre-Walker, A., and Keightley, P.D. (2007). The distribution of fitness effects of new mutations. Nat Rev Genet *8*, 610–618.

Faulks, S.C., Turner, N., Else, P.L., and Hulbert, A.J. (2006). Calorie restriction in mice: effects on body composition, daily activity, metabolic rate, mitochondrial reactive oxygen species production, and membrane fatty acid composition. J Gerontol a Biol Sci Med Sci *61*, 781–794.

Figge, M.T., Reichert, A.S., Meyer-Hermann, M., and Osiewacz, H.D. (2012). Deceleration of Fusion–Fission Cycles Improves Mitochondrial Quality Control during Aging. PLoS Comp Biol *8*, e1002576.

Fisher, R.A. (1930). The genetical theory of natural selection. (Oxford).

Florath, I., Butterbach, K., Müller, H., Bewerunge-Hudler, M., and Brenner, H. (2013). Cross-sectional and longitudinal changes in DNA methylation with age: an epigenome-wide analysis revealing over 60 novel age-associated CpG sites. Hum Mol Gen *23*, 1186–1201.

Frederico, L.A., Kunkel, T.A., and Shaw, B.R. (1990). A sensitive genetic assay for the detection of cytosine deamination: determination of rate constants and the activation energy. Biochemistry *29*, 2532–2537.

Garagnani, P., Bacalini, M.G., Pirazzini, C., Gori, D., Giuliani, C., Mari, D., Di Blasio, A.M., Gentilini, D., Vitale, G., Collino, S., et al. (2012). Methylation of ELOVL2 gene as a new epigenetic marker of age. Aging Cell *11*, 1132–1134.

García-Prat, L., Sousa-Victor, P., and Muñoz-Cánoves, P. (2013). Functional dysregulation of stem cells during aging: a focus on skeletal muscle stem cells. FEBS J *280*, 4051–4062.

Garland, T. (1982). The relation between maximal running speed and body mass in terrestrial mammals. J Zool, Lond *199*, 157–170.

Garlick, P.J., and Marshall, I. (1972). A technique for measuring brain protein synthesis. J Neurochem *19*, 577–583.

Gentilini, D., Mari, D., Castaldi, D., Remondini, D., Ogliari, G., Ostan, R., Bucci, L., Sirchia, S.M., Tabano, S., Cavagnini, F., et al. (2012). Role of epigenetics in human aging and longevity: genome-wide DNA methylation profile in centenarians and centenarians' offspring. Age (Dordr) *35*, 1961–1973.

Greaves, L.C., Elson, J.L., Nooteboom, M., Grady, J.P., Taylor, G.A., Taylor, R.W., Mathers, J.C., Kirkwood, T.B.L., and Turnbull, D.M. (2012). Comparison of mitochondrial mutation spectra in ageing human colonic epithelium and disease: absence of evidence for purifying selection in somatic mitochondrial DNA point mutations. PLoS Genetics *8*, e1003082.

Greaves, L.C., Nooteboom, M., Elson, J.L., Tuppen, H.A.L., Taylor, G.A., Commane, D.M., Arasaradnam, R.P., Khrapko, K., Taylor, R.W., Kirkwood, T.B.L., et al. (2014). Clonal expansion of early to mid-life mitochondrial DNA point mutations drives mitochondrial dysfunction during human ageing. PLoS Genetics *10*, e1004620.

Gredilla, R., Garm, C., Holm, R., Bohr, V.A., and Stevnsner, T. (2010). Differential age-related changes in mitochondrial DNA repair activities in mouse brain regions. Neurobiol Aging *31*, 993–1002.

Grosse, I., Buldyrev, S.V., Stanley, H.E., Holste, D., and Herzel, H. (2000). Average mutual information of coding and noncoding DNA. Pac Symp Biocomput *5*, 611–620.

Grounds, M.D. (1998). Age-associated changes in the response of skeletal muscle cells to exercise and regeneration. Ann N Y Acad Sci *854*, 78–91.

Guo, K.K., and Ren, J. (2006). Cardiac overexpression of alcohol dehydrogenase (ADH) alleviates aging-associated cardiomyocyte contractile dysfunction: role of intracellular Ca2+ cycling proteins. Aging Cell *5*, 259–265.

Guy, J., Qi, X., Koilkonda, R.D., Arguello, T., Chou, T.H., Ruggeri, M., Porciatti, V., Lewin, A.S., and Hauswirth, W.W. (2009). Efficiency and Safety of AAV-Mediated Gene Delivery of the Human ND4 Complex I Subunit in the Mouse Visual System. Invest Ophthalmol Vis Sci *50*, 4205–4214.

Guy, J., Qi, X., Pallotti, F., Schon, E.A., Manfredi, G., Carelli, V., Martinuzzi, A., Hauswirth, W.W., and Lewin, A.S. (2002). Rescue of a mitochondrial deficiency causing Leber hereditary optic neuropathy. Ann Neurol *52*, 534–542.

Haag-Liautard, C., Coffey, N., Houle, D., Lynch, M., Charlesworth, B., and Keightley, P.D. (2008). Direct estimation of the mitochondrial DNA mutation rate in Drosophila melanogaster. PLoS Biol *6*, e204.

Hamilton, W.D. (1966). The moulding of senescence by natural selection. J Theor Biol *12*, 12–45.

Hannum, G., Guinney, J., Zhao, L., Zhang, L., Hughes, G., Sadda, S., Klotzle, B., Bibikova, M., Fan, J.-B., Gao, Y., et al. (2013). Genome-wide methylation profiles reveal quantitative views of human aging rates. Mol Cell *49*, 359–367.

Hansen, K.D., Timp, W., Bravo, H.C., Sabunciyan, S., Langmead, B., McDonald, O.G., Wen, B., Wu, H., Liu, Y., Diep, D., et al. (2011). Increased methylation variation in epigenetic domains across cancer types. Nat Genet *43*, 768–775.

Hayflick, L. (2007a). Biological Aging Is No Longer an Unsolved Problem. Ann N Y Acad Sci *1100*, 1–13.

Hayflick, L., and Moorhead, P.S. (1961). The serial cultivation of human diploid cell strains. Exp Cell Res *25*, 585.

Hayflick, L. (2000). The future of ageing. Nature *408*, 267–269.

Hayflick, L. (2004). "Anti-aging" is an oxymoron. J Gerontol a Biol Sci Med Sci *59*, B573–578.

Hayflick, L. (2007b). Entropy explains aging, genetic determinism explains longevity, and undefined terminology explains misunderstanding both. PLoS Genetics *3*, e220.

Heglund, N.C., and Taylor, C.R. (1988). Speed, stride frequency and energy cost per stride: how do they change with body size and gait? J Exp Biol *138*, 301–318.

Heglund, N.C., Fedak, M.A., Taylor, C.R., and Cavagna, G.A. (1982). Energetics and mechanics of terrestrial locomotion. IV. Total mechanical energy changes as a function of speed and body size in birds and mammals. J Exp Biol *97*, 57–66.

Hetzer, M.W. (2013). Protein homeostasis: live long, won't prosper. Nat Rev Mol Cell Biol *14*, 55–61.

Heyn, H., Li, N., Ferreira, H.J., Moran, S., Pisano, D.G., Gomez, A., Diez, J., Sanchez-Mut, J.V., Setien, F., Carmona, F.J., et al. (2012). Distinct DNA methylomes of newborns and centenarians. Proc Natl Acad Sci USA *109*, 10522–10527.

Hochwagen, A., and Amon, A. (2006). Checking Your Breaks: Surveillance Mechanisms of Meiotic Recombination. Curr Biol *16*, R217–R228.

Holliday, R. (2010). Aging and the decline in health. Health *02*, 615–619.

Horvath, S. (2013). DNA methylation age of human tissues and cell types. Genome Biol *14*, R115.

Huang, P., Galloway, C.A., and Yoon, Y. (2011). Control of mitochondrial morphology through differential interactions of mitochondrial fusion and fission proteins. PLoS ONE *6*.

Hulbert, A.J. (2003). Life, death and membrane bilayers. J Exp Biol *206*, 2303–2311.

Hulbert, A.J. (2005). On the importance of fatty acid composition of membranes for aging. J Theor Biol *234*, 277–288.

Hulbert, A.J. (2008). The links between membrane composition, metabolic rate and lifespan. Comp Biochem Physiol, Part a Mol Integr Physiol *150*, 196–203.

Hulbert, A.J., and Else, P.L. (1999). Membranes as possible pacemakers of metabolism. J Theor Biol *199*, 257–274.

Hulbert, A.J., Pamplona, R., Buffenstein, R., and Buttemer, W.A. (2007). Life and death: metabolic rate, membrane composition, and life span of animals. Physiol Rev *87*, 1175–1213.

Hwang, J.S., Hwang, J.S., Chang, I., and Kim, S. (2007). Age-associated decrease in proteasome content and activities in human dermal fibroblasts: restoration of normal level of proteasome subunits reduces aging markers in fibroblasts from elderly persons. J Gerontol a Biol Sci Med Sci *62*, 490–499.

Irwin, M.H., Johnson, L.W., and Pinkert, C.A. (1999). Isolation and microinjection of somatic cell-derived mitochondria and germline heteroplasmy in transmitochondrial mice. Transgenic Res *8*, 119–123.

Irwin, M.H., Parameshwaran, K., and Pinkert, C.A. (2013). Mouse models of mitochondrial complex I dysfunction. Int J Biochem Cell Biol *45*, 34–40.

Isaksson, L., Enberg, J., Neutze, R., Karlsson, B.G., and Pedersen, A. (2012). Expression screening of membrane proteins with cell-free protein synthesis. Protein Expr Purif *82*, 218–225.

Itsara, L.S., Kennedy, S.R., Fox, E.J., Yu, S., Hewitt, J.J., Sanchez-Contreras, M., Cardozo-Pelaez, F., and Pallanck, L.J. (2014). Oxidative stress is not a major contributor to somatic mitochondrial DNA mutations. PLoS Genetics *10*, e1003974.

Jaramillo-Lambert, A., Harigaya, Y., Vitt, J., Villeneuve, A., and Engebrecht, J. (2010). Meiotic Errors Activate Checkpoints that Improve Gamete Quality without Triggering Apoptosis in Male Germ Cells. Curr Biol *20*, 2078–2089.

Jin, S.M., Lazarou, M., Wang, C., Kane, L.A., Narendra, D.P., and Youle, R.J. (2010). Mitochondrial membrane potential regulates PINK1 import and proteolytic destabilization by PARL. J Cell Biol *191*, 933–942.

Kennedy, S.R., Loeb, L.A., and Herr, A.J. (2011). Somatic mutations in aging, cancer and neurodegeneration. Mech Ageing Dev *133*, 118–126.

Kennedy, S.R., Salk, J.J., Schmitt, M.W., and Loeb, L.A. (2013). Ultra-Sensitive Sequencing Reveals an Age-Related Increase in Somatic Mitochondrial Mutations That Are Inconsistent with Oxidative Damage. PLoS Genetics *9*, e1003794.

Kenyon, C., Chang, J., Gensch, E., Rudner, A., and Tabtiang, R. (1993). A C. elegans mutant that lives twice as long as wild type. Nature *366*, 461–464.

Kenyon, C.J. (2010). The genetics of ageing. Nature *464*, 504–512.

Kilbourne, B.M., and Hoffman, L.C. (2013). Scale Effects between Body Size and Limb Design in Quadrupedal Mammals. PLoS ONE *8*, e78392.

Kim, N., and Jinks-Robertson, S. (2012). Transcription as a source of genome instability. Nat Rev Genet *13*, 204–214.

Kim, T.-W., Keum, J.-W., Oh, I.-S., Choi, C.-Y., Park, C.-G., and Kim, D.-M. (2006). Simple procedures for the construction of a robust and cost-effective cell-free protein synthesis system. Journal of Biotechnology *126*, 554–561.

Kirkwood, T.B. (1977). Evolution of ageing. Nature *270*, 301–304.

Kirkwood, T.B., and Holliday, R. (1979). The evolution of ageing and longevity. Proc R Soc Lond, B, Biol Sci *205*, 531–546.

Kirkwood, T.B., and Rose, M.R. (1991). Evolution of senescence: late survival sacrificed for reproduction. Philos Trans R Soc Lond, B, Biol Sci *332*, 15–24.

Kirkwood, T.B.L. (2005). Understanding the Odd Science of Aging. Cell *120*, 437–447.

Kirkwood, T. (1999). Time of Our Lives : The Science of Human Aging (Oxford University Press).

Kleiber, M. (1932). Body size and metabolism. Hilgardia *6*, 315–353.

Kondepudi, D., and Prigogine, I. (2014). Modern Thermodynamics (John Wiley & Sons).

Koshiba, T., Detmer, S.A., Kaiser, J.T., Chen, H., McCaffery, J.M., and Chan, D.C. (2004). Structural basis of mitochondrial tethering by mitofusin complexes. Science *305*, 858–862.

Kowald, A., and Kirkwood, T.B.L. (2011). Evolution of the mitochondrial fusion-fission cycle and its role in aging. Proc Natl Acad Sci USA *108*, 10237–10242.

Kram, R., and Taylor, C.R. (1990). Energetics of running: a new perspective. Nature *346*, 265–267.

Kraytsberg, Y., Kudryavtseva, E., McKee, A.C., Geula, C., Kowall, N.W., and Khrapko, K. (2006). Mitochondrial DNA deletions are abundant and cause functional impairment in aged human substantia nigra neurons. Nat Genet *38*, 518–520.

Kukat, C., Wurm, C.A., Spåhr, H., Falkenberg, M., Larsson, N.-G., and Jakobs, S. (2011). Super-resolution microscopy reveals that mammalian mitochondrial nucleoids have a uniform size and frequently contain a single copy of mtDNA. Proc Natl Acad Sci USA *108*, 13534–13539.

Larsson, N.-G. (2010). Somatic Mitochondrial DNA Mutations in Mammalian Aging. Annu Rev Biochem *79*, 683–706.

Lee, H.-S., Ma, H., Juanes, R.C., Tachibana, M., Sparman, M., Woodward, J., Ramsey, C., Xu, J., Kang, E.-J., Amato, P., et al. (2012). Rapid mitochondrial DNA segregation in primate preimplantation embryos precedes somatic and germline bottleneck. Cell Rep *1*, 506–515.

Li, Y., Wang, E., and Wang, Y. (1999). A modified procedure for fast purification of T7 RNA polymerase. Protein Expr Purif *16*, 355–358.

Liebermeister, W., Noor, E., Flamholz, A., Davidi, D., Bernhardt, J., and Milo, R. (2014). Visual account of protein investment in cellular functions. Proc Natl Acad Sci USA *111*, 8488–8493.

Lindahl, T. (1993). Instability and decay of the primary structure of DNA. Nature *362*, 709–715.

Lodato, M.A., Woodworth, M.B., Lee, S., Evrony, G.D., Mehta, B.K., Karger, A., Lee, S., Chittenden, T.W., D'Gama, A.M., Cai, X., et al. (2015). Somatic mutation in single human neurons tracks developmental and transcriptional history. Science *350*, 94–98.

Lotka, A.J., and Sharpe, F.R. (1911). A problem in age distribution. Philos Mag *21*, 435–438.

Mahony, S., Auron, P.E., and Benos, P.V. (2007). Inferring protein DNA dependencies using motif alignments and mutual information. Bioinformatics *23*, i297–i304.

Mbantenkhu, M., Wang, X., Nardozzi, J.D., Wilkens, S., Hoffman, E., Patel, A., Cosgrove, M.S., and Chen, X.J. (2011). Mgm101 Is a Rad52-related Protein Required for Mitochondrial DNA Recombination. J Biol Chem *286*, 42360–42370.

McClay, J.L., Aberg, K.A., Clark, S.L., Nerella, S., Kumar, G., Xie, L.Y., Hudson, A.D., Harada, A., Hultman, C.M., Magnusson, P.K.E., et al. (2013). A methylome-wide study of aging using massively parallel sequencing of the methyl-CpG-enriched genomic fraction from blood in over 700 subjects. Hum Mol Gen *23*, 1175–1185.

McKenzie, M., Trounce, I.A., Cassar, C.A., and Pinkert, C.A. (2004). Production of homoplasmic xenomitochondrial mice. Proc Natl Acad Sci USA *101*, 1685–1690.

McNab, B.K. (1966). The metabolism of fossorial rodents: a study of convergence. Ecology 712–733.

Medawar, P.B. (1952). An unsolved problem of biology.

Medvedev, Z.A. (1972). Possible role of repeated nucleotide sequences in DNA in the evolution of life spans of differentiated cells. Nature *237*, 453–454.

Miller, B.F., Robinson, M.M., Bruss, M.D., Hellerstein, M., and Hamilton, K.L. (2011). A comprehensive assessment of mitochondrial protein synthesis and cellular proliferation with age and caloric restriction. Aging Cell *11*, 150–161.

Miller, B.F., Robinson, M.M., Reuland, D.J., Drake, J.C., Peelor, F.F., Bruss, M.D., Hellerstein, M.K., and Hamilton, K.L. (2013). Calorie restriction does not increase short-term or long-term protein synthesis. J Gerontol a Biol Sci Med Sci *68*, 530–538.

Mitchell, H.H., Hamilton, T.S., Steggerda, F.R., and Bean, H.W. (1945). The chemical composition of the adult human body and its bearing on the biochemistry of growth. J Biol Chem *168*, 625–637.

Mitchell, T.W., Buffenstein, R., and Hulbert, A.J. (2007). Membrane phospholipid composition may contribute to exceptional longevity of the naked mole-rat (Heterocephalus glaber): a comparative study using shotgun lipidomics. Exp Gerontol *42*, 1053–1062.

Mitteldorf, J. (2010). Aging is not a process of wear and tear. Rejuvenation Res *13*, 322–326.

Moulton, C.R. (1923). Age and chemical development in mammals. J Biol Chem *57*, 79–97.

Nagy, K.A. (2005). Field metabolic rate and body size. J Exp Biol *208*, 1621–1625.

Narendra, D.P., Jin, S.M., Tanaka, A., Suen, D.-F., Gautier, C.A., Shen, J., Cookson, M.R., and Youle, R.J. (2010). PINK1 Is Selectively Stabilized on Impaired Mitochondria to Activate Parkin. PLoS Biol *8*, e1000298.

Niklas, K.J. (1994). Plant Allometry (University of Chicago Press).

Osman, C., Voelker, D.R., and Langer, T. (2011). Making heads or tails of phospholipids in mitochondria. J Cell Biol *192*, 7–16.

Pacy, P.J., Price, G.M., Halliday, D., and Quevedo, M.R. (1994). Nitrogen homoeostasis in man: the diurnal responses of protein synthesis and degradation and amino acid oxidation to diets with increasing protein intakes. Clin Sci *86*, 103–118.

Pamplona, R., Portero-Otín, M., Riba, D., Ruiz, C., Prat, J., Bellmunt, M.J., and Barja, G. (1998). Mitochondrial membrane peroxidizability index is inversely related to maximum life span in mammals. J Lipid Res *39*, 1989–1994.

Passos, J.F., Saretzki, G., Ahmed, S., Nelson, G., Richter, T., Peters, H., Wappler, I., Birket, M.J., Harold, G., Schaeuble, K., et al. (2007). Mitochondrial Dysfunction Accounts for the Stochastic Heterogeneity in Telomere-Dependent Senescence. PLoS Biol *5*, e110.

Pedersen, A., Hellberg, K., Enberg, J., and Karlsson, B.G. (2011). Rational improvement of cell-free protein synthesis. N Biotechnol *28*, 218–224.

Perez-Campo, R., López-Torres, M., Cadenas, S., Rojas, C., and Barja, G. (1998). The rate of free radical production as a determinant of the rate of aging: evidence from the comparative approach. J Comp Physiol B, Biochem Syst Environ Physiol *168*, 149–158.

Peters, R.H. (1986). The Ecological Implications of Body Size (Cambridge University Press).

Petersen, S., Saretzki, G., and Zglinicki, von, T. (1998). Preferential accumulation of single-stranded regions in telomeres of human fibroblasts. Exp Cell Res *239*, 152–160.

Pinkert, C.A., and Trounce, I.A. (2007). Generation of transmitochondrial mice: development of xenomitochondrial mice to model neurodegenerative diseases. Methods Cell Biol *80*, 549–569.

Pitts, K.R., Yoon, Y., Krueger, E.W., and McNiven, M.A. (1999). The dynamin-like protein DLP1 is essential for normal distribution and morphology of the endoplasmic reticulum and mitochondria in mammalian cells. Mol Biol Cell *10*, 4403–4417.

Plata, G., and Vitkup, D. (2013). Genetic robustness and functional evolution of gene duplicates. Nucleic Acids Res *42*, 2405–2414.

Pontzer, H. (2007). Effective limb length and the scaling of locomotor cost in terrestrial animals. J Exp Biol *210*, 1752–1761.

Porter, R.K., and Brand, M.D. (1995). Causes of differences in respiration rate of hepatocytes from mammals of different body mass. Am J Physiol *269*, R1213–1224.

Porter, R.K., Hulbert, A.J., and Brand, M.D. (1996). Allometry of mitochondrial proton leak: influence of membrane surface area and fatty acid composition. Am J Physiol *271*, R1550–1560.

Rakyan, V.K., Down, T.A., Maslau, S., Andrew, T., Yang, T.-P., Beyan, H., Whittaker, P., McCann, O.T., Finer, S., Valdes, A.M., et al. (2010). Human aging-associated DNA hypermethylation occurs preferentially at bivalent chromatin domains. Genome Res *20*, 434–439.

Rattan, S.I.S. (1996). Synthesis, modifications, and turnover of proteins during aging. Exp Gerontol *31*, 33.

Reeds, P.J., and Harris, C.I. (1981). Protein turnover in animals: man in his context. In Nitrogen Metabolism in Man, (London: Applied Science), pp. 391–408.

Reid, J.T., Bensadoun, A., and Bull, L.S. (1968). Some peculiarities in the body composition of animals. In Body Composition in Animals and Man.

Reilly, S.M., McElroy, E.J., and Biknevicius, A.R. (2007). Posture, gait and the ecological relevance of locomotor costs and energy-saving mechanisms in tetrapods. Zoology (Jena) *110*, 271–289.

Richardson, A., and Cheung, H.T. (1982). Current concepts: I. The relationship between age-related changes in gene expression, protein turnover, and the responsiveness of an organism to stimuli. Life Sci *31*, 605–613.

Riggs, J.E. (1994). Carcinogenesis, genetic instability and genomic entropy: insight derived from malignant brain tumor age specific mortality rate dynamics. J Theor Biol *170*, 331–338.

Rojo, M., Legros, F., Chateau, D., and Lombès, A. (2002). Membrane topology and mitochondrial targeting of mitofusins, ubiquitous mammalian homologs of the transmembrane GTPase Fzo. J Cell Sci *115*, 1663–1674.

Rossi, D.J., Jamieson, C.H.M., and Weissman, I.L. (2008). Stems Cells and the Pathways to Aging and Cancer. Cell *132*, 681–696.

Russell, K., Lobley, G.E., and Millward, D.J. (2003). Whole-body protein turnover of a carnivore, *Felis silvestris catus*. Br J Nutr *89*, 29–37.

Ryazanov, A.G., and Nefsky, B.S. (2001). Protein turnover plays a key role in aging. Mech Ageing Dev *123*, 207–213.

Santel, A., and Fuller, M.T. (2001). Control of mitochondrial morphology by a human mitofusin. J Cell Sci *114*, 867–874.

Santel, A., Frank, S., Gaume, B., Herrler, M., Youle, R.J., and Fuller, M.T. (2003). Mitofusin-1 protein is a generally expressed mediator of mitochondrial fusion in mammalian cells. J Cell Sci *116*, 2763–2774.

Schulz, C., Wood, C.G., Jones, D.L., Tazuke, S.I., and Fuller, M.T. (2002). Signaling from germ cells mediated by the rhomboid homolog stet organizes encapsulation by somatic support cells. Development *129*, 4523–4534.

Selman, C., Lingard, S., Choudhury, A.I., Batterham, R.L., Claret, M., Clements, M., Ramadani, F., Okkenhaug, K., Schuster, E., Blanc, E., et al. (2008). Evidence for lifespan extension and delayed age-related biomarkers in insulin receptor substrate 1 null mice. FASEB J *22*, 807–818.

Shanley, D.P., and Kirkwood, T.B. (2000). Calorie restriction and aging: a life-history analysis. Evolution *54*, 740–750.

Shyh-Chang, N., Daley, G.Q., and Cantley, L.C. (2013). Stem cell metabolism in tissue development and aging. Development *140*, 2535–2547.

Smirnova, E., Griparic, L., Shurland, D.L., and van der Bliek, A.M. (2001). Dynamin-related protein Drp1 is required for mitochondrial division in mammalian cells. Mol Biol Cell *12*, 2245–2256.

Smith, P.M., and Lightowlers, R.N. (2010). Altering the balance between healthy and mutated mitochondrial DNA. J Inherit Metab Dis *34*, 309–313.

Smith, R.E. (1956). Quantitative relations between liver mitochondria metabolism and total body weight in mammals. Ann N Y Acad Sci *62*, 405.

Sniegowski, P.D., Gerrish, P.J., Johnson, T., and Shaver, A. (2000). The evolution of mutation rates: separating causes from consequences. Bioessays *22*, 1057–1066.

Sousa-Victor, P., García-Prat, L., Serrano, A.L., Perdiguero, E., and Muñoz-Cánoves, P. (2015). Muscle stem cell aging: regulation and rejuvenation. Trends Endocrinol Metab *26*, 287–296.

Sousa-Victor, P., Gutarra, S., García-Prat, L., Rodriguez-Ubreva, J., Ortet, L., Ruiz-Bonilla, V., Jardí, M., Ballestar, E., González, S., Serrano, A.L., et al. (2014). Geriatric muscle stem cells switch reversible quiescence into senescence. Nature *506*, 316–321.

Speakman, J.R., Van Acker, A., and Harper, E.J. (2003). Age-related changes in the metabolism and body composition of three dog breeds and their relationship to life expectancy. Aging Cell *2*, 265.

Storch, J., and Kleinfeld, A.M. (1985). The lipid structure of biological membranes. Trends Biochem Sci *10*, 418.

Strang, K.T., and Steudel, K. (1990). Explaining the scaling of transport costs: the role of stride frequency and stride length. J Zool (London) *221*, 343–358.

Suda, T., Takubo, K., and Semenza, G.L. (2011). Metabolic regulation of hematopoietic stem cells in the hypoxic niche. Cell Stem Cell *9*, 298–310.

Suto, D., Ikeda, Y., Fujii, J., and Ohba, Y. (2006). Structural analysis of amino acids, oxidized by reactive oxygen species and an antibody against N-formylkynurenine. J Clin Biochem Nutr *38*, 107–111.

Szathmáry, E., and Smith, J.M. (1995). The major evolutionary transitions. Nature *374*, 227–232.

Tacutu, R., Craig, T., Budovsky, A., Wuttke, D., Lehmann, G., Taranukha, D., Costa, J., Fraifeld, V.E., and de Magalhães, J.P. (2012). Human Ageing Genomic Resources: integrated databases and tools for the biology and genetics of ageing. Nucleic Acids Res *41*, D1027–1033.

Tatar, M., Kopelman, A., Epstein, D., Tu, M.P., Yin, C.M., and Garofalo, R.S. (2001). A mutant Drosophila insulin receptor homolog that extends life-span and impairs neuroendocrine function. Science *292*, 107–110.

Tavernarakis, N., and Driscoll, M. (2002). Caloric restriction and lifespan: a role for protein turnover? Mech Ageing Dev *123*, 215–229.

Taylor, C.R., Heglund, N.C., and Maloiy, G.M. (1982). Energetics and mechanics of terrestrial locomotion. I. Metabolic energy consumption as a function of speed and body size in birds and mammals. J Exp Biol *97*, 1–21.

Thompson, R.F., Atzmon, G., Gheorghe, C., Liang, H.Q., Lowes, C., Greally, J.M., and Barzilai, N. (2010). Tissue-specific dysregulation of DNA methylation in aging. Aging Cell *9*, 506–518.

Tomasetti, C., and Vogelstein, B. (2015). Cancer etiology. Variation in cancer risk among tissues can be explained by the number of stem cell divisions. Science *347*, 78–81.

Torizawa, T., Shimizu, M., Taoka, M., Miyano, H., and Kainosho, M. (2004). Efficient production of isotopically labeled proteins by cell-free synthesis: a practical protocol. J Biomol NMR *30*, 311–325.

Tothova, Z., Kollipara, R., Huntly, B.J., Lee, B.H., Castrillon, D.H., Cullen, D.E., McDowell, E.P., Lazo-Kallanian, S., Williams, I.R., Sears, C., et al. (2007). FoxOs Are Critical Mediators of Hematopoietic Stem Cell Resistance to Physiologic Oxidative Stress. Cell *128*, 325–339.

Trindade, L.S., Aigaki, T., Peixoto, A.A., Balduino, A., Mânica da Cruz, I.B., and Heddle, J.G. (2013). A novel classification system for evolutionary aging theories. Front Genet *4*, 25.

Turner, N., Else, P.L., and Hulbert, A.J. (2003). Docosahexaenoic acid (DHA) content of membranes determines molecular activity of the sodium pump: implications for disease states and metabolism. Naturwissenschaften *90*, 521–523.

Turner, N., Hulbert, A.J., and Else, P.L. (2005). Sodium pump molecular activity and membrane lipid composition in two disparate ectotherms, and comparison with endotherms. J Comp Physiol B *175*, 77–85.

Twig, G., Elorza, A., Molina, A.J.A., Mohamed, H., Wikstrom, J.D., Walzer, G., Stiles, L., Haigh, S.E., Katz, S., Las, G., et al. (2008). Fission and selective fusion govern mitochondrial segregation and elimination by autophagy. EMBO J *27*, 433–446.

Verzijl, N., DeGroot, J., Thorpe, S.R., Bank, R.A., Shaw, J.N., Lyons, T.J., Bijlsma, J.W.J., Lafeber, F.P.J.G., Baynes, J.W., and TeKoppele, J.M. (2000). Effect of Collagen Turnover on the Accumulation of Advanced Glycation End Products. J Biol Chem *275*, 39027–39031.

Vijg, J., and Campisi, J. (2008). Puzzles, promises and a cure for ageing. Nature *454*, 1065–1071.

Wagner, S., Klepsch, M.M., Schlegel, S., Appel, A., Draheim, R., Tarry, M., Högbom, M., van Wijk, K.J., Slotboom, D.J., Persson, J.O., et al. (2008). Tuning Escherichia coli for membrane protein overexpression. Proc Natl Acad Sci USA *105*, 14371–14376.

Wai, T., Teoli, D., and Shoubridge, E.A. (2008). The mitochondrial DNA genetic bottleneck results from replication of a subpopulation of genomes. Nat Genet *40*, 1484–1488.

Waldera-Lupa, D.M., Kalfalah, F., Florea, A.-M., Sass, S., Kruse, F., Rieder, V., Tigges, J., Fritsche, E., Krutmann, J., Busch, H., et al. (2014). Proteome-wide analysis reveals an age-associated cellular phenotype of in situ aged human fibroblasts. Aging (Albany NY) *6*, 856–878.

Wallace, D.C. (1999). Mitochondrial Diseases in Man and Mouse. Science *283*, 1482–1488.

Wallace, D.C. (2010). Bioenergetics, the origins of complexity, and the ascent of man. Proc Natl Acad Sci USA *107*, 8947–8953.

Wang (2009). Modern thermodynamics – New concepts based on the second law of thermodynamics. Prog Nat Sci *19*, 125–135.

Wang, G., Shimada, E., Zhang, J., Hong, J.S., Smith, G.M., Teitell, M.A., and Koehler, C.M. (2012). Correcting human mitochondrial mutations with targeted RNA import. Proc Natl Acad Sci USA *109*, 4840–4845.

Waterlow, J.C. (2006). Protein turnover (Oxfordshire: CABI).

West, G.B., Brown, J.H., and Enquist, B.J. (1997). A general model for the origin of allometric scaling laws in biology. Science *276*, 122–126.

West, G.B., and Brown, J.H. (2005). The origin of allometric scaling laws in biology from genomes to ecosystems: towards a quantitative unifying theory of biological structure and organization. J Exp Biol *208*, 1575–1592.

West, G.B., Woodruff, W.H., and Brown, J.H. (2002). Allometric scaling of metabolic rate from molecules and mitochondria to cells and mammals. Proc Natl Acad Sci USA *99 Suppl 1*, 2473–2478.

White, C.R., and Seymour, R.S. (2005). Allometric scaling of mammalian metabolism. J Exp Biol.

Williams, G.C. (1957). Pleiotropy, Natural Selection, and the Evolution of Senescence. Evolution *11*, 398–411.

Yamada, Y., Kawamura, E., and Harashima, H. (2012). Mitochondrial-targeted DNA delivery using a DF-MITO-Porter, an innovative nano carrier with cytoplasmic and mitochondrial fusogenic envelopes. J Nanopart Res *14*, 1013.

Yang, W.C., Patel, K.G., Wong, H.E., and Swartz, J.R. (2012). Simplifying and streamlining Escherichia coli-based cell-free protein synthesis. Biotechnol Progress *28*, 413–420.

Yaniv, Y., Juhaszova, M., and Sollott, S.J. (2013). Age-related changes of myocardial ATPsupply and demand mechanisms. Trends Endocrinol Metab *24*, 495–505.

Yockey, H.P. (1974). An application of information theory to the Central Dogma and the Sequence Hypothesis. J Theor Biol *46*, 369–406.

Yoon, Y., Pitts, K.R., and McNiven, M.A. (2001). Mammalian dynamin-like protein DLP1 tubulates membranes. Mol Biol Cell *12*, 2894–2905.

Youle, R.J., and Narendra, D.P. (2011). Mechanisms of mitophagy. Nat Rev Mol Cell Biol *12*, 9–14.

Yu, H., Koilkonda, R.D., Chou, T.-H., Porciatti, V., Ozdemir, S.S., Chiodo, V., Boye, S.L., Boye, S.E., Hauswirth, W.W., Lewin, A.S., et al. (2012). Gene delivery to mitochondria by targeting modified adenoassociated virus suppresses Leber's hereditary optic neuropathy in a mouse model. Proc Natl Acad Sci USA *109*, E1238–1247.

Zangarelli, A., Chanseaume, E., Morio, B., Brugère, C., Mosoni, L., Rousset, P., Giraudet, C., Patrac, V., Gachon, P., Boirie, Y., et al. (2006). Synergistic effects of caloric restriction with maintained protein intake on skeletal muscle performance in 21-month-old rats: a mitochondria-mediated pathway. FASEB J *20*, 2439–2450.

Zglinicki, von, T. (2002). Oxidative stress shortens telomeres. Trends Biochem Sci *27*, 339–344.

Zhang, Y., Zhang, L., Zhang, L., Bai, J., Ge, H., and Liu, P. (2010). Expression changes in DNA repair enzymes and mitochondrial DNA damage in aging rat lens. Mol Vis *16*, 1754–1763.

Zheng, W., Khrapko, K., Coller, H.A., Thilly, W.G., and Copeland, W.C. (2006). Origins of human mitochondrial point mutations as DNA polymerase γ-mediated errors. Mutat Res *599*, 11–20.

Zhou, B.B., and Elledge, S.J. (2000). The DNA damage response: putting checkpoints in perspective. Nature *408*, 433–439.

Zhou, H.-X. (2010). Rate theories for biologists. Quart Rev Biophys *43*, 219–293.

Zimniak, P. (2008). Detoxification reactions: Relevance to aging. Ageing Res Rev *7*, 281–300.

de Magalhães, J.P., Costa, J., and Church, G.M. (2007). An analysis of the relationship between metabolism, developmental schedules, and longevity using phylogenetic independent contrasts. J Gerontol a Biol Sci Med Sci *62*, 149–160.

de Magalhães, J.P., Curado, J., and Church, G.M. (2009). Meta-analysis of age-related gene expression profiles identifies common signatures of aging. Bioinformatics *25*, 875–881.

van den Brink-van der Laan, E., Antoinette Killian, J., and de Kruijff, B. (2004). Nonbilayer lipids affect peripheral and integral membrane proteins via changes in the lateral pressure profile. Biochim Biophys Acta *1666*, 275–288.

Appendix 1 - Cell-Free Protein Synthesis Protocol

Buffers for extracts and cell-free reactions must be made from DNAse/RNAse-free water (use certified water from Teknova). Medium for *E. coli* cell culture can use MilliQ water. All instruments and glassware used in preparing extracts and cell-free synthesis reactions should be washed with autoclaved water containing 0.5% (v/v) DEPC and subsequently autoclaved.

Cell Extract (S12) Preparation

Buffers:

YTP Medium: 2x YT supplemented with 22 mM NaH_2PO_4 and 40mM Na_2HPO_4
Extract Buffer:
10 mM Tris-acetate, pH 8.2
14 mM magnesium acetate
60 mM potassium glutamate
1mM DTT

Adjust buffer pH with acetic acid.

Procedure:

NOTE: Timing on cultures and harvesting at mid-log phase is critical for extract performance. Keep cells and all buffers ice-cold for all steps following harvest.

1. Follow transformation protocol for Rosetta2 cells (Novagen), skipping addition of plasmid, and streak culture onto chloramphenicol-containing LB agar plate. Incubate plate overnight at 37°C (at least 15 hours).

2. Prepare mini-culture 1. Add 4 mL of YTP media + 30 µg/mL chloramphenicol to a 12 mL sterile culture tube and pre-warm to 37°C for 30 min.

3. Pick fresh colony from plate and inoculate mini-culture 1. Incubate at 37°C and 250 RPM for 8 hours.

4. 7 hours and 30 minutes after mini-culture 1 was started, prepare mini-culture 2. Add 50 mL of YTP media + 30 µg/mL chloramphenicol to a sterile 250mL Erlenmeyer flask and pre-warm to 37°C for 30 min.

5. Inoculate mini-culture 2 with 100 µL of mini-culture 1. Incubate at 37°C and 250 RPM for 8 hours.

6. 7 hours and 30 minutes after previous step, transfer 500 mL of YTP media + 30 µg/mL chloramphenicol to each of six 2 L stirrer flasks and pre-warm to 37°C for 30 minutes.

7. Add 5 mL of mini-culture 2 to each 2 L stirrer flask. Incubate at 37°C and 250 RPM until the culture OD600 reaches 1.5-2.0 (corresponding to mid-log growth phase). Check OD periodically with a 1:10 culture dilution for accuracy. **This step should take no longer than 3-3.75 hours; rapid growth and collection during mid-log phase is critical for extract quality.**

8. Cool cells on ice. Centrifuge at 6,200g for 15 min at 4°C. Aspirate supernatant. Record weight of wet cell pellet.

9. Resuspend cells by adding 20 mL of **ice-cold** extract buffer per gram of cells by shaking or knocking by hand. Do not pipet up and down. Centrifuge as per previous step and aspirate supernatant.

10. Repeat previous cell wash step.

11. Add 1.25 mL of **ice-cold** extract buffer for every gram of cells[1] and resuspend cell pellet by shaking or knocking by hand. Do not pipet up and down.

12. Aliquot 750 µL of cell solution to 1.5mL tubes. Sonicate each tube of cells on wet ice for 30 seconds continuously at a power setting of 5 (Fisher Scientific 550 Sonic Dismembrator, 1/16" probe 4417 (417-05) with coupler). Reuse tubes for subsequent rounds of sonication to minimize losses in yield.

13. Pool all sonicated fractions into 50 mL tube.

14. Centrifuge lysate at 12,000g for 15 min at 4°C.

15. Collect supernatant. Aliquot extract into volumes suitable for CFPS reaction sizes utilized in lab. Indicate volume on tubes. Flash freeze in liquid nitrogen. Store at -80°C.

T7 RNAP Preparation
Adapted from Yang et al. (2012).

Note: Yield is approximately 7g of wet cell pellet per liter of culture

Buffers:

Culture medium: LB broth with
100 μg/mL ampicillin

T7RNAP Lysis Buffer:
20 mM Tris, pH 8.0
10 mM EDTA
30 mM NaCl
1 mM DTT
10 mM β-Mercaptoethanol
5% glycerol
1x Roche Protease Inhibitor (add immediately before lysis)

T7RNAP FPLC Wash Buffer:
20 mM Tris, pH 8.0
1 mM EDTA
30 mM NaCl
1 mM DTT
5% glycerol

T7RNAP FPLC Elution Buffer:
20 mM Tris, pH 8.0
1 mM EDTA
1 M NaCl
1 mM DTT
5% glycerol

Procedure:

1. Transform BL21 or BL21(DE3) with pAR1219 plasmids according to standard procedures. Streak onto LB agar plates containing 100 μg/mL ampicillin for selection.

2. Inoculate 2 mL of culture medium with a colony from agar plate. Incubate at 37°C and 250 RPM for several hours or until medium is slightly turbid.

3. Transfer culture to 100 mL of culture medium. Incubate at 37°C and 250 RPM overnight.

4. Transfer 25 mL of culture to each of four 2L shaker flasks, each containing 1.25 L of culture medium. Incubate at 37°C and 250 RPM.

5. When OD600 reaches 0.6, induce T7 RNAP expression with 1 mM IPTG. Continue culturing for 5 hours.

6. Cool cells on ice. Centrifuge at 6,200g for 15 min at 4°C. Aspirate supernatant. Record weight of wet cell pellet.

7. Resuspend cells in 20 mL of lysis buffer per gram of cells by shaking or knocking by hand. Do not pipet up and down. Centrifuge as per previous step and aspirate supernatant.

8. Resuspend cell pellet by adding 1.25 - 1.5 mL of lysis buffer (with protease inhibitor) per gram of cells and pipetting up and down.

9. Sonicate cells on wet ice for 10 minutes continuously (power setting 7-8 with microtip). MONITOR SOLUTION TEMPERATURE – DO NOT ALLOW IT TO GET TOO HOT (>40°C).

10. Place solution back on ice while sonicating the other tubes.

11. Repeat the sonication step from step 9. (All cells should be sonicated for 20 minutes total.)

12. Centrifuge lysate at 10,000g for 15 minutes at 4°C. Collect supernatant. Solution can be flash-frozen in liquid nitrogen at this step for later processing.

13. Centrifuge supernatant from previous step in ultracentrifuge at 150,000g for 1 hour at 4°C (40k RPM on Ti60 rotor). Collect supernatant.

14. Purify T7RNAP by applying to anion exchange column (HiPrep DEAE FF 16/10). Elute over 6 column volumes (CV) using indicated buffers and collect fractions.

15. Concentrate fractions from anion exchange corresponding to conductivity values between 14 mS/cm and 22.5 mS/cm using 30kDa 20 mL spin columns (Vivaspin). Final volume should be ~1 mL for every 7 grams of cells.

16. Aliquot soluble fractions, flash-freeze in liquid nitrogen and store at -80°C.

17. Perform experiment to determine optimal T7RNAP concentration.

Quantifying T7 activity: Each new batch of T7RNAP should be tested in a CFPS reaction at different concentrations to determine relative activity.

25x 19 Amino Acid Mix Preparation
Adapted from Yang et al. (2012).

Note: L-Glutamate is omitted because it is included in the form of potassium glutamate and ammonium glutamate in the 10x Salt Solution.

Order of Addition	Reagent	Approx. pH After Addition	Approx. Dissolution Time (sec)
1	L-Arginine	10.65 – 10.68	30
2	L-Valine	8.99 – 9.20	180
3	L-Tryptophan	8.66 – 8.71	300
4	L-Phenylalanine	8.42 – 8.46	300
5	L-Isoleucine	8.31 – 8.34	480
6	L-Leucine	8.22 – 8.25	480
7	L-Cysteine	7.80 – 7.84	120
8	L-Methionine	7.73 – 7.75	240
9	L-Alanine	7.76 – 7.77	30
10	L-Asparagine	7.64 – 7.71	60
11	L-Aspartic Acid	5.35 – 5.41	180
12	L-Glycine	5.34 – 5.42	60
13	L-Glutamine	5.34 – 5.40	120
14	L-Histidine	6.46 – 6.54	240
15	L-Lysine	6.47 – 6.54	60
16	L-Proline	6.49 – 6.47	120
17	L-Serine	6.49 – 6.47	30
18	L-Threonine	6.50 – 6.54	30
19	L-Tyrosine	NA	NA

1. Obtain each of the reagents and set up the stir plate. Place a stir bar into an appropriately sized beaker. Add 87.5% of the final solution volume, autoclaved MQ water to the beaker.

2. Place the temperature probe into the water close to the edge of the beaker about half way into the water (without having the probe touching the beaker). Set the heating temperature to 37°C. Allow the water to reach temperature. **Any temperatures above 45°C for extended periods of time will decrease solution activity**.

3. Set the stir rate to 600 RPM. If the final volume is being scaled up, the stir rate should be set so that the bottom of the vortex forms just above the stir bar.

4. Weigh out the required quantity of each of the reagents. Add each of the reagents, one at a time according to the order of addition listed in the above table. After dissolution of each reagent, measure pH. Do not add the next reagent until the previous reagent is

fully dissolved. Use the "approx. dissolution time" and "approx. pH" as a guide. Repeat this step until tyrosine addition. After threonine has dissolved, allow the solution to mix for an additional 5 minutes.

5. Turn off heating on the heating/stir plate.

6. Pour the solution into a graduated cylinder to determine the volume. Add autoclaved MQ water to bring the total volume to the correct amount (approximately 5% of the final volume will be needed). **Sterile filtering the solution may decrease the activity of the final mixture by removing undissolved amino acids.** The solution should appear clear and colorless and relatively free of particulates. Freezing the solution at this point should not cause any precipitation.

7. Pour solution back into the beaker and resume stirring at 600 RPM. While mixing, add the required quantity of tyrosine to the solution and allow the suspension to mix for 5 minutes. **Note:** the tyrosine will not fully dissolve and will remain in suspension.

8. While still mixing, aliquot into tubes. Flash freeze the aliquots using liquid nitrogen and store at -80°C.

10X Nucleotide Solution Preparation
Adapted from Yang et al. (2012).

Buffer:

1. Add autoclaved MQ water to 80% of the final volume.

2. Weight out the required quantity of HEPES and pour into the mixing vessel. Allow to mix thoroughly.

3. Adjust the pH of the solution to pH 7.5 using HCl or KOH.

4. Add autoclaved MQ water to achieve final volume.

5. Sterile filter the solution through 0.22 μm filter.

Nucleotide Solution:

1. Obtain an appropriately sized mixing vessel and place it onto a stir plate. Place a stir bar into the bottom of the mixing vessel. Add 80% of the final volume, sterile-filtered nucleotide solution buffer to the vessel.

2. Set the stir rate to a sufficient mixing rate ensuring that splashing does not occur.

3. Add the specified quantity of malic acid to the solution. Ensure the complete dissolution of the material before proceeding with the next step.

4. Add the specified quantity of 2-oxoglutaric acid to the solution. Ensure the complete dissolution of the material before proceeding with the next step.

5. Add the specified quantity of succinic acid to the solution. Ensure the complete dissolution of the material before proceeding with the next step.

6. Add the specified quantity of folinic acid to the solution. Ensure the complete dissolution of the material before proceeding with the next step.

7. Add the specified quantity of DTT to the solution. Ensure the complete dissolution of the material before proceeding with the next step.

8. **Determine the pH of the solution before proceeding.** Adjust with HCl or KOH so that the pH is between pH 7.4 - 7.6.

9. Add the specified quantity of cAMP to the solution. Ensure the complete dissolution of the material before proceeding with the next step.

10. Add the required quantity of ATP into the beaker. Ensure the complete dissolution of the material before proceeding with the next step.

11. Add CMP, GMP, and UMP in that order, in a fashion similar to the ATP described above. Ensure the complete dissolution of the material before proceeding with the next step.

12. Add the specified quantity of tRNAs to the solution. Ensure the complete dissolution of the material before proceeding with the next step.

13. Determine the volume of the solution using a pipette or graduated cylinder. Add sterile-filtered nucleotide solution buffer to obtain the specified final volume.

14. Determine the pH of the solution. The pH should be approximately pH 7.4 - 7.6.

15. Aliquot into tubes. Flash freeze using liquid nitrogen and store at -80°C.

0.5M Magnesium Acetate Solution Preparation
Adapted from Yang et al. (2012).

Magnesium acetate is kept as a separate addition because the magnesium concentration for maximum protein production varies from one lot of cell extract to another. The typical optimal magnesium glutamate concentration for CFPS is 10-20 mM.

1. Obtain an appropriately sized mixing vessel and place it on the stir plate. Place a stir bar in the mixing vessel and set the heating temperature to 37°C. Add autoclaved MQ water to the vessel (75% of the final volume).

2. Set the stir rate to a high mixing rate, but avoid splashing.

3. Weigh out the required quantity of magnesium acetate in a weigh boat and pour the quantity into the mixing vessel.

4. Allow the magnesium acetate to dissolve at 37°C for 10 minutes with stirring.

5. Determine the volume of the solution using a pipette or graduated cylinder.

6. Add autoclaved MQ water to obtain the desired final volume. Allow the solution to stir at room temperature for 1 – 2 minutes until fully homogeneous.

7. Determine the pH of the solution and record the value. The pH should be approximately pH 6.4 - 6.5.

8. Sterilize by filtration through 0.22 μm filter.

9. Aliquot into tubes. Flash freeze using liquid nitrogen and store at -80°C.

Alternatively, for volumes of 10 mL or under prepare solution in sterile disposable 15 mL tube, vortex to mix, and filter sterilize through 0.22 μm filter. Aliquot as needed. Flash freeze using liquid nitrogen and store at -80°C.

10 mg/mL Creatine Kinase Solution Preparation
Adapted from Yang et al. (2012).

Buffer:

1. Transfer the required volume of glycerol to a clean mixing vessel.
2. Add autoclaved MQ water to 90% of the final volume.
3. Weight out the required quantity of potassium phosphate dibasic and pour the quantity into the mixing vessel. Allow to mix thoroughly.
4. Adjust the pH of the solution to pH 7.0 using HCl or NaOH.
5. Add the specified amount of NaCl.
6. Add autoclaved MQ water to achieve final volume.
7. Sterile filter solution through 0.22 μm filter.

Creatine Kinase Solution:

1. Transfer 85% of the final volume of freshly made, sterile-filtered creatine kinase buffer to clean tube.
2. Weigh out and add the specified volume of creatine kinase to the tube.
3. Allow to dissolve thoroughly using non-violent techniques (e.g. flicking tube or light pipetting is OK, do not vortex).
4. Add creatine kinase buffer to achieve final volume.
5. Aliquot into tubes. Flash freeze using liquid nitrogen and store at -80°C.

0.645M Creatine Phosphate Solution Preparation
Adapted from Yang et al. (2012).

Buffer:

1. Add autoclaved MQ water to 90% of the final volume.
2. Weight out the required quantity of HEPES and pour the quantity into the mixing vessel. Allow to mix thoroughly.
3. Adjust the pH of the solution to pH 7.0 using HCl or KOH.
4. Add autoclaved MQ water to achieve final volume.
5. Sterile filter solution through 0.22 μm filter.

Creatine Phosphate Solution:

1. Weigh out and add the specified volume of creatine phosphate to a clean, sterile 15 mL tube.
2. Transfer freshly made, sterile-filtered creatine phosphate buffer to the tube to 90% of the final volume.
3. Allow to dissolve thoroughly using non-violent techniques (e.g. flicking tube or light pipetting is OK, do not vortex). Solution must be clear.
4. Adjust to pH 7.0 using HCl or KOH.
5. Add creatine phosphate buffer to achieve final volume.
6. Aliquot into tubes. Flash freeze using liquid nitrogen and store at -80°C.

10X Salt Solution Preparation
Adapted from Yang et al. (2012).

1. Obtain an appropriately sized mixing vessel and place it on the stir plate. Place a stir bar in the mixing vessel.

2. Add autoclaved MQ water (45% of the desired final volume). Set the stir rate to a high mixing rate, but avoid splashing. Set the stir plate heating to 37°C.

3. Weigh out the required quantity of potassium glutamate and add into the beaker. Subsequent reagents can be added immediately.

4. Weigh out the required quantity of ammonium glutamate and add into the beaker.

5. Allow the salts to dissolve at 37°C for 10 minutes on the stir plate.

6. Determine the volume of the solution using a pipette or graduated cylinder.

7. Add autoclaved MQ water to obtain the desired final volume.

8. Allow the salts to dissolve at room temperature. This may take 10 minutes.

9. Obtain a pH reading for the solution once all components are completely dissolved. The pH should be approximately pH 7.2.

10. Aliquot into tubes. Flash freeze using liquid nitrogen and store at -80°C.

CFPS Main Reaction

Assemble on ice. Add in the order listed (enzymes last).

	Amounts		Stock Solution		Reaction Conc.	
DEPC-treated water	301.15	µL				
10X Salt Solution	250.00	µL	10	x		
25X Amino Acid Solution	100.00	µL	25	x		
10X Nucleotide Solution	250.00	µL	10	x		
S12 Extract	750.00	µL			30	% (v/v)
0.5M Magnesium Acetate Solution	50.00	µL	0.5	M	10.00	mM
0.645M Creatine Phosphate (CP) Solution	237.60	µL	0.645	M	61.3	mM
RNase inhibitor	2.50	µL	40	U/µL	40	U/mL
Complete EDTA-free Protease Inhibitor	25.00	µL	100	x	1	x
Detergent	375.00	µL	10	%	1.5	% (w/v)
DNA template	83.33	µL	450.00	ng/µL	15	µg/mL
IPTG	2.50	µL	400.00	mM	400	µM
T7RNAP	41.67	µL	6	mg/mL	100	µg/mL
10 mg/mL Creatine Kinase Solution	31.25	µL	10	mg/mL	125	µg/mL
Final Volume	2500.00	µL				

10X Nucleotide Solution

	Amounts		MW/Conc.		Reaction Conc.	
Hepes-KOH, pH 7.5					52.5	mM
Malic acid	147.50	mg	134.09	g/mol	4.4	mM
2-oxoglutaric acid	69.40	mg	146.1	g/mol	1.9	mM
Succinic acid	44.28	mg	118.09	g/mol	1.5	mM
Folinic acid	8.70	mg	511.5	g/mol	68	µM
DTT	65.56	mg	154.25	g/mole	1.7	mM
cAMP	59.07	mg	369.2	g/mole	0.64	mM
Adenosine 5'-Triphosphate Disodium Salt (ATP)	151.56	mg	551.14	g/mol	1.1	mM
Cytidine 5'-Monophosphate Disodium Salt (CMP)	78.02	mg	367.16	g/mol	0.85	mM
Guanosine 5'-Monophosphate Disodium Salt (GMP)	86.53	mg	407.18	g/mol	0.85	mM
Uridine 5'-Monophosphate Disodium Salt (UMP)	78.23	mg	368.15	g/mol	0.85	mM
tRNAs	43.75	mg			175	µg/mL
Solution Volume	25.00	mL				

Nucleotide Buffer, pH 7.5

Adjust pH with HCl or KOH

	Amounts		MW/Conc.		Buffer Conc.	
HEPES	6.255	g	238.3	g/mol	525	mM
Final Volume	50	mL				

10X Salt Solution

	Amounts		MW/Conc.		Reaction Conc.	
L-Glutamic acid potassium salt monohydrate	23.37	g	203.23	g/mol	230	mM
L-glutamic acid ammonium salt	2.25	g	164.2	g/mol	27.44	mM
Solution Volume	50.00	mL				

0.5M Magnesium Acetate Solution

	Amounts	MW/Conc.	Solution Conc.
MgOAc2 tetrahydrate	1.07 g	214.45 g/mol	0.5 M

Solution Volume 10.00 mL

0.645M Creatine Phosphate Solution

	Amounts	MW/Conc.	Solution Conc.
Sodium creatine phosphate dibasic tetrahydrate	2.11 g	327.14 g/mol	0.645 M

Solution Volume 10.00 mL

Creatine Phosphate Buffer, pH 7.0

Adjust pH with HCl or KOH

	Amounts	MW/Conc.	Buffer Conc.
HEPES	71.490 mg	238.3 g/mol	20 mM

Final Volume 15 mL

10 mg/mL Creatine Kinase Solution

	Amounts	MW/Conc.	Solution Conc.
Creatine Kinase (CK) from rabbit muscle	20.00 mg		10 mg/mL
Creatine Kinase Buffer			

Solution Volume 2.00 mL

Creatine Kinase Buffer, pH 7.0

Adjust pH with HCl or NaOH

	Amounts	MW/Conc.	Buffer Conc.
Potassium phosphate, dibasic	174.180 mg	174.18 g/mol	10 mM
NaCl	292.200 mg	58.44 g/mol	50 mM
Glycerol	50.000 mL		50 %

Final Volume 100 mL

25X Amino Acid Solution

	Amounts		MW/Conc.		Reaction Conc.	
L-Arginine monohydrochloride	173.79	mg	210.66	g/mol	1	mM
L-Valine	96.61	mg	117.1	g/mol	1	mM
L-Tryptophan	168.47	mg	204.2	g/mol	1	mM
L-Phenylalanine	136.29	mg	165.2	g/mol	1	mM
L-Isoleucine	108.24	mg	131.2	g/mol	1	mM
L-Leucine	108.24	mg	131.2	g/mol	1	mM
L-Cysteine	99.99	mg	121.2	g/mol	1	mM
L-Methionine	123.09	mg	149.2	g/mol	1	mM
L-Alanine	73.50	mg	89.09	g/mol	**1**	**mM**
L-Asparagine	108.98	mg	132.1	g/mol	1	mM
L-Aspartic Acid	109.81	mg	133.1	g/mol	1	mM
Glycine	61.93	mg	75.07	g/mol	1	mM
L-Glutamine	482.13	mg	146.1	g/mol	**4**	**mM**
L-Histidine monohydrochloride monohydrate	172.94	mg	209.63	g/mol	1	mM
L-Lysine monohydrochloride	150.65	mg	182.6	g/mol	1	mM
L-Proline	94.96	mg	115.1	g/mol	1	mM
L-Serine	173.42	mg	105.1	g/mol	**2**	**mM**
L-Threonine	98.26	mg	119.1	g/mol	1	mM
L-Tyrosine	149.49	mg	181.2	g/mol	1	mM
Solution Volume	33.00	mL				

100mM DTT Solution

Dissolve DTT in water. Aliquot and store at -20C

	Amounts		MW/Conc.		Solution Conc.	
DTT	154.25	mg	154.25	g/mol	0.1	M
Solution Volume	10.00	mL				

CFPS Reagents

Description	Supplier	SKU	Pack Size
2xYT medium, powder	EMD Millipore	4.85008.0500	500 g
Sodium phosphate, monobasic monohydrate, OmniPur	EMD Millipore	8290-500GM	500 g
Sodium phosphate, dibasic, heptahydrate, OmniPur	EMD Millipore	8210-500GM	500 g
Rosetta 2(DE3) Competent Cells	Novagen/EMD Millipore	71400-3	11 rxn
Water, Dnase- and RNAse- free, PCR-certified	Teknova	W3350	1 L
Trizma® base, BioPerformance certified	Sigma-Aldrich	T6066-100G	100 g
Glacial acetic acid			
Magnesium acetate tetrahydrate	Sigma-Aldrich	M5661-50G	50 g
L-Glutamic acid potassium salt monohydrate	Sigma-Aldrich	G1149-100G	100 g
DTT (DI-Dithiothreitol), biotechnology grade	Amresco	0281-5G	5 g
Phosphorylase B from rabbit muscle, for SDS-PAGE	Sigma-Aldrich	P4649-1VL	0.5 mg
21 L-Amino acids + Glycine	Sigma-Aldrich	09416-1EA	1 pack
Magnesium acetate tetrahydrate	Sigma-Aldrich	M5661-50G	50 g
L-Glutamic acid potassium salt monohydrate	Sigma-Aldrich	G1149-100G	100 g
L-Glutamic acid ammonium salt	MP Biomedicals	2180595.1	100 g
HEPES, OmniPur, Biotechnology Grade	EMD Millipore	5310-100GM	100 g
Adenosine 5’-triphosphate disodium salt hydrate	Sigma-Aldrich	A6419-1G	1 g
Cytidine 5’-monophosphate disodium salt	Sigma-Aldrich	C1006-1G	1 g
Guanosine 5’-monophosphate disodium salt hydrate	Sigma-Aldrich	G8377-1G	1 g
Uridine 5’-monophosphate disodium salt	Sigma-Aldrich	U6375-1G	1 g
Folinic acid calcium salt hydrate	Sigma-Aldrich	F7878-100MG	100 mg
L-(−)-Malic acid	Sigma-Aldrich	M7397-25G	25 g

α-Ketoglutaric acid / 2-Oxoglutaric acid	Sigma-Aldrich	K1128-5G	5 g
Succinic acid	Sigma-Aldrich	S3674-100G	100 g
tRNA from E. coli MRE 600	Roche	10109541001	100 mg
Adenosine 3’,5’-cyclic monophosphate, cAMP	Sigma-Aldrich	A9501-1G	1 g
Creatine kinase from rabbit muscle	Roche	10127566001	100 mg
Creatine phosphate disodium salt tetrahydrate	Roche	10621714001	5 g